

AD-A093 451

VIRGINIA UNIV CHARLOTTESVILLE DEPT OF MATERIALS SCIENCE F/6 20/2  
DISLOCATION CONCEPTS IN FRICTION AND WEAR.(U)  
DEC 80 D KUHLMANN-WILSDORF

N00014-76-C-1009

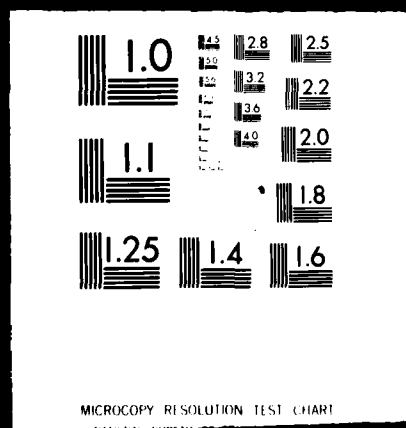
NL

UNCLASSIFIED

1 of 2  
AD-A093 451



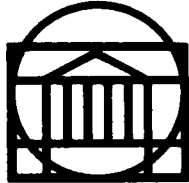
1 OF 2  
ADA  
093451



LEVEL

DTIC  
ELECTRA  
JAN 2 1981

RESEARCH LABORATORIES FOR THE ENGINEERING SCIENCES



# SCHOOL OF ENGINEERING AND APPLIED SCIENCE

UNIVERSITY OF VIRGINIA

Charlottesville, Virginia 22901

A Technical Report

DISLOCATION CONCEPTS IN FRICTION AND WEAR

Submitted to:

Office of Naval Research  
Materials Sciences Division  
Contract No. N00014-76-C-10009

Submitted by:

Doris Kuhlmann-Wilsdorf  
University Professor of Applied Science

DISTRIBUTION STATEMENT A  
Approved for public release;  
Distribution Unlimited

December 1980

80 12 31 053

AD A093451

DDC FILE COPY

### **RESEARCH LABORATORIES FOR THE ENGINEERING SCIENCES**

Members of the faculty who teach at the undergraduate and graduate levels and a number of professional engineers and scientists whose primary activity is research generate and conduct the investigations that make up the school's research program. The School of Engineering and Applied Science of the University of Virginia believes that research goes hand in hand with teaching. Early in the development of its graduate training program, the School recognized that men and women engaged in research should be as free as possible of the administrative duties involved in sponsored research. In 1959, therefore, the Research Laboratories for the Engineering Sciences (RLES) was established and assigned the administrative responsibility for such research within the School.

The director of RLES—himself a faculty member and researcher—maintains familiarity with the support requirements of the research under way. He is aided by an Academic Advisory Committee made up of a faculty representative from each academic department of the School. This Committee serves to inform RLES of the needs and perspectives of the research program.

In addition to administrative support, RLES is charged with providing certain technical assistance. Because it is not practical for each department to become self-sufficient in all phases of the supporting technology essential to present-day research, RLES makes services available through the following support groups: Machine Shop, Instrumentation, Facilities Services, Publications (including photographic facilities), and Computer Terminal Maintenance.

A Technical Report

DISLOCATION CONCEPTS IN FRICTION AND WEAR\*

Submitted to:

Office of Naval Research  
Materials Sciences Division  
Contract No. N00014-76-C-10009

Submitted by:

Doris/Kuhlmann-Wilsdorf  
University Professor of Applied Science

Department of Materials Science ✓

RESEARCH LABORATORIES FOR THE ENGINEERING SCIENCES

SCHOOL OF ENGINEERING AND APPLIED SCIENCE

UNIVERSITY OF VIRGINIA

CHARLOTTESVILLE, VIRGINIA

December 1980

\* To be published as Chapter 5 in "Fundamentals of Friction and Wear of Materials", 1980 ASM Materials Science Seminar, Editor D. A. Rigney, ASM.

Unclassified

SECURITY CLASSIFICATION OF THIS PAGE (When Data Entered)

REPORT DOCUMENTATION PAGE		READ INSTRUCTIONS BEFORE COMPLETING FORM
1. REPORT NUMBER - - -	2. GOVT ACCESSION NO. AD-A093 451	3. RECIPIENT'S CATALOG NUMBER - - -
4. TITLE (and Subtitle)  Dislocation Concepts in Friction and Wear		5. TYPE OF REPORT & PERIOD COVERED Technical Report 1980
		6. PERFORMING ORG. REPORT NUMBER - - -
7. AUTHOR(s)  Doris Kuhlmann-Wilsdorf		8. CONTRACT OR GRANT NUMBER(s)  N00014-76-C-1009 ✓
9. PERFORMING ORGANIZATION NAME AND ADDRESS Research Laboratories for the Engineer- ing Sciences, University of Virginia, ✓ Charlottesville, VA 22903		10. PROGRAM ELEMENT, PROJECT, TASK AREA & WORK UNIT NUMBERS  - - -
11. CONTROLLING OFFICE NAME AND ADDRESS Office of Naval Research Department of the Navy Arlington, VA 22217		12. REPORT DATE December 1980
		13. NUMBER OF PAGES 119
14. MONITORING AGENCY NAME & ADDRESS (if different from Controlling Office)		15. SECURITY CLASS. (of this report)  Unclassified
		15a. DECLASSIFICATION/DOWNGRADING SCHEDULE
16. DISTRIBUTION STATEMENT (of this Report)  Unlimited		
17. DISTRIBUTION STATEMENT (of the abstract entered in Block 20, if different from Report)  - - -		
18. SUPPLEMENTARY NOTES  - - -		
19. KEY WORDS (Continue on reverse side if necessary and identify by block number) friction, wear, delamination wear, coefficient of friction, wear coefficient, induction period, wearing-in, dislocation cells, texture, adhesion, surface films, micro-roughness.		
20. ABSTRACT (Continue on reverse side if necessary and identify by block number) Using dislocation concepts, primarily as relevant to geometrical considerations, and other basic facts concerning plastic proper- ties of crystalline materials, a number of qualitative and quan- titative relationships in the area of friction and wear are de- veloped. (i) The accepted model for friction and wear is expanded to in- clude the micro-roughness which must necessarily arise at con- tact spots on account of inhomogeneities in elastic and plastic		

DD FORM 1473

JAN 73

EDITION OF 1 NOV 65 IS OBSOLETE

Unclassified

SECURITY CLASSIFICATION OF THIS PAGE (When Data Entered)

Unclassified

deformation. (ii) A simple formula is proposed to describe the conditions under which adhesion is important. (iii) The concept of the "basic" case is introduced, which is sliding wear between average-rough and average-clean surfaces, such that adhesion as well as surface films can be neglected. (iv) A closer examination of the deformation process at indentations and underneath wear tracks shows that the reactive force balancing the normal force between the two sliding surfaces originates at considerably larger distances from the interface than the reaction to the tangential traction. (v) Based on this insight, an expression for the coefficient of friction in the "basic" case is derived. This is found to predict decreasing values of the coefficient of friction with decreasing crystal symmetry and, hence, decreasing numbers of "easy" crystallographic glide systems. (vi) This expression for the coefficient of friction predicts a number of effects which appear to be consistent with observations, dependent on surface texture, surface hardness, and surface temperature. (vii) The conditions under which surface films may be neglected are more closely examined, together with some effects of surface platings. (viii) Delamination wear is found to follow necessarily whenever the flow stress of the material near the surface is a function of the cumulative strain. (ix) Expressions for the wear coefficient and for the incubation period preceding "steady-state" delamination wear are derived and compared with available data. (x) The subsurface shear strain distribution underneath surfaces exposed to "steady-state" sliding wear is derived for the case that the applied shear stress, due to the tangential tractions, is balanced by the local shear strength as raised by work-hardening. The result depends on the prevailing work-hardening law. It is shown that one well-investigated case is explained in this manner, using a work-hardening law that appears to be common in wire drawing. (xi) Dislocation cells underneath worn surfaces are shown to be quite similar to those found in drawn wire, and evidence is presented, indicating that these cells are in accord with theoretical predictions based on dislocation theory. (xii) While either a hard or soft, very thin surface layer may be present, it is unlikely to be due to any esoteric dislocation reactions. However it is important to realize that dislocation cell walls are mobile by nature. Therefore dislocation cells do not deform homologously with the material. Therefore, also, the dislocation cells may generate the appearance of recrystallization then in fact none took place.

Accession For	NTIS	DTIC	U.S. Govt.	J. Education
By	Distribution	Availability	Disposal	
A				

Unclassified

### Abstract

Using dislocation concepts, primarily as relevant to geometrical considerations, and other basic facts concerning plastic properties of crystalline materials, a number of qualitative and quantitative relationships in the area of friction and wear are developed:

- (i) The accepted model for friction and wear is expanded to include the micro-roughness which must necessarily arise at contact spots on account of inhomogeneities in elastic and plastic deformation.
- (ii) A simple formula is proposed to describe the conditions under which adhesion is important.
- (iii) The concept of the "basic" case is introduced, which is sliding wear between average-rough and average-clean surfaces, such that adhesion as well as surface films can be neglected.
- (iv) A closer examination of the deformation process at indentations and underneath wear tracks shows that the reactive force balancing the normal force between the two sliding surfaces originates at considerably larger distances from the interface than the reaction to the tangential traction.
- (v) Based on this insight, an expression for the coefficient of friction in the "basic" case is derived. This is found to predict decreasing values of the coefficient of friction with decreasing crystal symmetry and, hence, decreasing numbers of "easy" crystallographic glide systems.
- (vi) This expression for the coefficient of friction predicts a number of effects which appear to be consistent with observations, dependent on surface texture, surface hardness, and surface temperature.
- (vii) The conditions under which surface films may be neglected are more closely examined, together with some effects of surface platings.
- (viii) Delamination wear is found to follow necessarily whenever the flow stress of the material near the surface is a function of the cumulative strain.
- (ix) Expressions for the wear coefficient and for the incubation period preceding "steady-state" delamination wear are derived and compared with available data.
- (x) The subsurface shear strain distribution underneath surfaces exposed to "steady-state" sliding wear is derived for the case that the applied shear stress, due to the tangential tractions, is balanced by the local shear strength as raised by work hardening. The result depends on the prevailing work-hardening law. It is shown that one well-investigated case is explained in this manner, using a work-hardening law that appears to be common in wire drawing.
- (xi) Dislocation cells underneath worn surfaces are shown to be quite similar to those found in drawn wire, and evidence is presented indicating that these cells are in accord with theoretical predictions based on dislocation theory.
- (xii) While either a hard or soft, very thin surface layer may be present, it is unlikely to be due to any esoteric dislocation reactions. However, it is important to realize that dislocation cell walls are mobile by nature. Therefore dislocation cells do not deform homologously with the material. Therefore, also, the dislocation cells may generate the appearance of recrystallization when in fact none took place.

### Acknowledgements

This research was prompted by an invitation to deliver a lecture at the "Fundamentals of Friction and Wear of Materials" ASM Seminar, Pittsburgh, October 1980. This led the writer to delve much more deeply into one area of the major topic of her research contract, namely development of improved electrical brushes, than would otherwise have been the case. This was a most rewarding experience, and many thanks are due to a number of colleagues without whose advice and encouragement the task might well not have been accomplished. Thus particular thanks are due to D. A. Rigney for extending the invitation to participate in the Seminar and for providing key information and publications. Other colleagues have variously given advice, pointed out crucial prior research results, and/or have provided micrographs, among whom special thanks are due to L. D. Dyer, J. P. Hirth, L. K. Ives, K. R. Lawless, E. Rabinowicz, N. P. Suh, H. G. F. Wilsdorf and J. B. P. Williamson. Last but by no means least, I should like to express my sincere gratitude to Commander Harold P. Martin whose support and encouragement has been unfailing.

# Table of Contents

	Page
Abstract - - - - -	3
Acknowledgements - - - - -	4
Table of Contents - - - - -	5
List of Figures - - - - -	6
INTRODUCTION - - - - -	8
WHAT MAKES A CONTACT SPOT STRONG AND HOW ARE ASPERITIES MAINTAINED? -	8
MICRO-ROUGHNESS AND PERSISTENT ASPERITIES OF CONTACT SPOTS - -	28
ADHESION AND SURFACE ROUGHNESS - - - - -	35
THE NUMBER OF SLIP SYSTEMS AND THE COEFFICIENT OF FRICTION - -	39
EFFECTS OF SLIDING DISTANCE, SLIDING DIRECTION, AND BULK TEXTURE ON THE COEFFICIENT OF FRICTION - - -	55
THE ROLE OF SURFACE FILMS- - - - -	58
SOME THOUGHTS ON GEOMETRICAL EFFECTS, SURFACE STRESS/STRAIN DISTRIBUTION, WEAR AND DELAMINATION - -	62
THE EFFECT OF CHANGES IN SURFACE HARDNESS ON THE COEFFICIENT OF FRICTION - -	65
WEAR RATE AND "WEARING-IN" - - - - -	71
THE NEAR-SURFACE SHEAR STRAIN DISTRIBUTION AS DETERMINED FROM WORK HARDENING - - -	85
DISLOCATION BEHAVIOR AND MICROSTRUCTURES - - - - -	92
SUMMARY AND OUTLOOK - - - - -	103
References - - - - -	106
Distribution List - - - - -	110

List of Figures

<u>Figure No.</u>	<u>Subject</u>	<u>Page</u>
1	Schematic representation of contact spot models	9
2	Micrographs of grooving on wear tracks (Courtesy L. K. Ives)	12
3	"Hot Spot" being a persistent contact spot (After J. P. Metzger)	15
4	Displacement field of worn copper pin (After J. H. Dautzenberg)	17
5	Displacement field and hardness distribution under wear track of worn brass (After W. Hirst and J. K. Lancaster)	17
6	Indentation on (100) face of copper (Courtesy L. D. Dyer)	18
7	Pattern of indentations as in Fig. 6 etched to reveal dislocations (Courtesy of L. D. Dyer)	19
8	Etched section through crystal as in Fig. 6 to reveal dislocation distribution underneath the surface (Courtesy L. D. Dyer)	20
9	Calculated elastic stresses under indentation (After R. M. Davies)	22
10	Surface topography and microhardness about rolling track on (100) copper surface (Courtesy L. D. Dyer)	24
11	Indentation on (100) face of copper with micro-roughness (Courtesy L. D. Dyer)	27
12	Persistent roughness in deep indentation (After A. J. W. Moore)	31
13	Irregular surface distortion due to wear (After N. P. Suh)	40
14	Irregular distortion of abraded surface (Courtesy L. K. Ives)	40
15	Surface wear texture in fcc metals (After J. P. Hirth and D. A. Rigney)	51
16	Dependence of friction coefficient on load (After F. P. Bowden and D. Tabor)	52
17	Correlated values of film resistance and coefficient of friction for silver graphite brushes	57
18	Interfacial temperatures as a function of sliding speed (After N. Saka, A. M. Elieche and N. P. Suh)	66
19	Sizes of contact spots ("a-spots") as a function of current passed through them (After T. Tamai and K. Tsuchiya)	68
20	Interfacial hardnesses derived from Fig. 19 (After T. Tamai and K. Tsuchiya)	68

<u>Figure No.</u>	<u>Subject</u>	<u>Page</u>
21	Coefficient of friction as a function of sliding speed (After E. Rabinowicz)	70
22	Coefficient of friction as a function of speed for extremely high velocities (After F. P. Bowden and D. Tabor)	70
23	Independence of coefficient of friction on externally applied temperature (After E. Rabinowicz)	72
24	Quantitative interpretation of subsurface shear strain distribution in terms of local work hardening (Measurements and diagram after J. H. Dautzenberg and J. H. Zaat)	79
25	Wear and friction coefficients for silver graphite brushes on various materials (After E. Rabinowicz and P. Chan)	82
26	Dependence of wear rate on sliding speed for brass (After W. Hirst and J. K. Lancaster)	84
27	Dislocation cell structures in drawn iron wire (Courtesy G. Langford and M. Cohen)	94
28	Dislocation cell structure beneath wear track in copper (Courtesy L. K. Ives)	95
29	Recrystallized grains beneath wear track in copper (Courtesy L. K. Ives)	98
30	Dislocation cell structure in thin copper film after sliding a sapphire ball on it (Courtesy K. R. Lawless)	101
31	As Fig. 30 but after a light anneal (Courtesy K. R. Lawless)	101

## DISLOCATION CONCEPTS AND FRICTION AND WEAR

### Introduction

The area of friction and wear is so vast that any single treatment or model cannot explain all, or even the majority of, measurements and observations. Further, for most purposes it is highly unlikely that detailed dislocation mechanisms can throw much light on friction and wear, for the reason that the sizes or volumina involved, e.g. the size of the wear debris, the depth of the deformed surface layer, and the diameter of the typical contact spot, are very large compared to the individual dislocation. The value of dislocation theory in the present context will therefore mostly be in the light it sheds on materials properties and their effects on friction and wear. The following discussion is, correspondingly, not attempting to analyze specific dislocation motions or reactions but uses knowledge of materials properties, as known in connection with dislocation behavior, to extend understanding of friction and wear in what is considered to be the "basic" case. This is the case of dry sliding after repeated passes between two parallel surfaces, neither extremely rough nor smooth, whose nominal area of contact is much larger than the load-bearing area of contact, and in which the two contacting materials are homogeneous, have no unduly thick or strong surface layers, and undergo no crystallographic or chemical transformations.

### What Makes a Contact Spot Strong and How are Asperities Maintained?

Very commonly, friction and wear are considered in terms of two apparently contradictory models, indicated in Fig. 1. Fig. 1A exemplifies the model of the adhesion theory. According to Bowden and Tabor<sup>(1)</sup> this theory is ultimately founded on the work of T. Desaguliers in 1784. Its modern development was pioneered mainly by R. Holm<sup>(2)</sup> in connection with electrical contacts

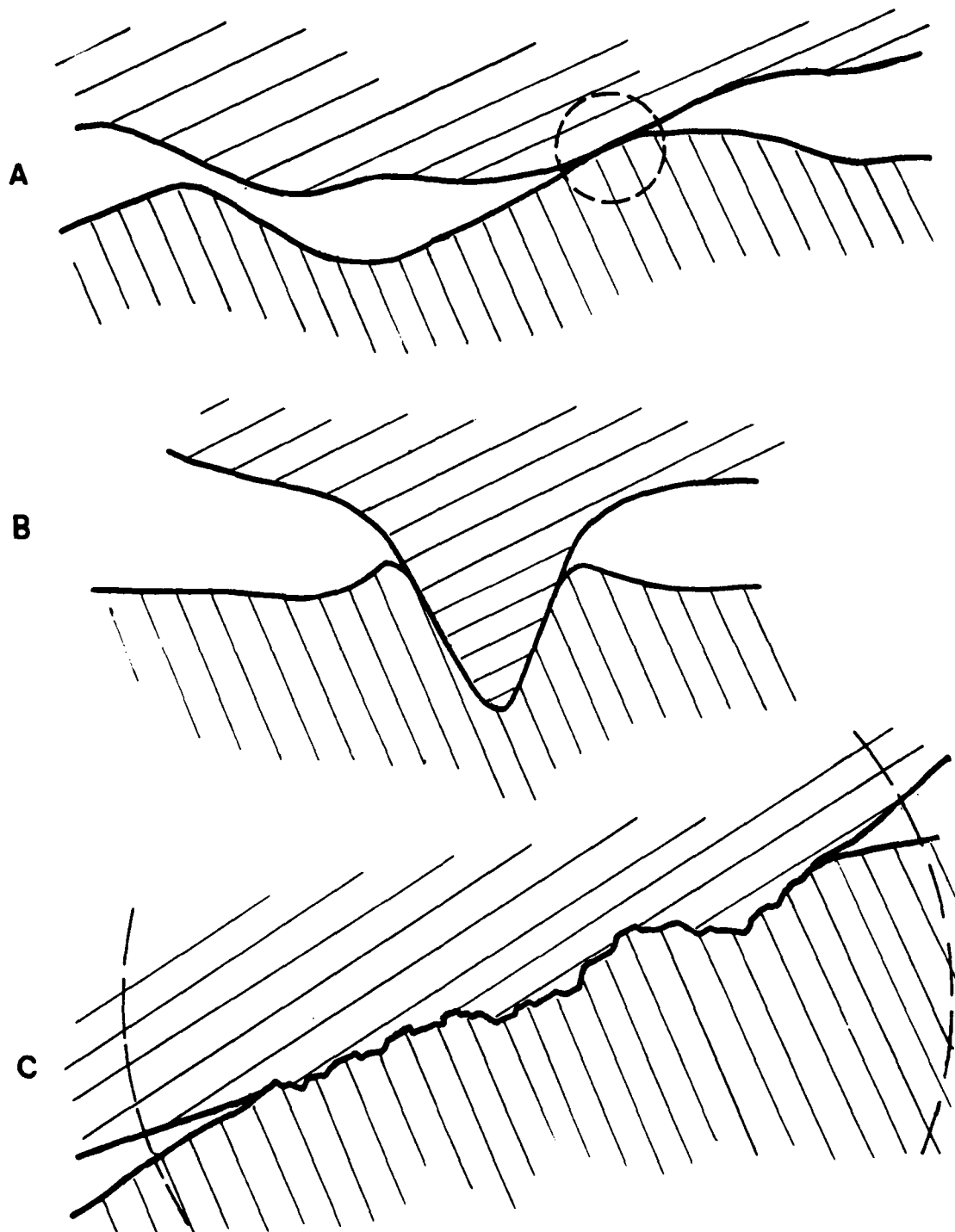


Fig. 1 Commonly accepted (A, B) and improved (C) models for friction and wear, based on adhesion (A) and on "plowing" of sharp asperities through the softer material (B), and (C) roughening of contact spots by micro-roughness generated through inhomogeneities of elastic and plastic deformation. A complete contact spot may consist of two or more interacting "hills". If so, (C) depicts one such hill rather than a complete contact spot. Also the micro-roughness is not believed to provide complete atomistic contact throughout, but more likely only over  $1/3$  to  $1/2$  of the area. Gap widths are almost certainly no more than a few hundred angstrom, and typically much less.

and by Bowden and Tabor as summarized in their books<sup>(3, 4)</sup>. In the adhesion theory of friction it is recognized that two sliding surfaces touch only at a number of separate contact spots which together amount to a small fraction of the geometrical contact area, as indicated in Fig. 1A. These contact spots are considered to be very strong, causing friction damage rather than permitting simple sliding of the two surfaces past each other, on the hypothesis that atomistic contact gives rise to adhesion, or local welding, stronger than the shear strength of the softer material underneath. This view has recently been vigorously criticized, especially by Bikerman<sup>(5)</sup> and, in regard to the wear mechanism, by N. P. Suh and coworkers<sup>(6)</sup>, after Rabinowicz<sup>(7)</sup>, although generally in favor of the theory, had already pointed out shortcomings of it: Most obviously, simply pressing or rubbing metals together does not give rise to sticking, as it would if the adhesion at contact spots was as general and strong as assumed in the adhesion theory of friction. If in fact the postulated strong adhesion of metals at their contact spots were to take place, metals could not be handled without some protective surface treatment, lest they stick together on mere contact much like cello tape.

On the plus side, it is true that cold welding (or frictional welding) is often observed. Indeed, it was its demonstration for the case of lead balls by Desaguliers, which originally launched the adhesion theory as outlined by Bowden and Tabor<sup>(1)</sup>. Further, the adhesion theory is effective in explaining the basic laws of friction. This is due to two fundamental assumptions of the theory. These are, firstly, that the total area of actual atomistic contact is proportional to the normal force between the two surfaces because, at the contact spots, plastic deformation of the softer of the two materials typically takes place to the point of saturation hardening; secondly,

that the adhesion or local welding between the two surfaces at the contact spots is always so strong that surface sliding is inhibited and, instead, shearing or fracture takes place in the subsurface layers, at least of the softer material. In this manner, the coefficient of friction is found independent of load as well as of apparent (overall geometric) area of contact and, within fairly wide limits, of roughness. With the further fact that the flow stress of crystalline materials tends to be little dependent on strain rate, the effective velocity independence of the coefficient of friction, again within fairly wide limits, is explained.

Fig. 1B, by contrast, is a model for the "ploughing" of asperities of the harder of the two materials through the softer. Indeed, it seems clear that some "ploughing", or perhaps better "grooving", takes place in friction, since wear tracks almost uniformly show fine grooves. Examples are shown in Fig. 2 due to L. K. Ives<sup>(8)</sup>. From this it may be seen that the asperities or particles which are generating the grooves are evidently rather long-lived, since the line pattern does not change significantly over the length of tracks shown in the micrographs. Specifically, the right part of Fig. 2 is included because it shows more clearly than the left part that the asperities or particles causing the grooves are on the micron size scale, at least in this example, and that the grooving is quite shallow for the most part.

The question which arises in this connection is how the asperities or particles responsible for this grooving are formed. Are they the same asperities which make contact spots of the type illustrated in Fig. 1A? To answer that question, one must try to evaluate the size of the average contact spot. This is not entirely straightforward because of uncertainty as to the number of contact spots which remains in spite of some superb research on the

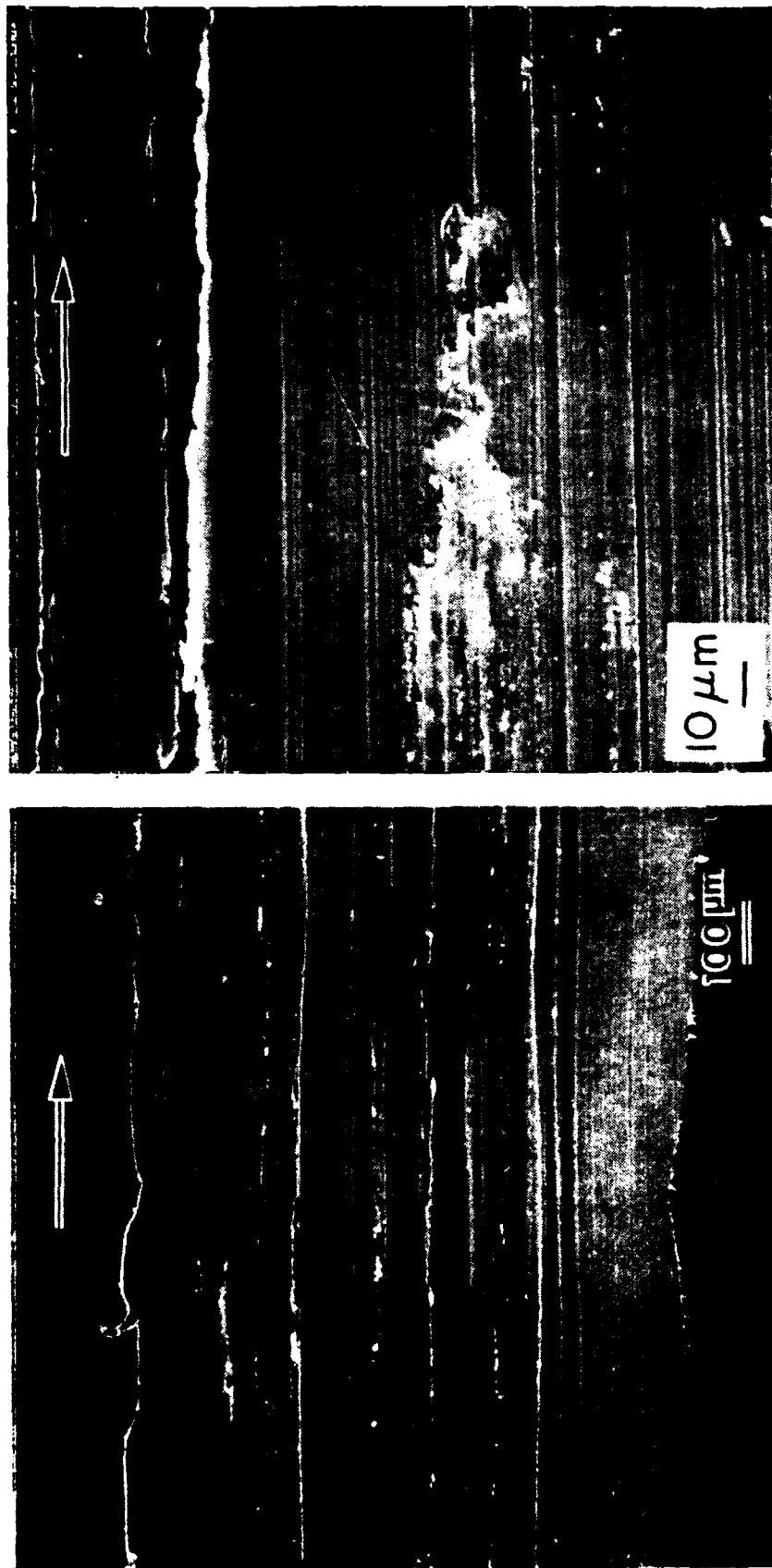


Fig. 2 Wear track on copper ring, tested under lubricated sliding condition, seen with two different magnifications as indicated. The grooving (which can be seen to consist of rather long scratches on the left part of the figure, and to be very shallow as seen on the right) is believed to be caused by micro-roughness of the kind indicated in Fig. 1C. While at actual contact spots, as in Fig. 1C, there is interlocking and relative rest between the two sides, grooving must occur at the sides of the contact spots and interacting "hills", and where surfaces are sufficiently separated to prevent locking but still within range of the highest asperities. The latter condition will routinely occur when contact spots of the kind in Fig. 1C are in the process of being released. "Grooving" is considered to contribute in the order of between 10% and 20% to the coefficient of friction, and only very little to wear. (Courtesy of L. K. Ives, ref. 8).

geometry of contacting surfaces (e.g. ref. 9-11). What, then, is the typical size of a contact spot? According to adhesion theory, and in accordance with much experimental evidence, the average load bearing area,  $A_b$  per contact spot, of altogether  $N$  contact spots between two surfaces pressed together with the force  $P$ , is

$$A_b \approx P/HN \approx \pi d^2/4 \quad (1)$$

if  $H$  designates the hardness of the softer of the two members. Much more will have to be said below about the "hardness" or "flow pressure",  $H$ , introduced here. At this point it is sufficient to assume that  $H$  is a fairly well defined materials constant and that eq. 1 is obeyed independent of the magnitudes of  $N$  and  $P$ .

For the majority of cases of interest, in practice as well as in the laboratory,  $P$  is in the order of 3 kg weight within, say, two orders of magnitude. Next,  $N$  is almost never a large number. For electrically conducting contact spots, Holm<sup>(12)</sup> found values of  $N$  up to 18 in a particular run of experiments, while recently  $N$  has been given by McNab<sup>(13)</sup> as between 10 and 50; and direct observations by means of infra-red microscopy by H. Kongsjorden, J. Kulsetås and J. Sletbak<sup>(14)</sup> revealed several separate temperature peaks over an apparent contact area of a few square millimeters. In fact, quite commonly  $N$  is still smaller than the quoted values, namely three, or two, or even one. The reason for this is thermal instability, a topic that is the subject of increasingly intense investigation, largely pioneered by Burton and co-workers<sup>(15)</sup>. Namely, frictional heat raises the temperature of contact spots and their surroundings, causing them to bulge out, thereby increasing the frictional force, with the resultant further rise in temperature. This process acts more powerfully

on larger than on smaller contact spots, eliminating the latter in favor of the former. Subsequent wear either causes a slow migration of these contact spots, or reduces the local stress at the one or several operative contact spots below a critical level when other spots take over. The result, by theory as well as by observation<sup>(16, 17)</sup> are the discussed one or only a very few contact spots per sliding interface, the so-called "hot spots", at least beyond some critical loads and speeds. Fig. 3 gives an example due to J. P. Netzel<sup>(17)</sup>.

To obtain some very rough impression of the size of a typical contact spot let, then,  $N$  be ten, and assume  $H = 50 \text{ kg}^*/\text{mm}^2$  at a load of three kilogram weight, i.e.  $P = 3 \text{ kg}^*$ . With these fairly typical numbers, eq. 1 yields  $A_b = 6 \times 10^{-3} \text{ mm}^2$  or  $d = 90 \text{ }\mu\text{m}$ . Similarly, in the experiments by Holm referred to above,  $d$  ranged between 70 and 126 microns. Such numbers are evidently much larger than the width of the average plowing asperity inferred from Fig. 2. In fact, considering eq. 1 it will be seen that, with  $N \leq 50$  and with  $H$  typically  $\leq 100 \text{ kg}^*/\text{mm}^2$ , contact spots of the size of the grooving in Fig. 2 could only arise with loads of several grams or less, whereas also for the case of Fig. 2 the computed contact spot diameter is about 100 microns.

Another problem, besides size considerations, with the model of a "ploughing" asperity is that in ploughing, such as in a farm field, the ploughed material is cut and heaped up on either side of the furrow and is not transported towards the end of the furrow. This kind of deformation is indeed often observed alongside grooves and furrows at the appropriate small scale. However, severe dragging in the direction of relative motion, to a depth much larger than the grooving, is very commonly observed in the subsurface regions, at least in the softer member. Figs. 4 and 5 give examples, due to



Fig. 3 "Hot spot", representing one persistent contact spot which is possibly composed of several interacting "hills", in the mating ring of a face seal after 45 minutes of operation. (Courtesy of J. P. Netzel, ref. 17).

Dautzenberg<sup>(18)</sup> and Hirst and Lancaster<sup>(19)</sup>, respectively. Thus we see that experimental evidence regarding subsurface strain distribution as given in Figs. 4 and 5 supports the adhesive model of friction according to Fig. 1A and not the ploughing model of Fig. 1B, whereas the topography of the wear track as shown in Fig. 2 supports the ploughing model, albeit with asperities on a much smaller scale than the size of the contact spots.

At this point a more detailed consideration of the deformation processes, in terms of dislocations, becomes useful: As seen, the strain distribution under wear tracks, e.g. as illustrated in Figs. 4 and 5, extends to a distance comparable to the estimated diameter of the average contact spot. This is not only in agreement with stress analysis such as performed by Davies<sup>(20)</sup> and Jahanmir and Suh<sup>(21)</sup>, but also with observations by L. D. Dyer<sup>(22)</sup> of strains and dislocation distributions about indentations (modelling the asperities at contact spots) in highly perfect single crystals. Fig. 6 due to Dyer shows the shape of an indentation made by a sapphire ball on the cube face of a copper single crystal, and Figs. 7 and 8 by Dyer show the resulting dislocation distribution. Admittedly, in this particularly soft material with its very low yield stress the indentation, as well as the zone through which dislocations spread, were larger for the same load than in an ordinary metal. Yet, the geometry is believed to be well represented, because the ratio of these two sizes is presumably largely independent of yield stress and, hence, choice of material, provided that the number of available slip systems is adequately large.

The point that in Fig. 8 the most intense dislocation concentration (indicative of the highest operative stress and hardening) is found well below the surface, in line with continuums theory<sup>(20, 21)</sup>, is gratifying.



Fig. 4 The displacement field of a worn copper pin, made visible by placing an aluminum foil between the two halves of the pin which was cut perpendicular to the sliding direction and pressed together before the wear test against SAE 1045 steel. 4 kg\* load. (Courtesy of J. H. Dautzenberg, ref. 18).

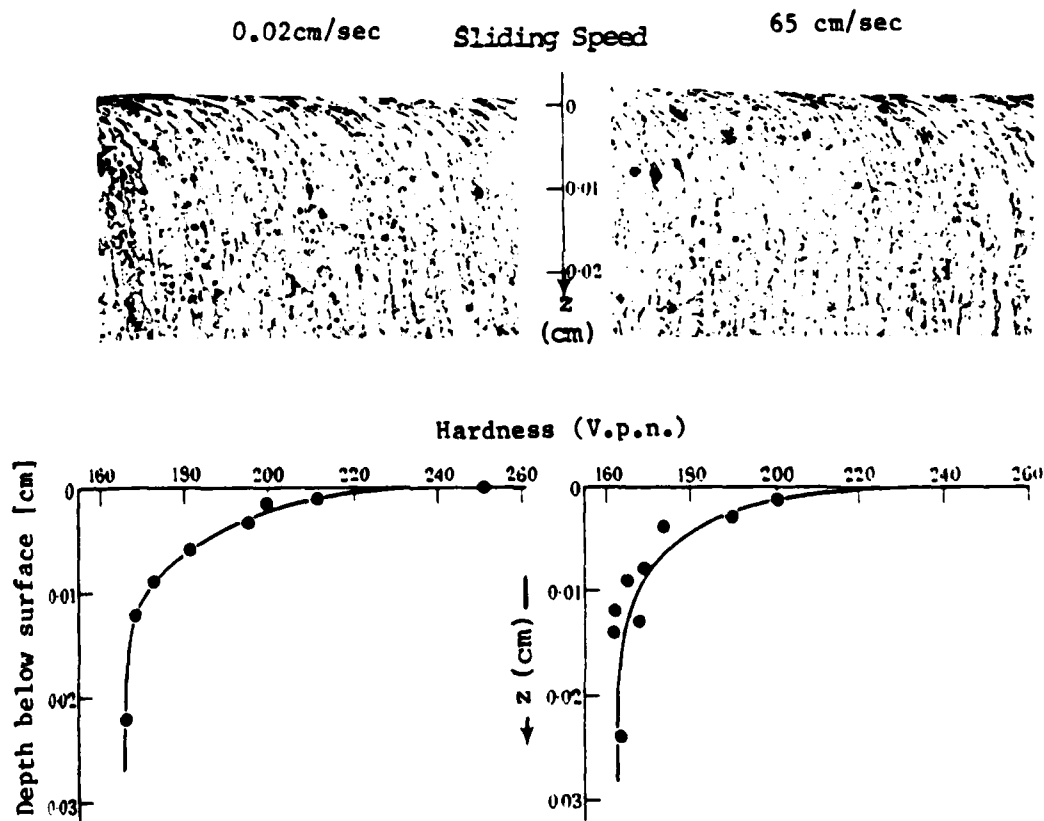


Fig. 5 Microstructure under wear track of 60/40 brass pins (top) and correlated hardness measurements (bottom) for two different sliding speeds under otherwise the same conditions. Note that the wear layer is roughly 120  $\mu\text{m}$  thick, which is considered to be comparable to the diameter of the average contact spot in this case, and at the same time to be a fairly representative value for contact spot diameters. Note that the thickness of the wear fragments was only  $\sim 3 \mu\text{m}$ . (After W. Hirst and J. K. Lancaster, ref. 19).

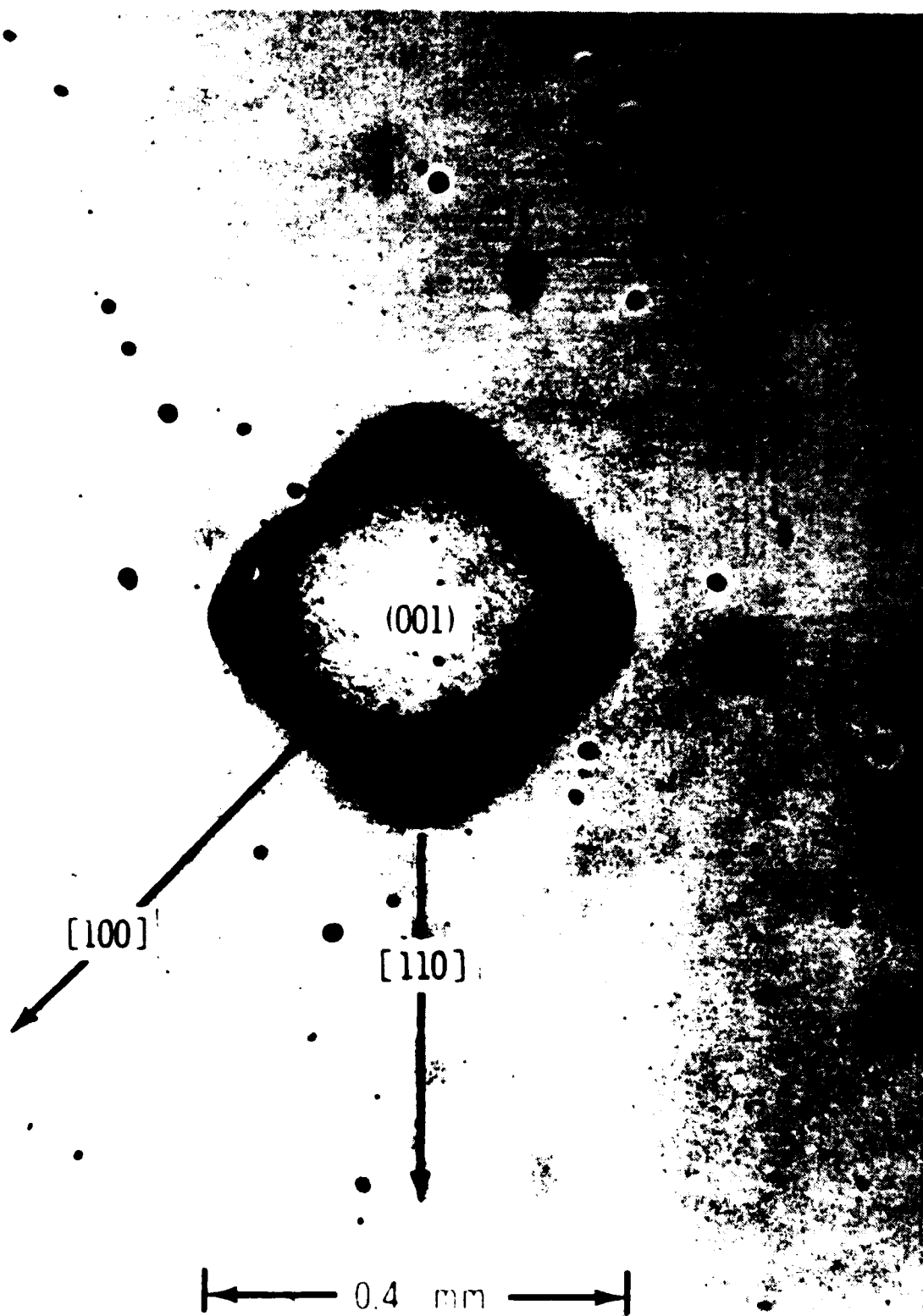


Fig. 6 Indentation made by a  $1/4"$  (6.35 mm) polished sapphire ball on the highly polished cube face of an especially perfect conner crystal, under 1 kg\* load. (Courtesy of L. D. Dyer, ref. 22).

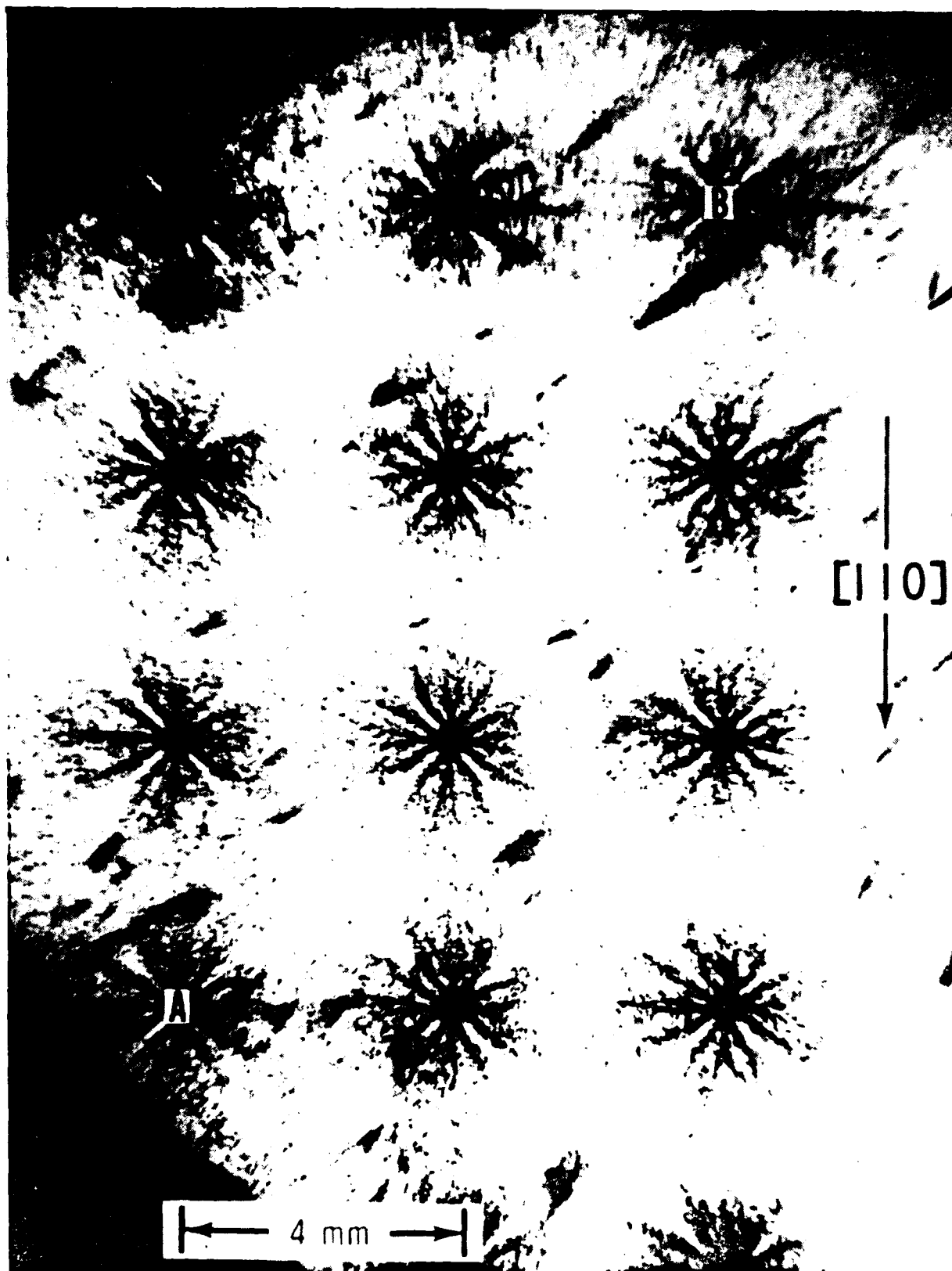


Fig. 7 Regularly arranged indentations of the kind shown in Fig. 6, made on the same crystal and etched to reveal dislocation intersections with the surface. (Courtesy of L. D. Dyer, ref. 22).

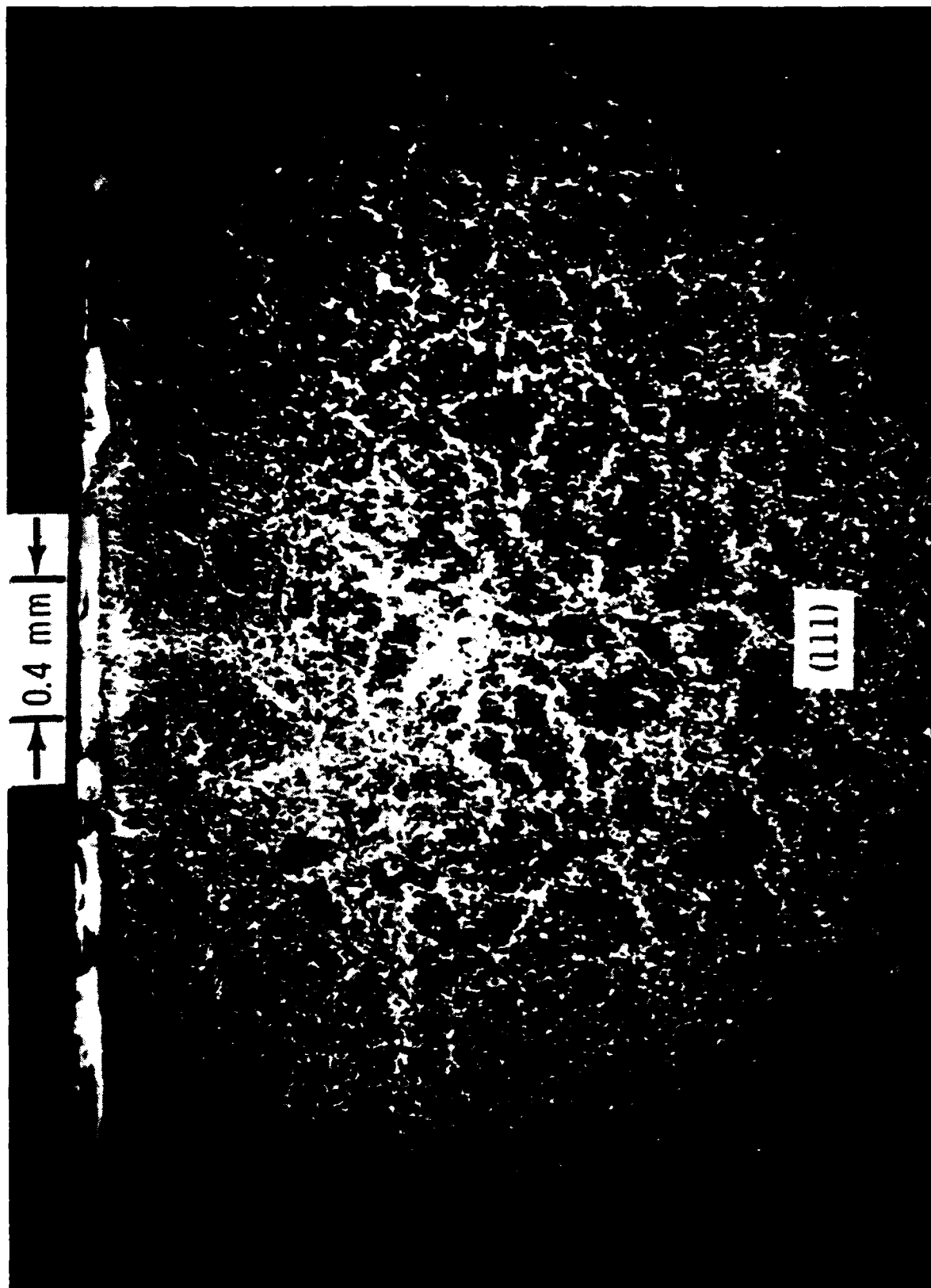


Fig. 8 Dislocation distribution beneath an indentation such as in Figs. 6 and 7, revealed by etching a polished section parallel to a  $\{111\}$  plane. It passes not through the center of the indentation but through the center of the dislocation concentration underneath, thereby somewhat underrepresenting the dislocation density directly at the surface at the indentation. Note also that, due to the obliqueness of the cut, vertical distances are expanded by about 20%. (Courtesy of L. D. Dyer, ref. 22).

Indeed, there is acceptable agreement between the observed dislocation distribution in Fig. 8 and stress maps obtained from theoretical stress analysis, as will be seen by comparison of Fig. 8 with Fig. 9. Clearly, stress analysis and observations on dislocations, both yield the result that the highest shear stresses and shear strains under an indenter or asperity occur somewhat below the surface and extend for a distance comparable with the size of the indentation. In turn, the range of the strong surface shear strain (Figs. 4 and 5) is of the same magnitude as the size of the contact spots, namely

$$d \approx \sqrt{A_b} \approx \sqrt{P/HN} \approx \sqrt{(P/H)/3} \quad (2)$$

found to be in the neighborhood of 0.1 mm in typical cases as explained. Therefore, there can be little doubt left that in friction and wear the surface layers are dragged along by strongly adhering contact spots, and that the asperities responsible for the grooving are of a quite different kind and of a much smaller size.

In order to obtain a possible answer as to the nature of the smaller asperities, consider yet another aspect of the deformation processes at contact spots of metals. To begin with, assume that, although mildly curved so as to produce localized plastically deformed contact spots, the two surfaces are ideally smooth. An examination of the two surfaces directly after pressing them together without sliding, might show that the harder of the two materials had retained a smooth surface. The same could, however, not possibly be true for the softer one, because there is absolutely no deformation process in crystalline materials which does not cause inhomogeneous distortions: if both objects had been single crystals, crystallographic slip would have caused slip lines and the corresponding surface roughening. Had

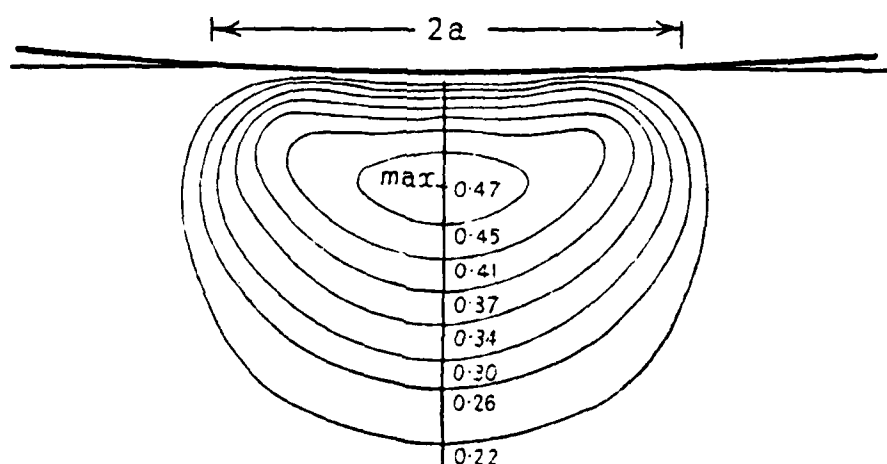


Fig. 9 Elastic distortion of a flat surface by an indenting sphere, and contour lines showing the values of the maximum shear stresses beneath the (elastic) indentation in units of the mean pressure exerted by the ball over the contacting area, according to D. Tabor (Fig. 24 of ref. 31), based on R. M. Davies, ref. 20.

there been twinning, this would have caused even greater roughening. Had there been grain boundaries in the softer material, this would further have added roughening due to differences in the hardness of the different grains depending on orientation. Fig. 10, also due to Dyer<sup>(23)</sup>, shows this anisotropy by inference, plus one perhaps yet more unexpected, namely that even for the same surface, (rolling) friction and hardness depend on the direction of relative motion. Correspondingly, different directions of relative motion give rise to different slip line patterns and different surface roughness, and incidentally also different coefficients of friction.

To all of those effects one must add elastic inhomogeneity: Specifically, elastic anisotropy in the softer material means that, depending on orientation, the elastic part of the deformation differs from crystallite to crystallite, along with peak hardness. As a result, the crystallites of the harder material are subject to different elastic strains, and hence reactive pressures, from one to the next crystallite of the softer partner also from this cause, besides responding differently even to the same pressure on account of their own elastic anisotropy. Thus the elastic compression in both materials differs from grain to grain on their own side, as well as from grain to grain on the opposite side, which differences translate into the corresponding variations of the plastic, permanent strain in the softer material. In addition, compatibility stresses at the grain boundaries must necessarily cause further rather abrupt changes in the plastic deformation of the softer material from one side to the other of any grain boundary, in both of the opposing surfaces.

Consider further that real materials are not ideally homogeneous, at best, and that they often contain second and third phases of greatly different hardness and elasticity. Also to be considered is the effect of entrapped



extraneous particles such as dust. Last, not least, if either or both of the materials had been covered by a brittle surface film, this might have cracked in a type of crazing pattern, with the correspondingly varied abrupt changes of the normal pressure transmitted across the interface and the plastic deformation in response thereto. Altogether, then, compressing two surfaces together must automatically and necessarily lead to micro-roughness. At the least, the depth of this micro-roughness must be on the scale of slip lines, and of the differences in plastic deformation normal to the interface that are complementary to the differences in the elastic deformation of grains. Note that such micro-roughness can never be rubbed off or otherwise vanish during wear, since it reestablishes itself in ever different configurations as wear occurs, and as through sliding the local conditions change continuously.

The depth of slip lines is very variable. It depends on strain, surface orientation, material, surface films, and loading conditions, including strain rate and temperature. Typically, the scale of roughness from this cause will be in the one hundred to one or a few thousand angstrom range. To estimate the roughness due to elastic anisotropy, let Young's modulus,  $E$ , vary by the amount of  $\Delta E$  as a function of orientation. The elastic compression of layer thickness  $d$  under pressure  $H$  is  $h = Hd/E$ . Therefore,  $\Delta h$ , the height difference resulting from the elastic deformation of a layer thickness  $d$  under compressive stress  $H$  at elastic anisotropy  $\Delta E/E$ , is given by

$$\Delta h \approx d(H/E)(\Delta E/E), \quad (3)$$

provided the grains are of a size larger than, or comparable to,  $d$ . Taking  $H/E \approx 5 \times 10^{-3}$ ,  $\Delta E/E \approx 0.2$ , and  $d \approx 0.1$  mm, as fairly typical numbers, one thus obtains  $\Delta h \approx 0.1$   $\mu$ m from this source. Note that this is just about the

scale of the roughness which appears to have caused the grooving in Fig. 2.

That micro-roughness is indeed generated at plastically deformed contacts, even if between two initially quite smooth surfaces free of grain boundaries, is directly documented by Fig. 11. This micrograph compares to Fig. 6 but was obtained at a much smaller load (namely 20 g\*) and using interference contrast to make slightest surface roughness visible. In Fig. 11, traces of slip lines can be seen in the indentation, plus small hillocks which might be due to materials inhomogeneities, or perhaps entrapped dust.

In light of the above considerations and experimental evidence, then, it seems certain that micro-roughness must be a ubiquitous feature at all contact spots. This conclusion permits a harmonious synthesis of the models in Figs. 1A and 1B; namely, the theoretical model for friction and wear ought to be modified by including in it the discussed micro-roughness, as shown in Fig. 1C. With this modification, the origin of the strength of the contact spots, and the reason why the subsurface material below the contact spots shears, in preference to simple sliding along the surfaces, is clarified.

The suggestion that surface roughness may lead to interlocking at contact spots is not new but, rather, goes back ultimately to Coulomb (1736-1806). As outlined by Bowden and Tabor<sup>(1)</sup>, Coulomb "recognized that adhesion might play some part in friction (but) rejected it as the main cause. He felt friction was due to the role of surface roughness..." -- all of which is entirely the standpoint developed above. Coulomb went on to consider the surface roughness at contact spots as if composed of ramps inclined, say, at an angle  $\phi$  to the macroscopic interface whence, for uphill sliding,  $\mu = \tan \phi$ . This notion of Coulomb's was criticized by John Leslie<sup>(1)</sup> in 1804 on the grounds that there was as much downhill as uphill sliding, and that there could be no net effect

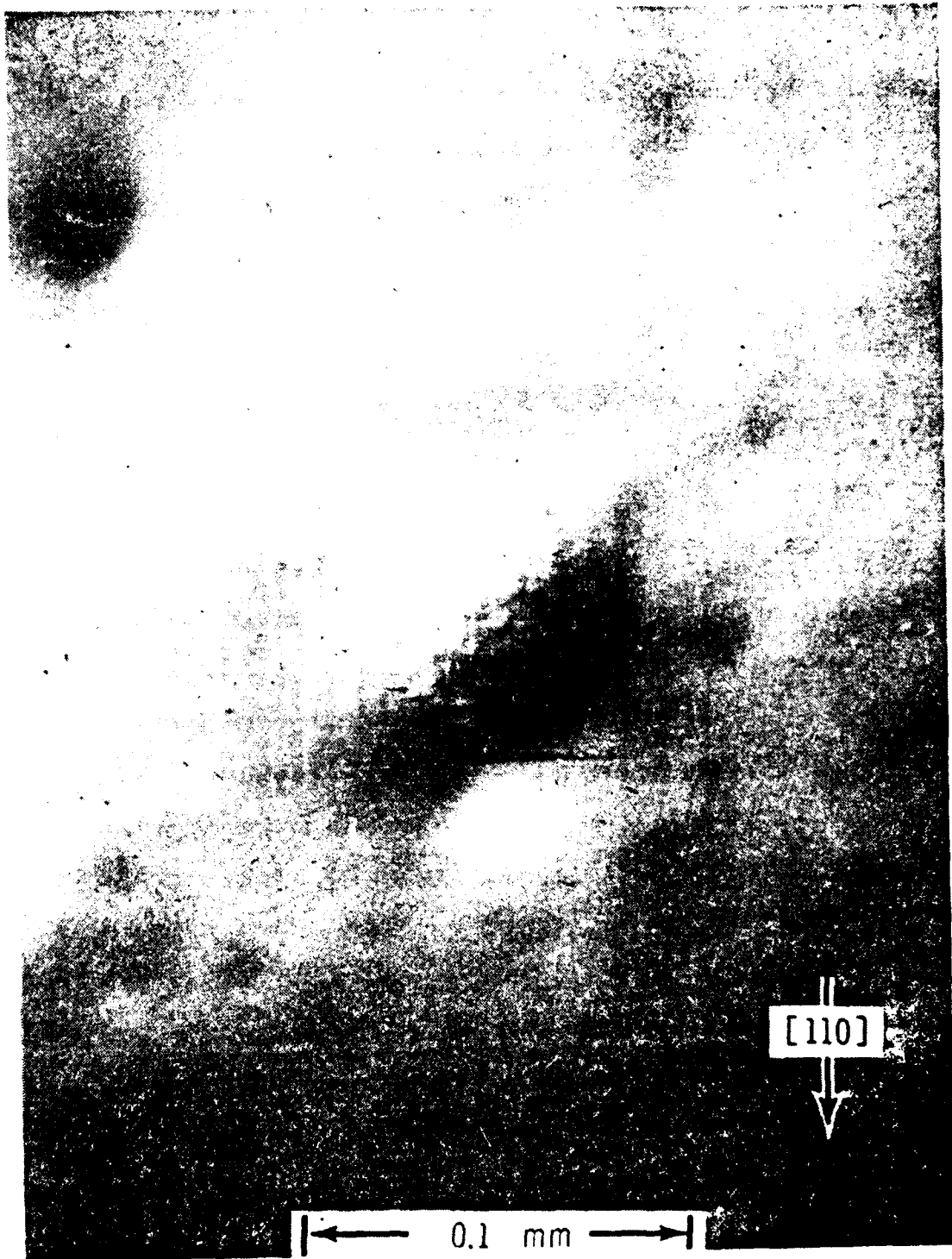


Fig. 11 As Fig. 6 but for a 20  $\alpha^*$  load and using interference contrast to reveal finest details in surface topography. Note the micro-roughness in the indentation, caused partly by slip lines, and partly due to other causes, including perhaps minute surface contamination or irregularities in the unseen oxide layer. (Courtesy of L. D. Dyer, ref. 22).

on the basis of Coulomb's mechanism on  $\mu$  for that reason. The approach in this paper differs from Coulomb's, in that the present model is based on the contention that interlocking by micro-roughness prevents relative motion, except via plastic deformation in the surface layer, at least over the area of the contact spots. This model, in turn, resembles the hypothesis put forth by Leslie in 1804<sup>(1)</sup>, it seems.

#### Micro-Roughness and Persistent Asperities of Contact Spots

The application of the model of Fig. 1C does not mean that local welding and/or noticeable adhesion does not occur at all, or is restricted to very clean conditions. For example, the cracking of brittle surface films must expose fresh surfaces at the contact spot interface. If that happens among materials of similar hardness, true adhesion can occur where film cracks on the two sides intersect, provided that they are wide enough for the underlying material to touch, perhaps after squeezing through the cracks by means of plastic flow. According to J. B. P. Williamson<sup>(24)</sup> that latter effect can be microscopically verified for two pieces of aluminum after pressing them together; much the same effect was earlier suggested by Whitehead<sup>(25)</sup>. Also, clean surfaces are continuously exposed in the course of wear, and these are capable of adhesion, especially at high pressures which have the effect of relatively increasing contact area to geometrical area and thus retarding recontamination. At any rate, whenever and to whichever degree adhesion and/or welding arise, they supplement the mechanical locking due to surface roughness and, if strong, they can be dominant and cause the corresponding effects.

Regardless of the relative strength of adhesion, (provided it is not dominant, a point to which we shall return later) the achievements of the adhesive theory of wear remain intact by the use of the model of Fig. 1C

since the essential assumptions remain unchanged: Namely, even more than in the unmodified adhesion theory, the typical load-bearing spot is not subject to sliding between the surfaces but deforms and/or shifts through subsurface plastic deformation. Secondly, as before, the total load-bearing area between the two surfaces remains to be (nearly) proportional to the normal force between them, subject to the limitations that the load be large enough to cause adequate local plastic deformation and small enough that only a minor fraction of the geometrical surface is in load-bearing contact.

The above statement that with and without micro-roughness the contact area is proportional to the load, and the more detailed properties of contact spots, deserve some elaboration. To begin with, it was shown by Archard<sup>(26)</sup> and Greenwood and Williamson<sup>(9)</sup> that, quite commonly, for large  $N$  a proportionality between  $NA_b$  and  $P$  comparable to eq. 1 may be expected even though the contact spots are not plastically deformed, whereas for a single asperity in elastic loading  $A_b$  is proportional to  $P^{2/3}$  according to the Hertzian solution<sup>(27)</sup>. This was found to be true especially when smaller protruberances were located on individual asperities. It would thus be expected to be true also for the model of Fig. 1C. Further,  $N$  was found to be proportional to  $P$  and, for Gaussian distributions,  $A_b$  to be independent of load.

Furthermore, micro-roughness on asperities has received repeated attention and Fig. 1C has to be interpreted in light of preceding work. Specifically, Fig. 1C is not meant to imply that microscopic contact is complete over all of the micro-roughness features indicated in Fig. 1C. From the viewpoint of materials science this is clear, assuming a very thin or no surface film, because of the inability of glide deformation along slip lines to produce smoothness, or true conformity to an opposing surface, on a scale less than

the distance between, and depth of glide on, active slip lines. While load is applied, elastic deformation will cause better conformity than plastic deformation alone can achieve. However, as will be discussed with a somewhat different viewpoint in connection with eqs. 4 to 9, a local pressure  $H$ , as exists at a contact spot, will not even out surface undulations beyond an angle of  $\sim 2H/\pi E$ . Assuming  $H/E \approx 5 \times 10^{-3}$  as before, this means that only undulations equal to, or less than, about  $0.2^\circ$  will be obliterated, which will be a small minority.

If, then, micro-roughness asperities due to inhomogeneous deformation are superimposed on the contact asperities, the considerations of Pullen and Williamson<sup>(11)</sup> apply. Their theory showed that peaks of interacting asperities on an indented region are flattened to the point that actual contact is close to 50%, provided that the surface and subsurface have the same hardness. That theory explains the intuitively most surprising persistence of roughness in macroscopic ball indentations that was first convincingly documented by A. J. W. Moore's<sup>(28)</sup> classical paper, as seen in Fig. 12.

Moore<sup>(28)</sup> had suggested that the hills in macroscopic indentations were persistent on account of preferential workhardening. Quite in line with our own preceding argument Moore realized that the indentation hardness controlling the compressing of the hills is that at a distance of their diameter below the surface, while the macro indentation conforms to the hardness at a distance of the macro indentation's diameter below the surface, more or less. Yet, although such hardness differences will be real enough, they are not the major reason for the persistence of hills in indentations, as was shown by Williamson and Hunt<sup>(10)</sup>. Rather, according to the theory and experiments by Pullen and Williamson<sup>(11)</sup>, flattening of hilltops is compensated by simultaneous rising of the valleys in the surface profile. This accounts for the volume displaced, and causes equilibrium to be established when the

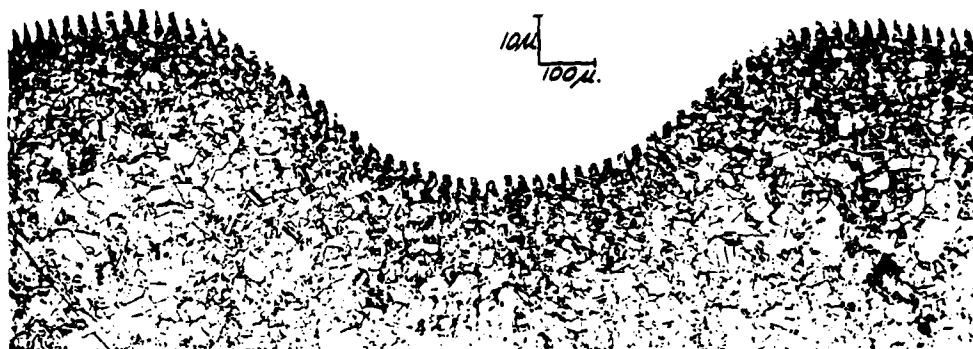


Fig. 12 Taper section of a deep indentation in annealed copper that had had a grooved surface made via turning on a lathe. Note the persistence of the "hills" in the indentation. However, it was noted that these hills were soon obliterated through sliding wear at the same load. (After A. J. W. Moore, ref. 28).

local pressure at the flattened hilltops is twice the average contact pressure over the indentation, while real contact occurs over only one half the area of the indentation, provided, that is, if the hardness is the same everywhere. When the hardness at the surface is  $H_s$  as compared to the bulk hardness  $H_b$ , Pullen and Williamson<sup>(11)</sup> find that the fraction of surface making real contact is  $H_b / (H_b + H_s)$  which reduces to  $\frac{1}{2}$  for  $H_b = H_s$ .

Pullen and Williamson<sup>(11)</sup> also consider the possible existence of a micro-roughness on the flattened hilltops as follows (ref. 11 p. 170): "if a large number of discrete micro-asperities exist on each asperity then in principle these also should act cooperatively and it can readily be shown that the degree of contact within the "real" contact area (now the nominal contact area of the micro-asperity population) would be two thirds." - assuming constant hardness throughout, that is.

This latter speculation was quite likely prompted by a very fine roughness on the flattened hilltops, in the order of, say,  $0.3 \mu\text{m}$ , visible on the surface profile tracings published by Pullen and Williamson<sup>(11)</sup> and Williamson and Hunt<sup>(10)</sup>. It is this which is here identified as the micro-roughness considered in this paper and indicated in Fig. 1C. The hills in the indentations may or may not have a true parallel for our present purposes. That uncertainty arises because the experiments in refs. 10 and 11 were conducted at pressures above the hardness of the specimen before the indentations or tests were made. Thus one might identify the hills with the contact spots during friction and wear, except that they are non-interacting in that case. On the other hand, it is widely believed that at low pressure the contact spots occur in clusters, with Pullen and Williamson<sup>(11)</sup> concluding: "Thus even at light loads when the contact spots occupy only a small fraction of the overall contact area they cannot, for most practical surfaces, be treated

as independent. As in local indentations, the real area of contact is not  $W/P$  as predicted by the classical theory but just half this; and the real pressure is not  $P$  but  $2P$ ."\*

In the further discussion in the present paper, it will be argued that the surface shearing deformation takes place below the level of the valleys in the micro-roughness or the valleys between the clusters of contact spots, as the case may be. The reason for this is that no systematic shear deformation is possible above that level. Therefore, the results of Pullen and Williamson do not affect eq. 1, provided  $A_b$  is taken to be the (average) area over which correlated hills and micro-asperities make contact with the opposing member, while  $N$  is the (average) number of spots at which systematic shear takes place at any one moment. A "contact spot" will therefore mean that local region over which interacting contact spots are distributed and participate in what is in effect a single larger indentation.  $A_b$  will be the average area of such regions and  $N$  their average number.

The above details may be less important for wear than might initially be thought because the persistence of hills and valleys observed by Moore<sup>(28)</sup>, which triggered the subsequent work by Williamson and coworkers<sup>(10, 11)</sup>, is typical for stationary contacts only. In relative sliding the hills are rapidly obliterated, but it appears that the micro-roughness is preserved (see ref. 28 p. 237 and Figs. 11 and 12). Even so, it is possible, if not probable, that on average there is more than one hill per contact spot also during sliding.

Having thus clarified the meaning of  $A_b$  and  $N$  as used throughout this paper, a similar clarification is needed in regard to the hardness,  $H$ . Indeed, this is a thornier problem, in spite of the fact that it is usually agreed among researchers that hardness is a materials property which, in wear, may be

---

\*Footnote: The symbols  $W$  and  $P$  in the above quote correspond to  $P$  and  $H$ , respectively, in this paper.

assumed to be independent of the load, the number of contact spots, and their shape. One particular difficulty encountered for our present purposes is that the hardness (defined as the "Meyer hardness" see ref. 29, for example, namely  $H = P/NA_p$  with  $A_p$  the projected area of the indentation as in eq. 1) depends on the relative depth of indentation. Measured values of  $H$ , obtained from single ball indentations, rise rapidly from zero to a kind of saturation value while the ratio of depth of indentation to ball radius rises from zero to 3%<sup>(30-33)</sup>. This initial rise of hardness with increasing depth of indentation coincides with the stress range before all requisite slip systems are activated. Beyond this range, the hardness is equal to  $2.8 \sigma_y$ <sup>(30, 31)</sup> or  $H \approx 3 \sigma_y$ , if  $\sigma_y$  is the yield stress in tension (say, the stress of 0.2% plastic strain), more or less. However, the plastic deformation made by the ball indenter (and equivalently by the harder side meeting an asperity on the softer) workhardens the material. As a consequence the measured value of  $H$  continues to rise.

Tabor<sup>(30, 31)</sup> has shown that the measured hardness approximates the hardness which the material would have if it were subjected to a tensile strain of  $\epsilon = 0.1 d/r$  beyond the existing state, wherein  $d$  is the diameter of the indentation and  $r$  is the radius of the indenting ball. It is therefore possible to infer the tensile stress-tensile strain curve, i.e.  $\sigma(\epsilon)$ , of an annealed material from hardness measurements made with different ball sizes and loads, substituting  $2.8 H$  for  $\sigma(\epsilon)$  and  $0.1 d/r$  for  $\epsilon$ .

Translating this result into the conditions in sliding friction, one might thus say that  $H$  equals  $2.8 \sigma_y^*$ , where  $\sigma_y^*$  is the yield stress of the material (at a distance  $\sqrt{A_p}$  below the surface) after it has been work hardened beyond its original state as if by a tensile strain of  $0.1\sqrt{A_p}/r$ .

As a further complication,  $H$  is somewhat rate dependent, increasing with decreasing time of indentation. This effect is strong for soft materials, but for rather hard materials the dynamic hardness is practically constant<sup>(20, 30)</sup> and is equal to (or very close to)  $2.8 \sigma_y^*$  as defined above.

#### Adhesion and Surface Roughness

About the rim of any contact spot an annular region exists in which the opposing surfaces are separated by only a very small gap width<sup>(34)</sup>. In Fig. 1C, for example, the region at issue is that where the two surfaces include a small angle, just inside of the circle. Electric tunneling in that annular zone, believed to span a gap width in the order of 5 angstroms, has lately been investigated<sup>(35, 36)</sup>. Similarly one must expect adhesive forces of interaction to act across that gap. The extent of that annular zone, relative to the load bearing area  $A_b$ , increases with the number of contact spots and decreases with increasing load. Above all, it is a strong function of surface smoothness, increasing with decreasing surface roughness: As the load per contact spot decreases, so that the individual contact spots shrink in size and the surface distortion due to local plastic deformation decreases, so, evidently, the annular gap up to some fixed distance of separation increases in relative area. Similarly, decreasing the pre-existent surface curvature causes a size increase in the discussed annular zone.

One may make a very rough estimate of the strength of the adhesive forces across the annular gap as follows: If the total interfacial energy of the two sides is reduced by  $\Delta\gamma$  when they are in atomistic contact, as compared to their being separated by a distance  $s$  equal to the range of the adhesive forces, then the average attractive stress between the two sides at distance  $s$  is

$$p_\gamma \approx \Delta\gamma/s = \Delta\gamma/nb, \quad (4)$$

expressing  $s$  as a multiple of  $b$ , the atomic diameter. Presumably, the range of adhesive forces is a few or several angstroms, so that  $n = 2$  appears to be a reasonable estimate. Now, in a material of elastic modulus  $E$ , a sine wave of displacement

$$u = A \sin \frac{2\pi}{\lambda} x \quad (5)$$

is elastically flattened by a pressure<sup>(16)</sup>

$$p_A = \pi EA/\lambda \quad (6)$$

From equations 4 and 5 one may find the maximum surface waviness such that it would be flattened by adhesive forces and, hence, give rise to complete contact between the two surfaces. In this, it is helpful to employ a rough empirical relationship between the surface tension  $\gamma$ , the atomic diameter  $b$ , and Young's modulus  $E$ , namely

$$\gamma \approx Eb/20. \quad (7)$$

The relative change of total surface energy may therefore be written

$$\Delta\gamma/2\gamma \approx 10\Delta\gamma/Eb, \quad (8)$$

assuming that the surface energy and elastic constants are similar on the two sides.

From equating the two pressures,  $p_A$  and  $p_Y$ , and using eq. 8, one finds the maximum value of the average angle of surface inclination due to roughness such that adhesive forces will establish complete atomistic contact over the surface,

$$(2A/\lambda)_{crit} \approx \theta_{crit} \approx (\Delta\gamma/\gamma)/10\pi n. \quad (9)$$

With  $n = 2$ , as introduced above, and  $\Delta\gamma/\gamma \leq 1$ , it correspondingly follows that very strong adhesive effects must arise for surface waviness with average surface inclinations between the two surfaces smaller than, or about equal to,

$$\theta_{\text{crit}} \approx 0.015 (\Delta\gamma/\gamma) \leq 0.9^\circ. \quad (10)$$

For surface roughnesses much larger than the limiting value given by eq. 10, which are indeed most common due to preceding surface preparation as well as due to sliding and the discussed micro-roughness, the annular zones of adhesion must necessarily be rather small compared to the load-bearing interface,  $A_b$ . In fact, the typical surface waviness is  $\theta \approx 5^\circ$ . Therefore adhesive forces can be neglected in very many cases, especially since generally  $(\Delta\gamma/\gamma)$  is evidently quite small, witness the fact that it is not possible to mend fractured objects by simply pressing the two sides together, however perfect may be the geometrical match between the two surfaces.

The reason for the low values of  $\Delta\gamma/\gamma$  commonly experienced is, of course, that the adhesive forces are screened by surface films. Such films form almost instantaneously in atmospheric air. Obvious conditions under which strong adhesion arises are, therefore, twofold. Firstly, when eqs. 9 and/or 10 are fulfilled, i.e. in the case of very planar, highly polished, clean surfaces making contact under almost any pressure. Secondly, when surface films are eliminated faster than they can reform. This may readily occur under moderate to high pressures, especially in protective atmospheres or in vacuum when, during wear, new surfaces are made and quickly covered by relatively large contact spots in which air access is inhibited.

For strong adhesion to occur, surface waviness in accordance with eqs. 9 and 10 is most important when the surfaces are relatively at rest. However, it is intuitively clear that adhesion as manifested by seizing can spread via

local plastic deformation when surface films are destroyed through relative motion, especially when motion is slow and/or occurs under high pressures, even if the initial surface should be rough and eq. 10 not be obeyed. These expectations appear to be in general agreement with observation.

For completeness sake, a few more details regarding adhesion may be in order: the concept of compatibility, linking the expected degree of friction and wear among pairs of materials to their alloying behavior, championed by Rabinowicz<sup>(37, 38)</sup>, may be theoretically linked to epitaxial behavior. Namely, the value of  $\Delta\gamma/\gamma$  in eqs. 9 and 10 would seem to be the same as that which controls epitaxy and plays a considerable role there<sup>(39-41)</sup>. One may thus expect that materials which are known to form good epitaxial systems, namely those with large  $\Delta\gamma/\gamma$  in the clean state, are those which are "compatible" in the sense of Rabinowicz, and are those in which adhesive effects are strong. To the extent that sliding wear under high pressure lays bare new uncontaminated surfaces which are at least partly and temporarily shielded from contamination, "compatibility" is thus very relevant if "seizing" is experienced.

Turning to the other extreme, namely contacts under light loads, one may estimate the contribution made by adhesive forces on the basis of the Hertzian contact as discussed by Holm<sup>(2)</sup>: The average diameter of  $N$  plastically deformed load-bearing contact spots, modelled as formed by lightly indenting, locally spherical asperities of radius  $r_c$  contacting a flat surface under load  $P$ , is according to eq. 1

$$d = \sqrt{4P/\pi H N} \quad (11)$$

However, as explained, the average contact spot is surrounded by an annular zone, whose outer diameter may be given by the symbol  $d_t$ , within which adhesive forces act. If, again, the gap width within which this effect is significant

is taken to be  $s = nb$ , then by simple geometry<sup>(34)</sup>

$$d_t = \sqrt{d^2 + 8r_c nb} = \sqrt{(4P/\pi HN) + (8r_c nb)} \quad (12)$$

As seen before,  $d \approx 0.1$  mm within a factor of ten or so, i.e.  $10^{-6} \text{m}^2 \leq d^2 \leq 10^{-10} \text{m}^2$  in the majority of cases. By comparison, with  $10^{-3} \text{m} \leq r_c \leq 10^{-5} \text{m}$  as a reasonable range, with  $n \approx 2$  and with  $b \approx 3 \times 10^{-10} \text{m}$ , one obtains  $5 \times 10^{-14} \leq 8r_c nb \leq 5 \times 10^{-12}$ , i.e. orders of magnitude smaller than  $d^2$ . Therefore, spreading of contact spots is not going to occur to any noticeable extent except under the conditions of high pressure, and/or great cleanliness and surface smoothness outlined above.

#### The Number of Slip Systems and the Coefficient of Friction

According to the model of Fig. 1C, with or without the action of adhesive forces, sliding requires shear deformation of the weaker of the two materials, being sheared off, or carried along by the stronger at least for short distances. However, as clarified by Figs. 6, 7, 8 and 10 it is not possible to shear or drag a surface element without propagating the shear deformation into the surrounding material. In other words, the crosssectional area over which shearing must occur is larger than the actual load-bearing area of the contact spot and indeed larger than  $A_0$ . Certainly it is impossible to drag along a surface element without deforming also surrounding material. This is dramatically obvious in cases of rather strong roughness in which literally material may be pulled over parts of the original surface, as in Figs. 13 and 14, and in extreme cases giving rise even to the burying of extraneous material under material dragged along by contact spots, as shown in Fig. 14. Thus both, the cases of no relative motion and great simplicity (Figs. 6, 7 and 8), as well as of surface turbulence of rather extreme magnitude (Figs. 13 and 14), suggest that the area sheared in sliding is larger than



Fig. 13 Highly irregular deformation at the interface between a thick gold plating and its AISI 1020 steel substrate underneath the wear track of an AISI 521 00 steel slider. (Courtesy of N. P. Suh, ref. 6 p. 4).

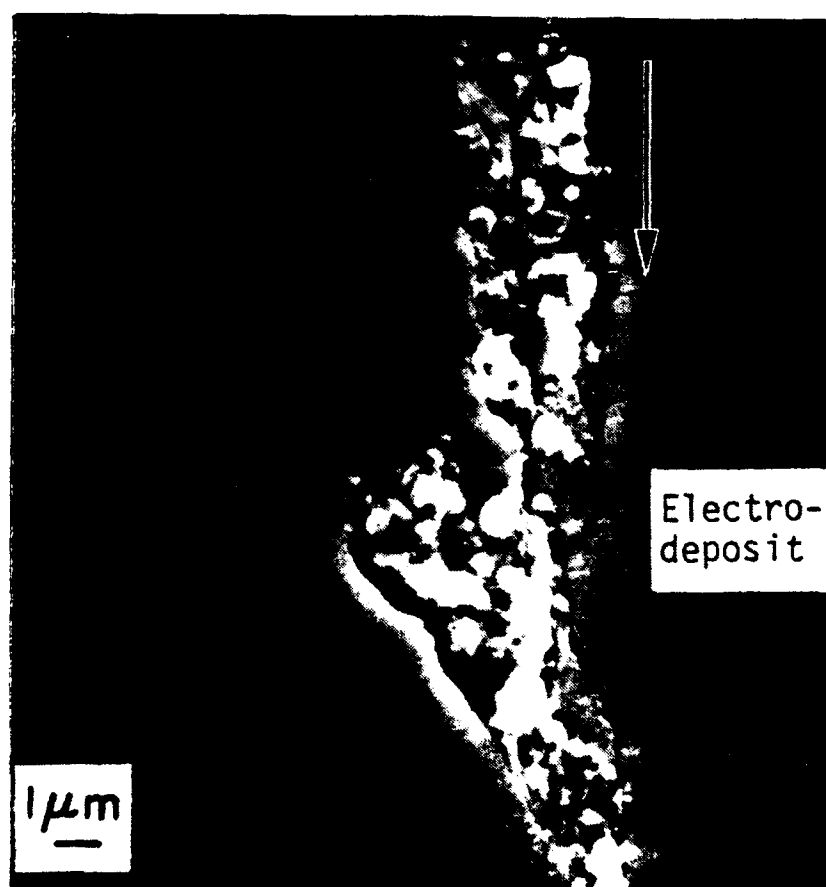


Fig. 14 Abraded copper surface showing highly irregular surface deformation to the point that some of the abrading sand particles have become embedded. (Courtesy of L. K. Ives, ref. 6).

the area bearing the normal load by some constant  $c$ . This constant  $c$ , which is estimated to lie between 1.5 and 5, is liable to be subject to variations depending on geometry and load.

Using the above result we may write for  $\mu$ , the coefficient of friction,

$$\mu = \frac{F_t}{P} = \frac{NcA_b \tau_s}{NA_b H} = \frac{c\tau_s}{H} \quad (13)$$

where  $F_t$  is the tangential force required for sliding, and  $\tau_s$  is the flow stress of the softer material in regard to shear parallel to the surface.

From dislocation theory it is known that plastic deformation of crystalline materials deforming in glide occurs if, and as soon as, the momentary critical resolved shear stress is exceeded on any crystallographic slip system. It appears to have been overlooked in the past that both, the magnitude of the critical resolved shear stress and the factor relating the applied stress to the resolved shear stress on the controlling slip system(s), are different for the surface, at which the shear strain is concentrated, and the subsurface region, in which the hardness is controlled.

Fortunately, for purposes of theory, the plastic strains concerned (in the subsurface region establishing load-bearing indentations and near the surface during sliding) are frequently so large, and/or workhardening is so small, that one may assume that saturation flow stress is attained everywhere. If so,  $\tau_s$  and  $H$  are related in a simple manner. Namely, in agreement with the discussion in the preceding section.

$$H = 2.8 \sigma_y. \quad (14)$$

where  $\sigma_y$  is the saturation tensile stress (for the present assumed to be constant). Further, in single glide the saturation resolved shear stress,  $\tau_y$ ,

is correlated with  $\sigma_y$  via the so-called Schmid factor,  $m_b$ , as

$$\tau_y = \sigma_y m_b = \sigma_y (\cos \lambda \cos \chi) \quad (15a)$$

where  $\lambda$  and  $\chi$  are the angles made by the compression axis with the active slip directions and slip plane normals, respectively. In eq. 15, meant to be used in connection with eq. 14, the subscript b has been used as a reminder that the relevant deformation takes place somewhere in the interior and thus may be taken to reflect the orientation in the bulk. Specifically in regard to indentations (i.e. eqs. 14 and 15 together),  $m_b$  depends on crystal orientation or texture, of course. It's value is not easily found in view of the complexity of the deformation, as exemplified in Figs. 7 and 8.

The conditions at the surface are different. In that case the applied shear stress, parallel to the interface in sliding direction, must be resolved into the active slip planes and slip directions carrying the surface shear. However, if single rather than multiple glide occurs, i.e. if slip continues on only one set of parallel glide planes and in only one glide direction, the active slip plane and slip direction reorient to be parallel to the plane and direction of shear, respectively. This has been well-known ever since Schmid and Boas' fundamental work<sup>(42)</sup>. Directly at the surface, where the shear deformation is very large as seen in Figs. 4 and 5, a crystal texture should therefore develop such that the "easiest" crystallographic glide plane is parallel to the surface, and the easiest glide direction therein is parallel to the direction of sliding. The factor relating applied stress to resolved shear stress in the top layer, should therefore be nearly unity when, or if, shear in the top layer is confined to only one single slip system. In that case  $\tau_s = \tau_y$ , whence with eqs. 13, 14 and 15

$$\mu = cm_b/2.8 \quad (16)$$

One other consideration intervenes here, namely that it is as yet uncertain under which circumstances and for what materials single glide is realized in the surface layers during sliding wear. The most simple geometrical concepts outlined above would lead one to expect single glide at the surface but in its totality the deformation in wear is very complicated, as discussed above, and multiple slip would seem to be rather more likely than single glide. In that case, on account of the very large shear strains achieved at the surface, one expects the development of some symmetrical orientation in which two or more glide systems are equally highly stressed.

The simplest example in this connection is that of layer-type crystals. These have only one crystallographic slip plane, namely the basal plane, within which, however, there commonly are three non-parallel glide directions according to three directions of atomic close packing. In single glide, the surface texture would be that described already, namely with the basal plane parallel to the surface and a close packed direction parallel to the direction of wear. However, even in the absence of any alternative mode of plastic deformation it is equally well possible that the strain at the surface settles down to double glide on two equivalent glide directions, thus generating a surface texture in which the direction of wear bisects the angle between the two.

Similarly, in crystal systems with more than one "easy" glide plane (meaning all but layer-type and hcp crystals with a  $c/a$  ratio larger than ideal) multiple glide on more than one glide plane could well be expected. The resulting texture, if consisting of but one component, should then be one in which the surface is symmetrical in regard to two or perhaps three, or even four, different slip systems.

The discussed principles may be illustrated by experimental evidence for the case of wire drawing: In wire drawing the wire axis of bcc metals is

parallel to  $\langle 110 \rangle$ , i.e. not parallel to the  $\langle 111 \rangle$  slip direction but symmetrical to two pairs of two  $\langle 111 \rangle$  directions each. Fcc metals have a double fiber texture in which different grains have either  $\langle 100 \rangle$  or  $\langle 111 \rangle$  parallel to the wire axis. Since  $\langle 110 \rangle$  is the slip direction in fcc metals, as already mentioned, again the texture axes are symmetrical to more than one of the  $\langle 110 \rangle$  slip directions, namely symmetrical to four  $\langle 110 \rangle$  directions in the case of  $\langle 100 \rangle$ , and three for  $\langle 111 \rangle$ .

Low stacking fault energy causes a distinct dissociation of  $\frac{1}{2}\langle 110 \rangle$  dislocations into two  $\frac{1}{6}\langle 112 \rangle$  partials, to the effect that cross slip as well as dislocation intersections are inhibited to a degree depending on the width of dissociation. This, in turn, has the effect of impeding the simultaneous action of different slip systems. In this light, it is understandable why low stacking fault energies shift the fcc wire drawing texture so as to favor the  $\langle 111 \rangle$  component, as was first pointed out by N. Brown<sup>(43)</sup>. Similarly, therefore, one may suspect that the wear texture, and hence wear behavior, of fcc and hcp metals depend on stacking fault energy, a point to which we shall return later.

In rolling textures of metals the same principles may be perceived, albeit with some complications. The rolling texture of bcc metals is  $\langle 110 \rangle$ ,  $\{100\}$ , naming first the rolling direction and then the plane of the sheet. That of hcp metals can be  $\langle 11\bar{2}0 \rangle$ ,  $\{0001\}$ , as would be expected on the most simple model for single glide, but generally the hcp rolling texture is variable, depending on the number of slip systems and twinning modes participating<sup>(44)</sup>. In fcc metals,  $\langle 112 \rangle$  is parallel to the rolling direction (i.e. midway between two  $\langle 110 \rangle$  slip directions) but the texture in regard to the plane parallel to the rolling plane is not well defined. For pure fcc metals the average orientation of many grains is best represented as  $\{123\}$  parallel

to the sheet, it seems<sup>(45)</sup>, while for fcc alloys (i.e. low stacking fault energies) it is more nearly {110}. However, especially for pure fcc metals, the texture has at least two components, much like the fcc drawing texture.

One may ask why nature should prefer multiple glide, entailing short mean free dislocation paths and profuse dislocation intersections, before single glide with potentially much longer free paths, thus fewer dislocations generated per unit of glide and much fewer dislocation intersections. It is here suggested that the reason may be found in the specifics of sub-boundary formation as follows: With gratifying regularity, under a host of different deformation conditions, the dislocation density,  $\rho$ , is found to depend on  $(\tau - \tau_0)$ , i.e. the resolved shear stress in excess of the intrinsic frictional stress,  $\tau_0$ , as

$$\rho = [(\tau - \tau_0)/\alpha Gb]^2 \quad (17)$$

with  $\alpha \approx 0.4$  (within a factor of two, say),  $b$  the Burgers vector, and  $G$  the shear modulus. The great increase of dislocation density during plastic deformation, which in accordance with eq. 17 occurs while  $\tau$  rises in the course of work hardening, arises via mutual dislocation trapping into low-energy configurations. In unidirectional deformation, whenever several independent crystallographic slip systems exist and dislocations are not significantly dissociated into partials, these low energy configurations typically are, or approach, low-angle boundaries arranged into characteristic networks, commonly referred to as "cell walls" forming a "cell structure".

It could be shown theoretically that the energy of cell walls decreases with increasing number of participating non-parallel Burgers vectors, meaning dislocations belonging to different slip systems<sup>(46)</sup>, especially in strongly elongated cells in which tilt walls predominate. The effect of twist components

in the cell wall structure modifies this result to the effect that there is not much additional gain in specific dislocation energy stored in the cell walls when the number of non-parallel Burgers vectors rises above three<sup>(47)</sup>. It follows, therefore, that an accumulation of dislocations with just one type of Burgers vectors strongly attracts dislocations of other types. Among these, the dislocations belonging to highly stressed glide systems are evidently favored by the externally imposed forces. The discussed tendency for the simultaneous operation of two or more glide systems counteracts the impediment against intersecting glide that otherwise exists for all types of dislocations; and it overcomes it, unless the dislocations are substantially extended and intersect only with great difficulty, thereby inhibiting dislocation cell formation.

Theory further shows that the number of possible low-angle boundaries, and hence of cell walls, is truly stupendous, and that cell walls in any arbitrary orientation can be made of any three or more independent Burgers vector directions, provided only that the dislocation densities are free to adjust<sup>(48)</sup>. Therefore it is difficult to predict the cell structure that will form under different circumstances, but the proclivity for multiple glide, whenever several independent "easy" crystallographic slip systems exist and dislocation intersections are not impeded through unduly large dislocation dissociation, is readily understood from the above principles.

Later on, more will be said about dislocation cells in relation to friction and wear. The topic has been introduced here mainly in preparation for the later discussion and could have been omitted at this point. Namely, the macroscopic effect of the discussed dislocation and cell wall properties is simply that multiple glide takes place readily, and that the resolved shear stresses on different, simultaneously acting glide systems are quite similar. On this

basis, i.e. that, locally, all simultaneously acting glide systems continue to have the same critical resolved shear stress throughout workhardening, plus the fact first pointed out by Taylor<sup>(49)</sup> that five independent glide systems are necessary and sufficient for all grains in an aggregate to deform homologically with the external strain, most textures can be generated via computer modelling<sup>(44)</sup>. However, the fact that deforming single crystals also break up into crystallites, separated by cell walls with gradually increasing angles of misorientation, cannot be so simply explained but requires understanding of the dislocation mechanisms introduced above. In this light, the effect of dislocation dissociation into partials is to selectively increase the critical resolved shear stress of otherwise equivalent crystallographic slip systems.

Returning to the problem at hand, namely to find the coefficient of friction in accordance with eqs. 13 to 15 for the general case, we need to relate  $\tau_s$ , the shear flow stress at the surface, to  $\tau_y$ , the critical resolved shear stress of the slip systems operating at the surface, via the appropriate Schmid factor. To do this, we make use of the general relationship between the applied stress,  $\sigma_{ij}$ , and the resolved shear stress on the various (operative) slip systems, of which eq. 15a is but a specific case. Namely<sup>(44)</sup>

$$\tau_y = \frac{1}{2} \sum \sigma_{ij} (\cos \alpha_i \cos \beta_j + \cos \alpha_j \cos \beta_i) = \sum \sigma_{ij} m_{ij} \quad (18)$$

with  $\alpha$  and  $\beta$  referring to the respective slip directions and slip plane normals. For the case of the surface shear stress generated by sliding, say, along the  $z$  plane in  $x$  direction, eq. 18 simplifies to one single term. Namely, in that case  $\sigma_{zx} = \sigma_{xz} = \tau_s$  is the only stress component, and

$$\tau_y = m_s \tau_s = \tau_s \cos \alpha_x \cos \beta_z. \quad (19)$$

where  $\alpha_x$  is the angle which the slip direction includes with the sliding

direction, and  $\beta_z$  is the angle which the slip plane makes with the plane of sliding. Eq. 19 is a simplification in that the resolved shear stress is in truth a function of  $z$ , a point to be discussed below. For the present purpose  $s\tau_y$  stands for the resolved shear stress at the level of maximum strain rate.

The Schmid factor in eq. 19 has been given by the symbol  $m_s$  in order to remind the reader via the subscript  $s$  that it is governed by the conditions in the topmost surface layers, in which the critical resolved shear stress is  $s\tau_y$ . By contrast, in the sub-surface layers the critical resolved shear stress is  $b\tau_y$ , i.e.

$$b\tau_y = b\sigma_y m_b = H_b m_b / 2.8. \quad (15b)$$

By combining eqs. 13, 14, 15b and 19, one thus obtains for the coefficient of friction

$$\mu = \frac{c\tau_s}{H} \approx \frac{c s\tau_y \cos \lambda \cos \chi}{2.8 b\tau_y \cos \alpha_x \cos \beta_z} \approx \frac{c s\tau_y m_b}{2.8 b\tau_y m_s} \quad (20a)$$

for all cases in which slip is the sole mode of plastic deformation.

In order to obtain a quantitative value for  $\mu$ , one must consider the likely values of the relevant Schmid factors  $m_b$  and  $m_s$ . As was shown by Dyer<sup>(22, 23)</sup> most crystallographically possible "easy" glide systems do in fact operate below and about an indentation, which is not surprising considering the complexity of the imposed strain and G. I. Taylor's rule that five independent slip systems are required for the general deformation<sup>(49)</sup>. Further, as was discussed, at any one spot all simultaneously acting equivalent slip systems have about the same Schmid factor and critical resolved shear stress

value, while at the same spot no equivalent slip system operates whose Schmid factor is much smaller. It follows that  $m_b$  rises with  $M$ , the number of crystallographically possible "easy" slip systems: If  $M$  is larger than five, the value of  $m_b$  decreases when  $M$  drops, i.e. as the choice of "easy" slip systems decreases, because increasingly those in less favorable orientations are forced to act. If  $M$  is less than five, "easy" slip systems must be supplemented by slip systems with intrinsically larger values of  $\tau_y$ , or else twinning or cracking will result. Thus  $m_b$  in eq. 20 depends not only on orientation, as was demonstrated by Fig. 6, for example, but even more so on crystal structure.

Reliable determinations of  $m_b$  for asperity contacts, at different degrees of flattening and for different crystal types and orientations, would require arduous calculations and/or experiments of the kind conducted by Dyer<sup>(22, 23)</sup>, a task evidently entirely out of the range of the present paper. However, some very simple arguments permit to clarify the basic concepts involved as follows.

For the case of polycrystals  $m_b$  is the larger, the higher the number of independent glide systems is. To the extent that an indentation parallels a compression test,  $(\lambda + \chi) \geq 90^\circ$  in eq. 20a, and the Schmid factor  $m_b$  cannot be larger than 0.5. This value of  $m_b = 0.5$  would be realized if every crystallographic plane could act as slip plane, and every direction as slip direction. In essence, amorphous materials and glassy metals have that property so that, for them,  $m_b = 0.5$ . Among the metals, it seems that aluminum at elevated temperatures comes closest to this ideal, when it can glide on all  $\{111\}$  and  $\{100\}$  planes in the twelve  $\langle 110 \rangle$  directions. Therefore aluminum, when sliding so as to elevate surface temperature to, say  $300^\circ\text{C}$  and above, should have an  $m_b$  value near  $\frac{1}{2}$ , and thus the highest coefficient of friction among the crystalline metals, given the same value of the other parameters in eq. 20a.

The next largest  $m_b$  values are expected for bcc metals, since in them  $\langle 111 \rangle$  serves as slip direction, and, in pencil glide, most if not all planes in the  $\langle 111 \rangle$  zone may act as slip plane, especially in the non-refractory ones. From the research on textures referred to before,  $m_b = 0.44$  appears to be the most likely estimate for the case of pencil glide.\* A somewhat lower value of  $m_b$  is predicted for fcc metals with their  $\frac{1}{2}\langle 110 \rangle$ ,  $\{111\}$  slip systems, namely  $m_b \approx 0.33$  for polycrystals under the constraints of "polyslip"<sup>(50)</sup>.

In typical hcp metals the basal plane is the only strongly preferred glide plane, with the three closest-packed directions in it serving as slip directions. i.e.  $M = 3$  in this case. Depending on  $c/a$  ratio, twinning or glide on pyramidal planes will supplement these glide systems or cracking will occur. In any event, lack of at least five "easy" slip systems will cause the hardness to be relatively higher than indicated by eq. 15b, to the same effect as if  $m_b$  were lower than geometrically determined. If, then,  $\tau_y$  is taken to be the critical resolved shear stress of the basal plane,  $m_b \approx 0.25$  may be a reasonable estimate for hcp metals.

Conditions are still more restrictive for layer-type materials. In these, cracking on account of insufficiency of glide systems is presumably wide-spread since for them glide on the basal plane is the only mode of plastic deformation. The most extreme case is presented by very hard materials such as carbides and nitrides, which lack any effective glide systems or other modes of plastic deformation and thus are brittle. For these, therefore, the hardness to shear strength ratio is abnormally high, which is formally expressible as abnormally low  $m_b$  values.

---

\*Footnote: The inverse of the Schmid factor,  $m_b$ , under discussion is the Taylor factor for polyslip. That Taylor factor has been tabulated for various cubic slip modes by G. Y. Chin in "Work Hardening in Tension and Fatigue" (Ed. A. W. Thompson, AIME, Warrendale, PA, 1977) p. 45.

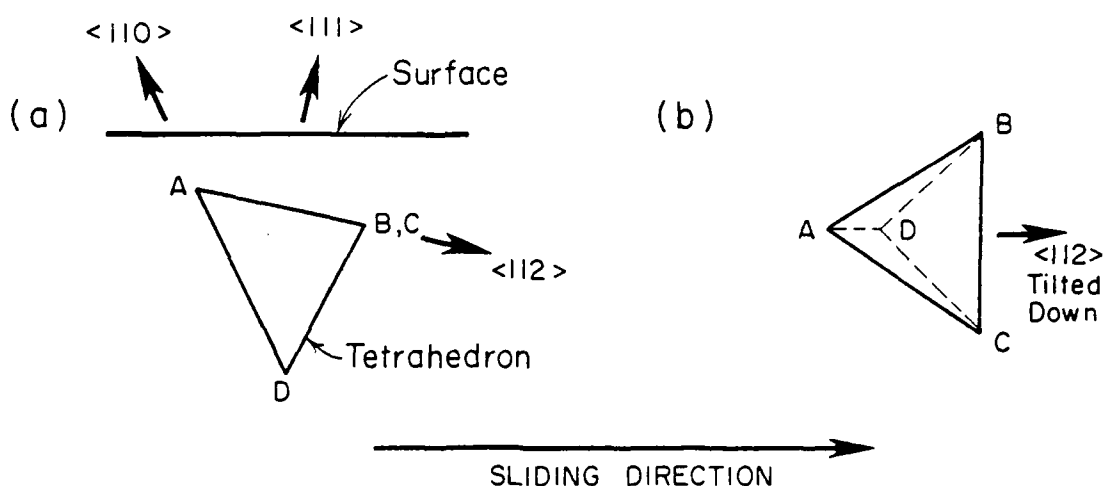


Fig. 15 Surface texture geometry reported for sliding wear in fcc metals, clarified by means of Thompson's tetrahedron, composed of the four  $\{111\}$  slip planes as bounded by the six  $\langle 110 \rangle$  slip directions. Also for hcp metals and for layer-type materials the slip plane, namely the basal plane in that case, is nearly parallel to the surface in the wear texture. Section normal to surface at left, top view at right. (Courtesy of J.P.Hirth and D.A.Rigney, ref.51).

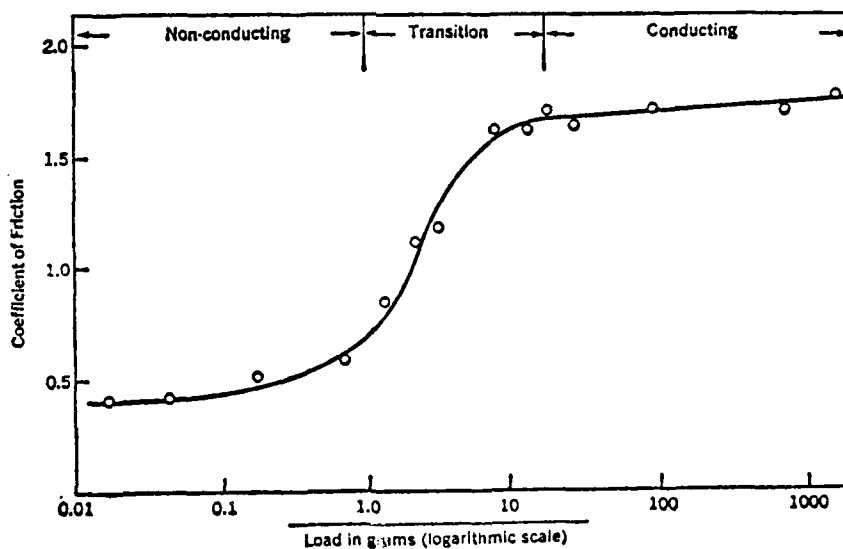


Fig. 16 Dependence of the friction coefficient of copper versus a hard steel slider as a function of load, using slow speed and well-controlled conditions. This is Fig. 38 in ref. 4 to which the authors, F. P. Bowden and D. Tabor, write: Below 1 gm. the friction is low ( $\mu \approx 0.4$ ) and the surfaces are electrically insulating; sliding occurs within the oxide film on the copper surface. Above 100 gm. the friction is high ( $\mu \approx 2$ ) and the surfaces become electrically conducting. The oxide is penetrated giving metallic contact and increased interfacial adhesion. According to the theory in this paper the above explanation is modified to exclude sliding within the oxide layer, and seeing the "basic" case realized at low loads.

Turning next to the  $m_s$  values in eq. 20 it is evident that these are apt to be larger and be less dependent on crystal type than  $m_b$ , because the applied surface tractions and resulting strains are close to simple shear, and therefore the number of participating slip systems smaller, i.e. one, two or three. If single glide obtains, the final texture would cause  $m_s = 1$ , with  $\alpha_x = \beta_z = 0$  in eq. 19.

Hirth and Rigney<sup>(51)</sup> have recently made a literature survey regarding surface textures due to sliding wear or abrading. As might be expected, these resemble, or may be identical with, the corresponding rolling textures. Fig. 15 due to Hirth and Rigney<sup>(51)</sup> indicates the surface wearing texture for fcc metals. The textures for hcp and bcc metals, and for layer-type crystals, can be derived from Fig. 15 by substituting, for  $\{111\}$ , the pertinent crystallographic slip plane, (namely the basal plane for hcp and layer-type crystals, and  $\{110\}$  for bcc metals). In this light, considering the texture of Fig. 15, it seems clear that once the surface texture is established the value of  $m_s$  cannot be much lower than  $m_s = 0.8$  in accordance with eq. 19, with  $m_s = 1$  as the upper limit.

Altogether, therefore, with  $m_s$  not very variable in the fully "run-in" specimen, the coefficient of friction is found roughly equal to  $m_b$ , if  $s_y^\tau = b_y^\tau$  as would be true for very hard or not workhardenable materials. Namely, with  $(c/2.8 m_s)$  not far from unity in accordance with the above discussion, eq. 20a then reduces to

$$\mu \approx m_b \quad (20b)$$

for the "standard case" after the "run in" period. Correspondingly, the  $m_b$  values outlined above are indicative of the value of the coefficient of

friction in steady state, namely,  $m_b = 0.5$  for aluminum at mildly elevated temperature,  $m_b = 0.44$  for bcc metals deforming in pencil glide,  $m_b = 0.33$  for fcc metals,  $m_b = 0.25$  for hcp metals, and perhaps  $m_b = 0.15$  for layer-type materials. Finally, for ultra-hard brittle materials, the coefficient of friction on this basis should be quite low, e.g. 0.15 or even less, because formally  $m_b$  would be very low (indeed perhaps zero). From a different viewpoint one would rephrase this latter result, saying that brittle materials have a low coefficient of friction because they lack any efficient mechanism to convert mechanical work into heat.

The above values presumably play the role of lower limits because, generally,  $s_y^{\tau} > b_y^{\tau}$  on account of workhardening in the course of surface shear, as seen for example in Fig. 5. Secondly,  $m_s$  rises during the run-in period before the surface texture is established and may start out at much lower values than 0.8. Third, the work expended in grooving must be added, which is generally presumed to account for 10% or 20% of the coefficient of friction. Finally, on new surfaces, "prow formation" as discussed recently by Antler<sup>(52)</sup> will add to the sliding resistance and thus to  $\mu$ . Conversely,  $c$  may have been overestimated. This question is difficult to resolve at this point: It is considered that the effect of the micro-roughness to modify local pressures and actual surface contact by a factor of perhaps 2 or even 3 in accord with the investigations by Williamson and co-workers<sup>(10, 11)</sup> does not influence our considerations because, unnoticed, micro-roughness was there all along and was implicitly incorporated into the factor  $2.8 = H/\sigma_y$  without this having been realized. The same cannot be said of the possible clustering of interacting hills into any one contact spot. The effect of such clustering would be to put a lower limit on  $c$ , namely  $c = 2$  in soft materials and up to 3 in harder ones<sup>(10, 11)</sup>. These are lower limits

because, to the thus enlarged average contact spot area, the previously considered plastically deformed zone about the spot must be added.

Actual values of the coefficient of friction appear to follow the order of the dependence of  $m_b$  values on number of slip systems<sup>(51, 53)</sup> outlined above. Specifically, it has often been noted that hcp metals have a lower coefficient of friction than fcc metals (e.g. refs. 51, 53, 54), and bcc metals have a higher friction coefficient than these, while layer-type crystals, foremost among them graphite and molybdenite, have such low coefficients of friction (namely, in the order of 0.15) that they are widely used as lubricants.

A correlation between the friction coefficient and the number of slip systems and/or stacking fault energy, was previously suggested by Heilman and Rigney<sup>(53)</sup>, Rigney and Glaeser<sup>(55)</sup>, and Hirth and Rigney<sup>(56)</sup>. In the context of the present theory the connection of coefficient of friction with stacking fault energy has already been explained. It comes about because low stacking fault energies, in fcc as well as hcp metals, act to reduce the effective number of slip systems, and thus  $m_b$  and  $\mu$ .

One is hard put to give actual experimental values for  $\mu$  so as to test eq. 20a and thereby to place some limits on the constant  $c$ . The following appear to be somewhat representative for the "standard case" to which eq. 20a applies: For layer-type crystals a lower limit value of the friction coefficient in the order of 0.1; about 0.4 for fcc metals; for bcc metals about 0.5 and, finally, closer to 0.25 for hcp metals.

One must hedge in quoting such values because we restricted our considerations to the average-clean, average-rough, well run-in sample, and disregarded lubrication, strong or thick surface layers, and adhesion which is expected to be strong in vacuum, exceptionally planar and smooth surfaces, or high pressures. Regrettably, measurements of the friction coefficient are frequently given without

clarifying the conditions under which they were obtained. Furthermore, in line with the prevailing focus on the adhesion theory, measurements under very clean conditions were usually believed to be more meaningful, and therefore these are mostly reported. In fact, values of the friction coefficient below unity are often believed to be artifacts due to an assumed lubricating effect of surface impurities or surface films. The above discussion will have shown why a reexamination of friction data for dry sliding between average-clean, average-rough surfaces would be highly desirable, indeed essential if eq. 20a is to be tested, with the possible outcome that these conditions will be established as the standard case, from which all others may be derived by considering the various modifying factors.

Effects of Sliding Distance, Sliding Direction, and Bulk Texture  
on the Coefficient of Friction

The preceding interpretation of friction coefficients in terms of slip geometry accounts for, respectively predicts, some special effects. Firstly, as long as surface texture is not fully established,  $m_s$ , the Schmid factor for the shear deformation at the surface, changes. Generally  $m_s$  tends to rise, perhaps up to unity as was explained. This should cause the friction coefficient to drop during run-in by up to almost a factor of two even in cubic crystals, and more in materials of lower symmetry. Conversely, workhardening through surface deformation increases  $s_y^{\tau}$  while  $b_y^{\tau}$  remains rather stable, causing the coefficient of friction to rise proportionately. Therefore one must expect substantial changes of  $\mu$  during run-in which could go either way, and which could (indeed often should) show an intermediate extremum.

Secondly, for the fully run-in condition there should exist an orientation dependence on the direction of wear. Namely, if a texture should have been established in which the active slip direction is parallel to the direction

of sliding, the friction coefficient is expected to have a minimum value (say  $\mu_0$ ) when testing in the initial direction of sliding, while in other directions  $\mu$  should be inversely proportional to the corresponding (lower) direction cosine in accordance with eq. 20a. In case of the perfect texture, i.e.  $\alpha_x = \beta_z = 0$ , this means that  $\mu = \mu_0 / \cos \phi$  where  $\phi$  signifies the angle between the direction of testing and the original sliding direction, or the nearest equivalent slip direction in the slip plane parallel to the surface. Of such equivalent slip directions there are two (besides the original one) on the hexagonally close-packed slip planes of fcc, hcp and layer-type substances, but only one on the {011} slip plane of bcc metals slipping parallel to  $\langle 111 \rangle$ .

For any texture in which the sliding direction is midway between two slip directions, e.g.  $\langle 112 \rangle$  in fcc metals with {111} nearly parallel to the surface as in Fig. 15, the coefficient of friction is predicted to have a maximum in the original sliding direction. In agreement with that prediction Moore<sup>(28)</sup> found the coefficient of copper that had been grooved by turning on a lathe (which presumably generated the discussed  $\langle 112 \rangle$ {111} texture) to be 0.6 in dry sliding parallel to the grooves, but 0.57 at  $45^\circ$  to the grooves. For an accurate  $\langle 112 \rangle$ {111} texture the expected ratio of  $\mu$  in the two directions is  $\cos 30^\circ : \cos 15^\circ = 0.60 : 0.54$ , and for {111} somewhat tilted against the surface, as in the actual texture, the predicted coefficient at  $45^\circ$  should correspondingly be moderately higher than 0.54 but below 0.60, in good agreement with Moore's measurement.

Eq. 20a further indicates a dependence of the friction coefficient on any pre-existent texture in the bulk of the material. This offers the hypothetical opportunity of reducing friction coefficients via suitable choices of textures. Some indirect support for this contention is provided by Fig.

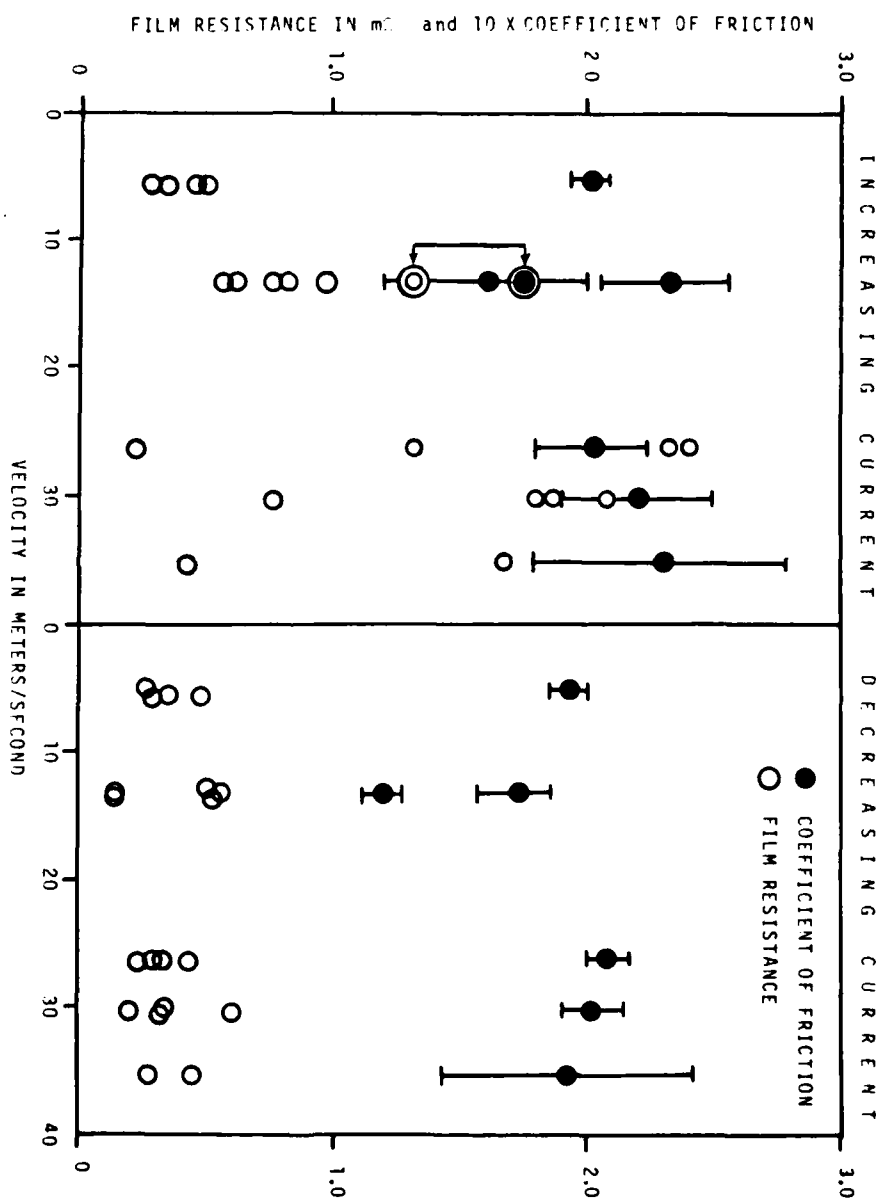


Fig. 17 Values of the coefficient of friction and of the electrical resistance of the surface film for an electrical silver graphite brush (75w/o Ag) sliding on a polished copper ring, measured during the same experiment (see ref. 60). Note that the film resistance varies irregularly by as much as a factor of ten on increasing current, indicating correspondingly large changes in the film thickness and/or structure, while the coefficient of friction changes only within about  $\pm 25\%$  and without any correlation with the film resistance. On decreasing the current, the film resistance changes much less but the coefficient of friction more than on increasing current. Clearly, therefore, there is no direct correlation between coefficient of friction and film character, at least not in this case.

10, in conjunction with Dyer's<sup>(23)</sup> observation that the coefficients for rolling friction were 0.0045 for rolling in [100] direction, and 0.0059 for rolling in [110] direction.

#### The Role of Surface Films

Much evidence exists in support of the contention that the coefficient of friction and/or adhesion are greatly influenced by surface films. Thus substantial effects can result even from very minor contaminations of either or both of the two contacting surfaces, as elaborated by Bowden and Tabor<sup>(3, 4)</sup> and Rabinowicz<sup>(7)</sup> as well as numerous other workers, e.g. J. R. Whitehead<sup>(57)</sup>, K. L. Johnson and D. V. Keller<sup>(58)</sup>, and D. H. Buckley<sup>(59)</sup>. Fig. 16 from the book by Bowden and Tabor<sup>(4)</sup> gives an example including in the legend the interpretation advanced by these authors.

In view of the wide acceptance of the adhesion theory of friction, it is not surprising that authors commonly ascribe decreases in the coefficient of friction following the introduction of some contaminants to the lubricating effect of surface layers, including those which are only several atomic layers thick, much as Bowden and Tabor in their interpretation of Fig. 16. However, not at all infrequently major changes in the nature of the surface films do not cause any significant, reproducible changes in the coefficient of friction. Examples may be found in refs. 60 and 61. Fig. 17, presenting data extracted from ref. 60 illustrates the latter phenomenon.

The model of Fig. 1C and the preceding considerations are clearly incompatible with the assumption that very thin surface films act as lubricants. In fact, the theory presented in this paper does not leave room for any major effects of surface films except under a number of specific circumstances, including at least one of the following: (1) films of a thickness comparable

to, or larger than, the micro-roughness. (ii) Films so strong that they compete with the strength of a layer thickness comparable to  $\sqrt{A_b}$  of the softer material. (iii) Films of a kind to inhibit the formation of micro-roughness. (iv) Films which form hard wear debris particles.

Note that films falling under point (i) may significantly reduce the coefficient of friction, and thus be truly lubricating, provided their shear strength is low. Soft platings such as discussed by Peterson in this volume provide examples. Films of group (iii) can also reduce the coefficient of friction, especially if they are very hard, and those in group (iv) can reduce  $\mu$  by providing particles which separate the two surfaces while either rolling between them like balls in a ball race, or plowing through either or both sides. The wear rate in the last case could be affected either way, but more likely it is increased. Hard platings, such as discussed by Ramalingam in this volume, tend to belong to both (ii) and (iii).

Any of the above possibilities, plus perhaps a number of others not considered, singly and in combination, will surely be realized under a bewildering variety of different circumstances and will thus give rise to the correspondingly varied effects. The range of effects that one may expect in connection with films of types (i) to (iv) is further increased on account of the surface temperature changes which, at constant pressure and velocity, accompany changes in the coefficient of friction, and which at the same time can influence surface films in various ways.

Ordinary thin surface films on nominally clean surfaces, meaning films not visible to the naked eye, i.e. of thickness between, say, twenty and two hundred angstroms, are unlikely to fall into any of the above categories, except perhaps (iv). Therefore, materials with surface films not thick or strong

enough to be classed under any of the four points enumerated above will be included in the "basic" case. Conversely, it requires the local absence of any film whatever, including monatomic adsorption layers, to permit strong adhesion<sup>(58, 59)</sup>, and furthermore, all "ordinary" films down to monatomic layers on the two surfaces, have a significant electrical resistance.

In light of the above considerations, and in agreement with Bowden and Tabor's own interpretation, the transition shown in Fig. 16 is seen as one between the "basic" case including an invisible surface film, and surface film removal through wear which exposes new surface under conditions in which re-contamination is inhibited. Now true adhesion takes place, and the measured coefficient of friction correspondingly rises steeply.

It requires very well-controlled conditions of loading in order to obtain a virtually constant coefficient of friction when there is a significant adhesive force between the two sliding objects, e.g. as was seemingly the case in Fig. 16 and similar measurements by Whitehead<sup>(57)</sup> that were performed in the same laboratory. At least in the latter case<sup>(57)</sup>, the data points indeed were averages of a large number of individual measurements which showed wide scatter, including stick slip. More importantly yet, the sliding took place only on fresh tracks and at a very slow speed (namely 0.008 cm/sec), and the load was kept constant in any one test. Similar conditions were observed by Buckley<sup>(59)</sup>.

These conditions are important because the meaning of the coefficient of friction is ambiguous when true adhesion is present. Namely, the coefficient of friction is given by  $\mu = F_t/P$  according to eq. 13. If adhesion is dominant,  $F_t$  is presumably controlled by the highest value of  $P$  attained in any one test, since any increase of  $P$  increases the true area of contact

irreversibly. Albeit, it does not require that  $F_t$  depend reversibly on  $P$  in order to collect "coefficient of friction" data. Therefore, using samples which cling together not only when  $P = 0$  but even if under slight tension, meaning negative values of  $P$ , while the adhesive junctions provide a finite value for  $F_t$ , permits obtaining values for  $\mu$  between minus and plus infinity, including zero. Bikerman<sup>(5)</sup> has previously made this same point.

Cases, as that of Fig. 16, in which  $\mu$  is found constant within a wide range of  $P$ , even though adhesion is significant, are those in which the force of adhesion is proportional to  $P$ . While this is sometimes observed (e.g. Fig. 45 of ref. 62) they are by no means general<sup>(58)</sup>.

The converse phenomenon of the above, i.e. independence of measured coefficients of friction (in the  $0.2 \pm .05$  range as in Fig. 17, and in the  $0.4 \pm 0.1$  range in ref. 61), in the presence of drastic changes in the nature of the surface film, is also easily understood: As long as the films are not belonging to categories (i) to (iv) above, they are unlikely to have any significant influence on the coefficient of friction. At the same time the fact that in both, refs. 60 and 61 (and in Fig. 17), the coefficients of friction, although not subject to systematic changes, yet show substantial irregular variations, is a further argument in favor of the earlier conclusion that the number of contact spots can be quite low. Namely, in both refs. 60 and 61 conditions were such as to cause considerable local heating, i.e. favoring a small number of contact spots. Further, in both cases local materials differences at the contact spots would have been erratic and not insignificant because composite materials were used. It is thus believed that the erratic behavior of the friction coefficient in Fig. 17 reflects local materials differences as the few acting contact

spots begin, grow and decay.

Some Thoughts on Geometrical Effects, Surface Stress/Strain Distribution,  
Wear and Delamination

Repeated reference has been made to the elevated temperature that may exist at the contact spots, and to the resultant temperature gradients towards the interior. The analytical problems involved in determining the local temperatures on the two sides of the sliding contact are formidable and no detailed treatments are so far available. Similarly, only scattered measurements of contact spot temperatures are available. Much excellent work has indeed been done in this most vital area (e.g. refs. 2, 15, 33). Even so, much remains to be done.

Some aspects of temperature effects become especially evident when the coefficient of friction is considered in terms of mechanical energy being converted into heat, rather than in terms of forces as was done so far. That viewpoint has a distinguished history which was recently reviewed by Rigney and Hirth<sup>(63)</sup>, and a new treatment has recently been proposed by Hirth and Rigney<sup>(51, 63)</sup>. These authors, as also Dautzenberg<sup>(18)</sup>, emphasize that only plastic deformation can be the mechanism by which the observed conversion of mechanical energy into heat can take place during friction. They also emphasize that this conversion does not take place at the interface but mainly in the sub-surface regions of the softer of the two materials. One may add that the less thermally conductive tends to be hotter than the more thermally conductive and tends to develop the hot spots, given similar hardnesses and an extended geometrical interface<sup>(15, 16)</sup>. Besides, for geometrical reasons, in a pin and ring combination only the pin can develop hot spots, which is no doubt one important reason why the same materials combination can show different coefficients of friction and wear when pin and ring materials are interchanged.

These considerations are highly significant because of the general rule

that hardness decreases with temperature. As a consequence the softer material (as judged from tests at ambient temperature) must be expected to wear rather faster when used as the pin than the ring. Further, material transport, while primarily going from the softer to the harder as judged at ambient temperature, should have a superimposed tendency for going from the pin to the ring. Thus, while Fig. 1C leads to the conclusion that the softer material always transfers faster to the harder material than vice versa, it is also true that, on account of geometry and coefficients of thermal conductivity, and the differences in local temperature at the contact spots resulting therefrom, the roles may be inverted as judged from relative hardness at ambient temperature. According to Holm (ref. 12, footnote to p. 238) Bowden and Hughes were the first to emphasize that fact.

Hirth and Rigney have made a qualitative analysis of the coefficient of friction based on stress and strain distribution in the subsurface regions, primarily in the softer material<sup>(51, 63)</sup>. The standpoint in this paper differs from their treatment in assuming that no recovery takes place. Consider, then, the resolved shear stress causing the surface strain, such as depicted in Figs. 4 and 5. It is due to the tangential tractions applied at the contact spots. Let us assume that it is adequately represented by

$$\tau(z) = \{z_0/(z + z_0)\}_s \tau_y, \quad (21)$$

say (although the subsequent argument does not depend on the specific form of  $\tau(z)$ ), where  $z_0$  is comparable to  $d$ , i.e.  $\sqrt{A_0}$  of eq. 1. Here, as before,  $s \tau_y$  is the resolved shear stress at the surface. For the case of homogeneous materials, we shall specify its position, identified as  $z = 0$ , more precisely as the level of maximum strain rate. Thus  $z = 0$  will be located at the level of the valleys between interacting hills making up the contact spot, and

for the case of only one hill per contact spot  $z = 0$  will be at the level of the valleys of the micro-roughness.

The resolved shear stress  $\tau(z)$  must be in equilibrium with the local flow stress of the material which, to a first order approximation at small strains, depends on shear strain  $\gamma$  and shear strain rate  $\dot{\gamma}$  as, say,

$$\tau(\gamma, \dot{\gamma}) = \tau_0 + \Theta_{II}\gamma + a\dot{\gamma} \quad (22)$$

where  $\Theta_{II}$  is the linear workhardening coefficient and  $a$  a constant which typically decreases with temperature.

On the assumption that one may treat the different layers of  $z = \text{constant}$  as gliding and workhardening independently (vindicated by the results to be discussed later), one may therefore write

$$\tau(z) = {}_s\tau_y - \Theta_{II}\{\gamma_s - \gamma(z)\} - a\{\dot{\gamma}_s - \dot{\gamma}(z)\} \quad (23)$$

where the subscript  $s$  refers to values at  $z = 0$ . Combining eqs. 21 and 23 yields

$$\dot{\gamma}(z) = \dot{\gamma}_s - {}_s\tau_y z / \{a(z + z_0)\} - \Theta_{II}\{\gamma(z) - \gamma_s\} / a. \quad (24)$$

Now, if steady state were reached, meaning that the strain rates at the various values of  $z$  were independent of time, the respective strains would be  $\gamma = \dot{\gamma}t$  with  $t$  the elapsed time of testing, presumed to be large compared to the "run-in" period. Correspondingly, in steady state eq. 24 would render the clearly time dependent expression

$$\dot{\gamma}(z) = \dot{\gamma}_s - {}_s\tau_y z / \{a(z + z_0)\} - \Theta_{II}\{\dot{\gamma}(z) - \dot{\gamma}_s\}t / a, \quad (25)$$

an evident contradiction.

This paradoxical result points up the impossibility of reaching steady state in sliding friction as long as the local hardness depends on the cumulative local strain, actually quite independent of the specific forms of  $\tau(z)$  and  $\tau(\gamma, \dot{\gamma})$ . In this light, it is evident that any steady-state equilibrium in sliding wear can only be dynamic in either of two ways, or a combination thereof. Namely, hardening can cease without fracture, or fracture can occur. The former can be realized via continuous annealing, which is the assumption made by Rigney and Hirth<sup>(51, 63)</sup>. However, in most cases of practical interest the hardness gradients at worn surfaces are real (e.g. Fig. 5) and temperature effects on the coefficient of friction are minor (e.g. Fig. 23) so that it is highly probable that no dynamic recovery takes place. In that case, to the extent that the consideration of the problem in terms of somewhat independently acting layers is valid, fracture must occur. Such fracture must take the form of delamination for the reason that, statistically, cracking will always occur where stress/strain conditions of fracture are first reached, which will necessarily be at some more or less well-defined value of  $z$ .

#### The Effect of Changes in Surface Hardness on the Coefficient of Friction

The temperatures at the interface of contact spots can be quite high, indeed they can easily reach the melting point. Fig. 18 gives a recent example due to Saka, Eleiche and Suh<sup>(64)</sup>. In the preceding discussion, repeated reference was made to the mechanical effects of such temperature increases at the contact spots. Also, they can cause transformations, especially importantly, of course, in the case of steels (compare the chapter on "Wear of Steels" by O. Vingsbo in this volume). Correspondingly, as a function of depth below the surface, zones of different phases can be formed with their own characteristic microstructures and hardnesses, and leading on occasion to very pronounced effects on wear rates<sup>(65)</sup>.

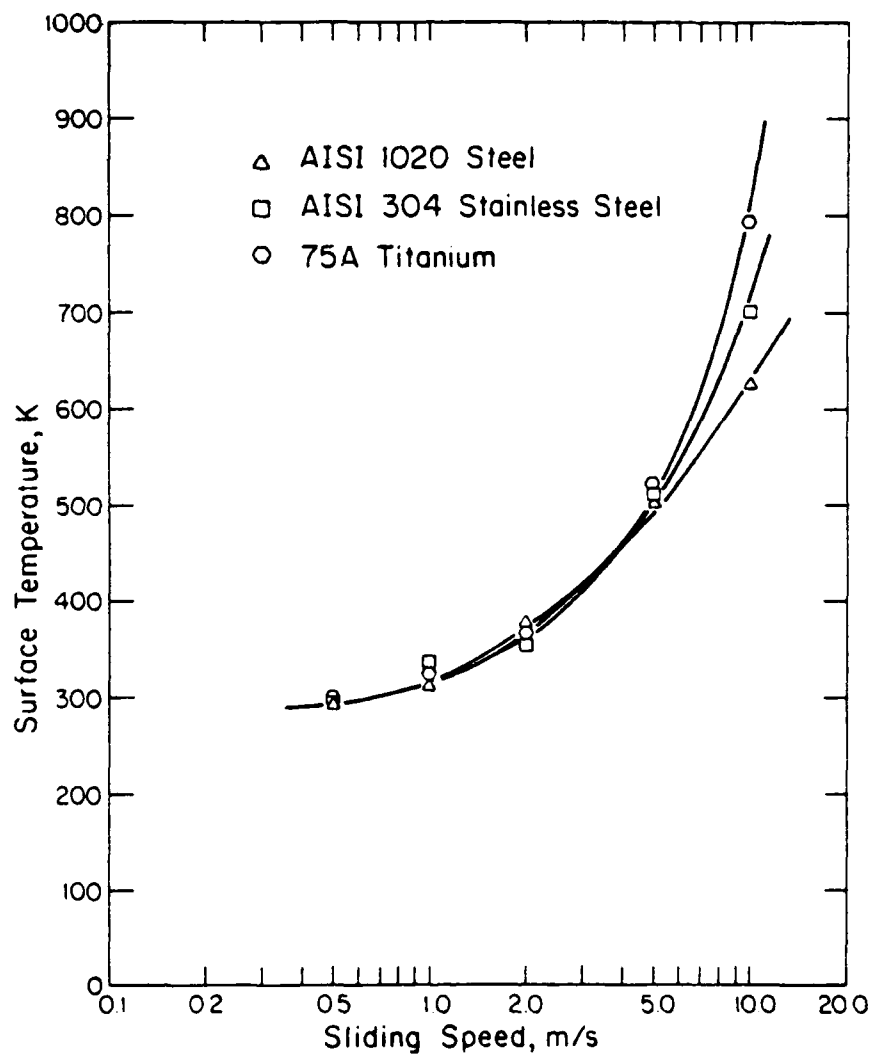


Fig. 18 Average temperatures at the interface between different materials as indicated and a 52100 AISI steel ring on which they slide under a 49 N load, as dependent on sliding speed. (Courtesy of N. Saka, A. M. Eleiche and N. P. Suh, ref. 64).

However, in the present paper no further attention will be paid to this complication, since it is viewed as a deviation from the "basic" case as defined above.

A very illuminating study of the effect of temperature on the area of contact spots and the materials hardness derivable therefrom has recently been published by Tamai and Tsuchiya<sup>(66)</sup>. Figs. 19 and 20 present their results. In that case, the temperature variation was generated by passing current between the contacting materials while these were at rest and the contact spot was under direct observation, thus permitting measurements that would otherwise not have been possible.

The data in Figs. 19 and 20 are not surprising. The purpose of presenting them is to document that the softening expected to accompany temperature rises does indeed occur, and that it causes the corresponding increase in the load-bearing area  $A_b$ . It will hardly be doubted that in this connection it is immaterial that the temperature increase was due to Joule heat rather than frictional heat. However, whether heating is due to electrical currents or friction, or both, there will be a strong temperature gradient away from the surface.

At significant values of peak temperature the gradient will not be as strong in the case of friction heat than Joule heat<sup>(63)</sup>, but can certainly be very strong in both cases, e.g. presumably in the order of  $50,000^{\circ}\text{C}/\text{cm}$  in the case of Fig. 18. Correspondingly, there can be strong gradients in (momentary) flow stress. This will cause an additional concentration of the shear strain parallel to the sliding direction in the topmost surface layers, beyond what would be expected from considerations such as given in eqs. 21 to 25, and yet further accentuated because greater strain rates in turn lead to greater heating. Therefore it must be understood that  $s\tau_y$  and  $b\tau_y$  in eq. 20a refer to their

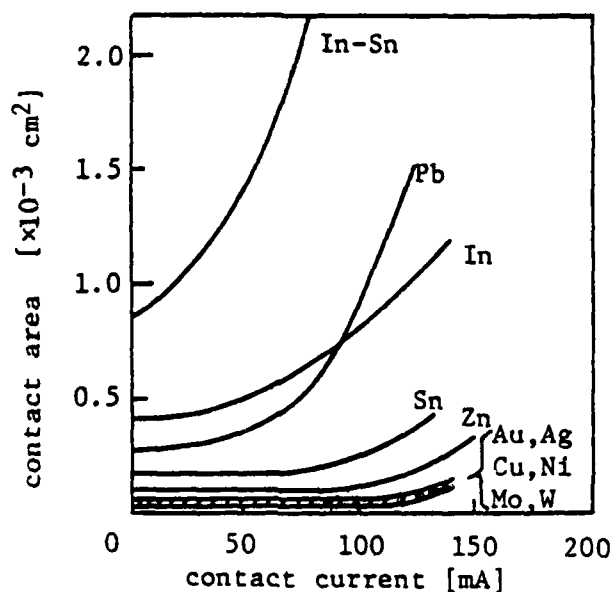


Fig. 19 Size of current-conducting contact spot (one "a-spot") formed at the polished end of a wire, pressed against a glass surface provided with a thin, transparent conducting layer, under a 100 g\* load, as a function of current. With increasing current, the interfacial temperature is raised and the contact spot size increases correspondingly. (After T. Tamai and K. Tsuchiya, ref. 66).

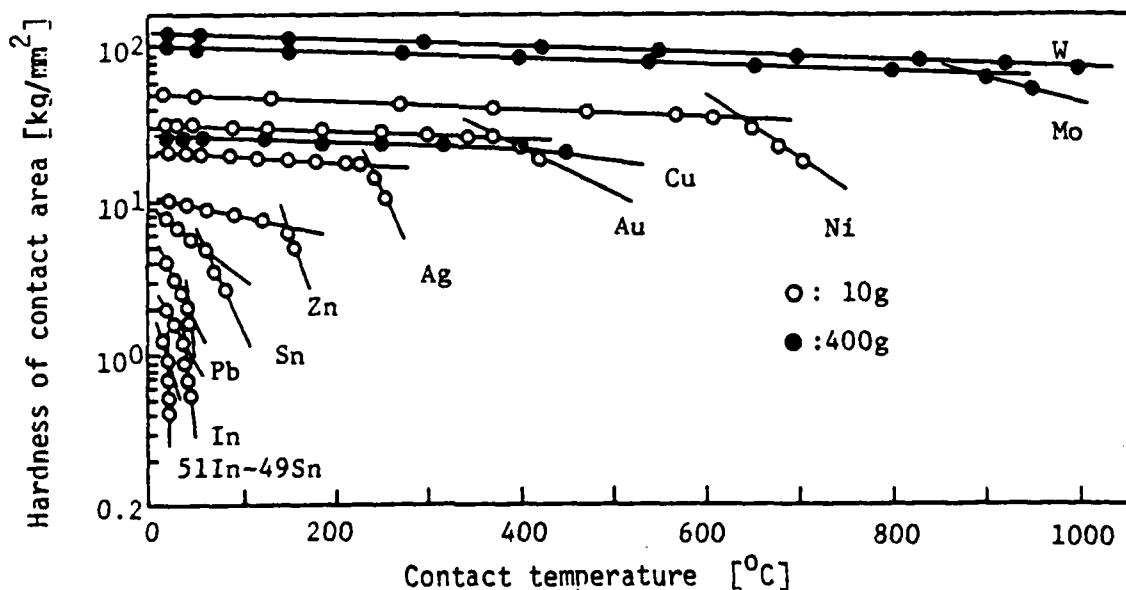


Fig. 20 Dependence of hardness of the wire materials in Fig. 19 derived from the data in that figure. (After T. Tamai and K. Tsuchiya, ref. 66).

values during sliding, which are not necessarily identical with those determined afterwards, such as in Fig. 5, especially not when the temperature differences between surface and slightly lower subsurface regions are so large that significant differences of flow stress values are caused thereby. To emphasize this point, eq. 20a may be rewritten as

$$\mu = \frac{c m_b s \tau_y(\gamma_s, \dot{\gamma}_s, T_s)}{2.8 m_s b \tau_y(\gamma_b, \dot{\gamma}_b, T_b)} \approx m_b \frac{s \tau_y(\gamma_s, \dot{\gamma}_s, T_s)}{b \tau_y(\gamma_b, \dot{\gamma}_b, T_b)} \quad (20c)$$

where, again, the subscript s refers to the layer at  $z = 0$  as defined and b to the subsurface region at  $z \approx \sqrt{A_b}$ . Eq. 20c qualitatively predicts the dependence of the coefficient of friction on sliding speed and during run-in.

On account of eq. 20c, for "steady state" conditions, one expects a gradual decrease of friction coefficient with sliding speed, namely by a factor of two or a few between very slow relative motion and a sliding speed just below that causing superficial melting, commensurate with the decrease of critical resolved shear stress between ambient temperature and several degrees below melting. The estimated factor of "two or a few" is meant to be a rough guide, with actual figures hopefully eventually determinable with the aid of eq. 20c. At still higher speeds, when surface melting occurs, the coefficient of friction will drop to very low levels since then  $s \tau_y(\gamma_s, \dot{\gamma}_s, T_s) = 0$  and dynamic effects of the liquid metal take over.

Available data are in qualitative accord with the above prediction. An example is given in Fig. 21 for the range in which the surface remains solid, and Fig. 22 in regard to extremely high speeds (achieved by Beams' method<sup>(67)</sup>) up to surface melting. Already Bowden and Tabor<sup>(1, 3)</sup> and Rabinowicz<sup>(68)</sup> clearly realized that different effects of temperature on  $F_t$  and  $H$  (eq. 13) are

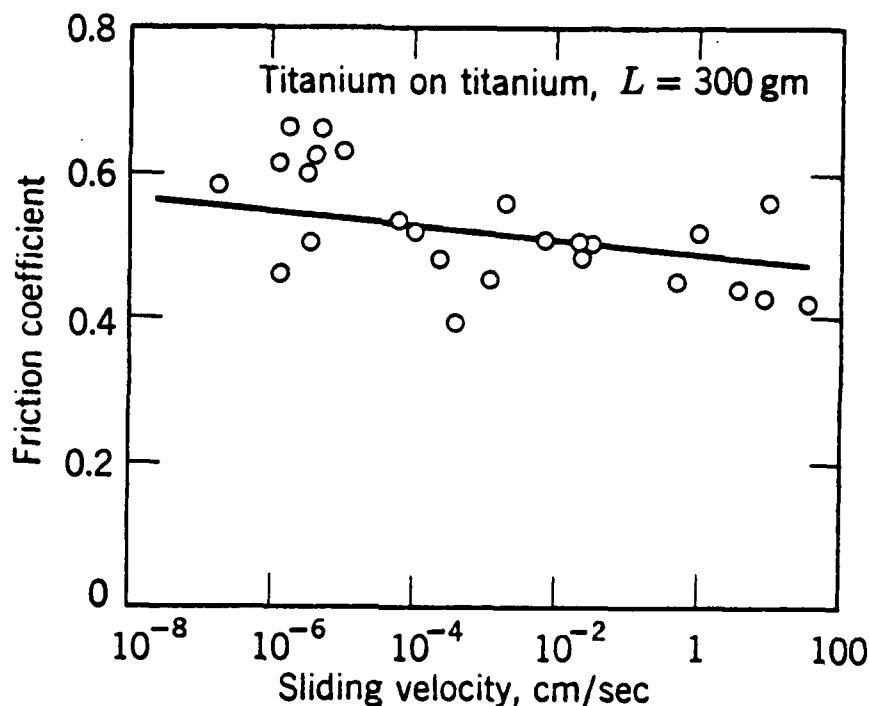


Fig. 21 For hard materials, the coefficient of friction declines slowly with speed, as in this example. (After E. Rabinowicz, Fig. 4.12, ref. 4).

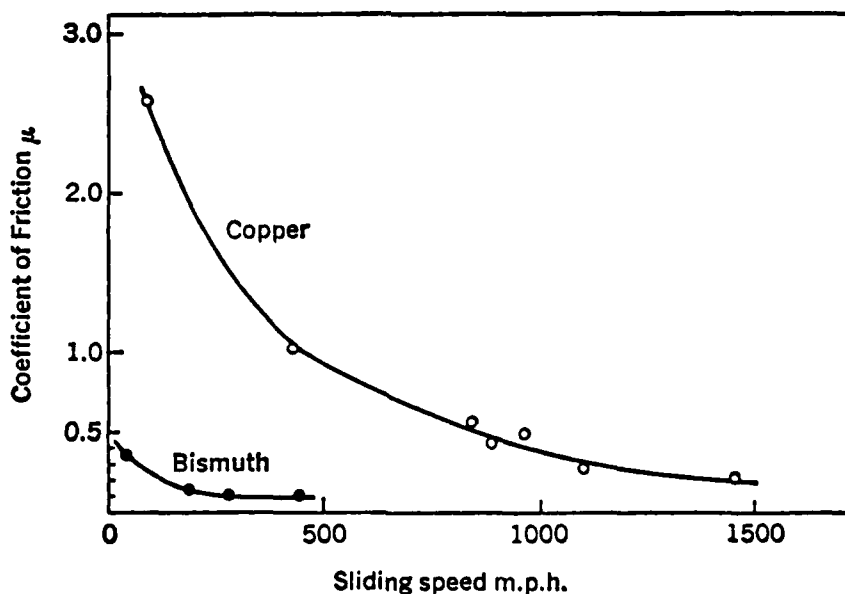


Fig. 22 Friction coefficient of a steel ball rubbing against copper and bismuth at extremely high speeds. Modest vacuum. With copper the friction falls to a relatively low value at sliding speeds of 1,500 m.p.h. due to the formation of a thin molten surface film of copper. With bismuth, where the melting point is much lower, the drop-off in friction occurs at a correspondingly lower speed. (Figure and legend after F. P. Bowden and D. Tabor, ref. 4, Fig. 42).

responsible for the typical decline of the friction coefficient with sliding speed, and Rabinowicz pointed out explicitly that temperature changes per se were not the cause, giving Fig. 23 as proof.

One aspect of eqs. 20a and 20c is the prediction of a rapid increase in  $\mu$  due to workhardening in the surface, raising  $s\tau_y$  as compared to  $b\tau_y$  during "run-in" provided that (i) the softer of the two materials is initially in a condition to permit strong workhardening, and (ii) the surface temperature does not quickly rise into the softening range. Now, the initial rise of  $s\tau_y$  is rather more rapid than the increase of  $m_s$  due to surface texture formation. Therefore, during run-in a rapid rise of  $\mu$  could be followed by a mild decrease before equilibrium is established. It seems possible that at least some of the  $\mu(t)$  curves during running-in reported by Feinle and Feller<sup>(69)</sup> record this phenomenon.

#### Wear Rate and "Wearing-In"

There is no universal relation between wear rates and coefficient of friction. Intuitively, one would expect that high friction coefficients are correlated with high wear rates on the grounds that much energy is expended when friction is high. However, the derivation of the coefficient of friction leading to eqs. 20a and c) does not give any grounds for a correlation between wear rates and friction.

The question of wear has so far been touched upon only once, namely in connection with eq. 25 which showed up the fact that no true steady state can be reached in sliding friction unless strain hardening ceases due to continuous annealing, which as indicated already is not normally expected to happen. Typically, therefore, hardening will proceed until fracture takes place, presumably within that zone parallel to the surface where fracture conditions

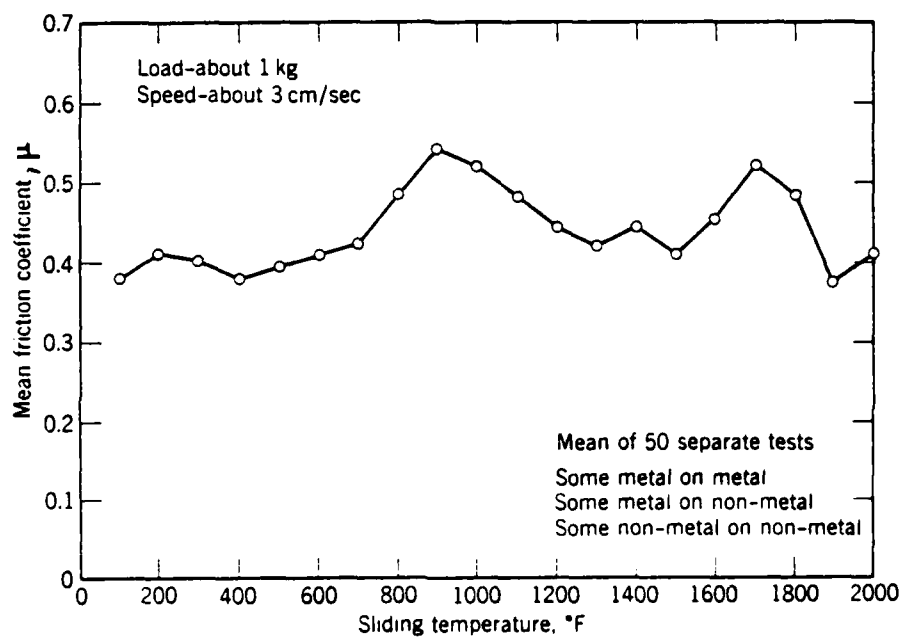


Fig. 23 The friction coefficient is insensitive to externally applied temperature changes, as was demonstrated by E. Rabinowicz with this figure representing measurements of over fifty widely varying materials combinations. (Fig. 4.33, ref.7).

are reached first. This, then, brings up the question where fracture will take place.

To begin with, one should distinguish between the interface at which actual contact takes place between the two materials and the zone (mainly in the softer of the two) within which strong shear in the direction of sliding takes place. In recognition of that distinction, in the preceding considerations the origin of the z-axis (pointing downwards into the softer material as in Fig. 5) was placed at the average level of the valleys in the micro-roughness for an otherwise continuous contact spot, or at the level of the valleys between the interacting hills if the contact spot is composed of such. This was done because above those levels, due to the constantly changing geometry, the slip planes are broken up into a multitude of disjointed and mutually misaligned regions, permitting no systematic glide. For the same reason, this zone cannot be the source of the typical flake-like wear debris that is so very generally observed. On the other hand, small pieces of material projecting from either of the two materials into valleys (between hills and/or the micro-roughness) of the other, are doubtlessly sheared off in large numbers even after very slight relative movements, including those occurring coincidentally with macroscopical loading and unloading of pieces relatively at rest.

Evidently, more particles of the softer should be so sheared off and cling to the harder than vice versa, but both transfers should take place profusely in terms of numbers of particles, albeit involving only very small volumina. Also, once the two surfaces are macroscopically separated, and the configurations of the micro-roughnesses have changed in response to the load reduction, many of the sheared off particles will simply fall off, or be attracted back

to their own original side by adhesive forces. Further, pre-existing roughnesses will have much the same effect until obliterated.

It appears that all of these conclusions are in adequate agreement with observations. Specifically it is a well-known rule that, preferentially, the softer material moves onto the harder. Yet already Moore<sup>(28)</sup> noted that iron can be found on a copper surface over which hard steel has been sliding. However, the wear debris from this cause will be small, namely on the scale of the micro-roughness.

The larger wear particles which cause the bulk of wear are "delaminated" via cracking parallel to the surface<sup>(6)</sup>. Systematic crack formation in the zone of positive z-values (using our previous coordinate system) will typically require some time: Shear strain will have to accumulate until the deformability of the material in shear has been exhausted. Whether there is an additional requirement for delamination because shear stresses by themselves may not be sufficient cause for crack nucleation and propagation is not considered in the present paper. That question is even now the object of doubt and disagreement: Fleming and Suh<sup>(70)</sup> have emphasized the role of sub-surface tensile stresses normal to the surface behind the moving contact spot, while Rosenfield<sup>(71)</sup> believes compressive/shear stresses to be much more important, and Jahanmir and Suh<sup>(21)</sup> have concentrated attention on inclusions as likely sites for crack nucleation.

In the present paper the stand will be taken that cracking will occur whenever and wherever a critical shear strain is reached. The value of that critical shear strain will depend on numerous parameters including perhaps the local normal stress, and it will require considerable further research before it can be theoretically predicted. The salient point is that it is not

believed that crack nucleation sites are ever scarce, with and without inclusions. Not only can cracks start at grain boundaries, but as was shown by Gardner, Pollock and Wilsdorf<sup>(73-75)</sup> for the case of tensile stress, and postulated by Rigney and Glaeser<sup>(51, 55)</sup> for the case of wear, cell walls, or joints between them, provide crack nucleation sites.

With this, a few simple conclusions regarding the dependence of wear on hardness and surface coatings emerge: First off, the shear strain is largely concentrated in the softer material so that delamination-type wear (which by present consensus tends to account for the bulk of wear, as indicated already) will be concentrated mainly in the softer partner, whence the rule that wear decreases sharply with increasing hardness. The same protective effect of hardness can be achieved by thin hard platings, especially if they inhibit the formation of micro-roughness so that in favorable cases true sliding may be expected. Soft platings, by contrast, are beneficial when they concentrate the shear in themselves and are of a kind either not to workharden at all, like indium, or to continuously anneal under the prevailing temperature at the surface.

For homogeneous samples, some simple quantitative relationships regarding wear rates and induction times derive directly from the model as follows: Fracture is expected to occur by cracking parallel to the surface, within the shear-stressed layer, of thickness  $\sqrt{A_b} \approx z_0$  according to eq. 21, once a critical local shear strain,  $\gamma_{crit}$ , is reached, thereby generating wear particles of thickness

$$t = \sqrt{A_b}/n = \sqrt{P/NH}/n. \quad (26)$$

Here  $n$  is a number depending on the position of the critically deformed layer below the interface which however is insensitive to changes in  $P$ . The critical

shear strain will be some multiple of  $\bar{\gamma}$ , the average shear strain in the deformed zone, say  $\gamma_{crit} = \bar{\gamma}/f$  with  $f$  smaller than unity. In turn, the average shear strain is

$$\bar{\gamma} = (NA_b/A_t)L/\sqrt{A_b} = N\sqrt{A_b} L/A_t = \sqrt{PN/H} L/A_t \quad (27)$$

where  $A_t$  is the total, macroscopic area of contact and  $L$  is the distance of sliding. Eq. 27 follows because the displacement  $L$  of the contact spots of total area  $NA_b$  is averaged over the whole area of macroscopic contact, whereas the thickness of the deformed zone is taken to be  $\sqrt{A_b}$ .\* Once steady state is reached, the volume of wear particles produced when the deformed layer undergoes a shear deformation  $\bar{\gamma}$  may thus be written

$$V_w = A_t t \bar{\gamma} / f \gamma_{crit} = \sqrt{PN/H} t L / f \gamma_{crit} \quad (28)$$

since the volume of wear particles will total  $A_t t$  when  $\bar{\gamma} = f \gamma_{crit}$ . Combining eqs. 26 and 28 we thus obtain

$$V_w = (PL/H) / (nf \gamma_{crit}) = ZPL/H. \quad (29)$$

The last formulation gives the empirical formula for wear rate in the form preferred by Holm (ref. 12 pp. 233 ff.).

Equation 29 refers to steady state, whereas there must be an incubation period during which  $V_w/L$  on account of the formation of delaminated wear particles rises from zero to its steady-state value. The sliding distance to reach steady state is that for which  $\bar{\gamma} = \gamma_{crit}/f$ , i.e. from eq. 27 and eq. 1

$$L_{inc} = A_t \sqrt{H/NP} \gamma_{crit} / f \quad (30)$$

---

\*Footnote: As will be further shown below, the deformed zone is in fact significantly thinner than  $\sqrt{A_b}$ . In the present context the effect of this is to underestimate the parameter  $n$ . However, the lower limit of  $n$  in the present consideration was obtained from data in which the deformed layer thickness was insufficiently well specified. Therefore it seemed safer to proceed as above.

During the incubation period, smoothing of surface roughnesses with the associated shearing off of particles goes on, leading to the overall transfer of softer material to the harder, which then comes to a dynamic equilibrium. Depending on the material loss due to this process the wear rate in the incubation period can be larger or smaller than in steady state.

It is evident that eq. 29 represents the well-known law of wear which says that the wear volume is proportional to the load as well as the sliding distance and is inversely proportional to the hardness. The wear coefficient deduced from eqs. 26 to 29 is related to the formulations of Holm (ref. 32 p. 233), and of Rabinowicz (ref. 7 p. 138) as

$$(nf\gamma_{crit})^{-1} = Z = k/3 \quad (31)$$

Experimental data yield a very wide range of values for  $Z$ . Holm (ref. 12 p. 237-239) lists values for the softer contact (metal) member between  $Z = 2 \times 10^{-6}$  and  $2 \times 10^{-3}$  in air, and up to  $2.7 \times 10^{-2}$  for two like metals. Correspondingly, one must compare reasonable values of  $(nf\gamma_{crit})$  with that range, i.e. check whether

$$30 \leq (nf\gamma_{crit}) \leq 5 \times 10^5. \quad (32)$$

For the particular cases of Ni, Cu and Au each sliding on itself, Soda, Kimura and Tanaka<sup>(76)</sup> found that the thickness of the wear fragments was proportional to the thickness of the deformed surface layer in the range from  $12\mu\text{m} \leq t \leq 43\mu\text{m}$  with  $n = 4$ .

This is a most welcome support for eq. 26 and at the same time provides what may be presumed to be the lower limit of  $n$ . Namely, as has been known for a long time, and is also apparent from the quoted  $Z$  values, the heaviest

wear occurs when two like materials slide on each other. Holm explains that phenomenon (ref. 12 p. 240) on the grounds that "... the contact area (is) prescribed by the strength of the softer member. But the harder member prescribes the structure of the surface." Therefore, when both members are the same, both deform and "the contact surface is in a labile state and will attain a wavy structure" (Holm p. 240). Consequently, the gradient of shear deformation from the surface inward is lower, and the region in which systematic glide in which fracture can occur begins at a relatively greater depth below the interface, when like material slides on like than in any other situation. For all other cases  $n$  is therefore bound to be larger. Thus, for example, in the investigation by Hirst and Lancaster<sup>(19)</sup> to which Fig. 5 pertains, the thickness of the wear particles was only about three micrometers, i.e.  $n \approx 40$ . It is, of course, extremely unlikely that this should coincidentally also be the maximum value for  $n$ , and  $n = 100$  would appear to be a very conservative value for the maximum.

The lower limit of  $f$  is about 0.2, and the value of  $\gamma_{crit}$  is typically comparable to  $\gamma_s$ , as will be shown presently. Therefore eq. 32a implies

$$40 \leq \gamma_{crit} \leq 5000 \quad (32b)$$

These values seem to be entirely reasonable, seeing that Dautzenberg<sup>(18)</sup> and Dautzenberg and Zaat<sup>(77)</sup> determined shear strain values of  $\gamma_s \approx 120$  and  $\gamma_s \approx 700$  respectively, for copper sliding on steel\*. However, the limits of eq. 32b are too conservative. Namely, some additional insights may be gained by the use of Fig. 24 by Dautzenberg and Zaat<sup>(77)</sup>, into which the interpolation curve

$$\gamma = \gamma_s \exp(-mz/z^*) \quad (33)$$

---

\*Footnote: Note that their "effective strain"  $\bar{\delta}$  is  $\gamma/\sqrt{3}$ .

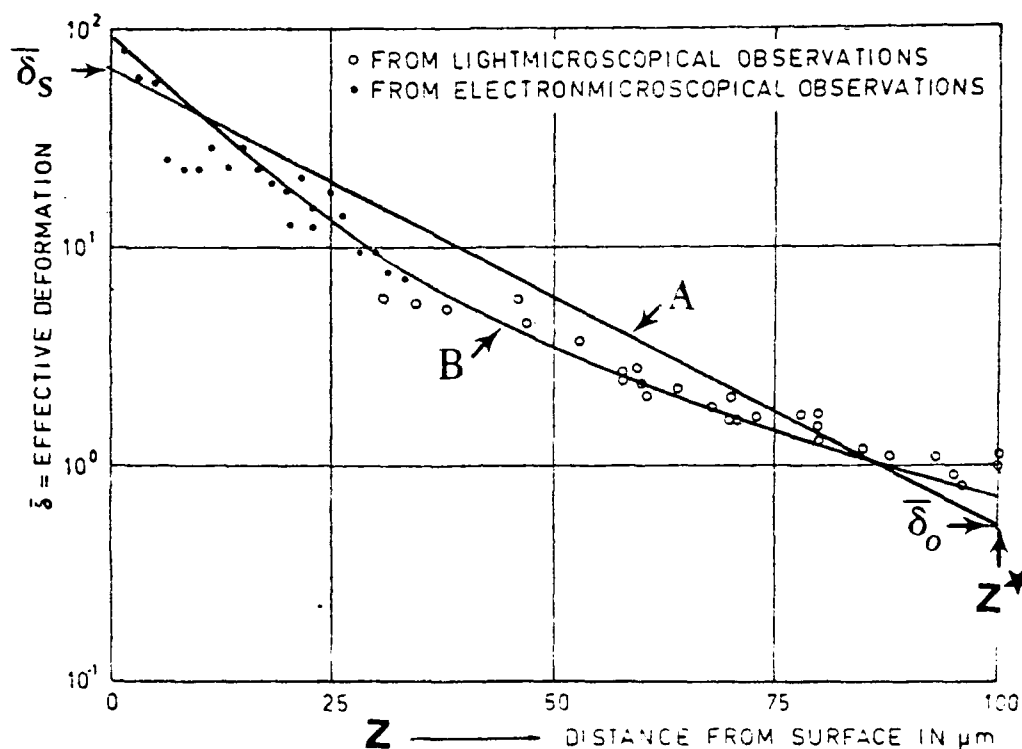


Fig. 24 Subsurface shear strain (in terms of "effective" strain  $\bar{\epsilon} = \gamma/\sqrt{3}$ ) in an 8 mm dia. polished OFHC copper pin slid on a normalized polished SAE 1045 steel ring at 2 m/sec under 4 kg\* load. The interpolation curve A represents eq. 33 for the case of  $m = 5$  with  $z^* = 0.1$  mm and  $\bar{\epsilon}_s = 70$ , whence  $\bar{\epsilon}_0 = \bar{\epsilon}_s/150$ . The interpolation curve marked B represents eq. 48a, again with  $m = 5$  and with  $\bar{\epsilon}_s = 100$ . Thus curve B is the predicted strain dependence when the applied tangential stress drops off as  $(1+z/z_0)^{-1}$  and a logarithmic workhardening law prevails. (Diagram, excepting interpolation curves, due to J. H. Dautzenberg and J. H. Laatz, ref. 77).

has been entered with  $\gamma_s = 70 \times \sqrt{3}$  and  $m = 5$ . Eq. 33 is the type of interpolation suggested by Heilmann and Rigney<sup>(53)</sup>. In effect eq. 33 defines  $z^*$ , being the thickness of the strongly sheared layer, as that distance at which  $\gamma(z^*) = \gamma_s \exp(-m) = \gamma_s/150$ , in this case yielding  $z^* = 100 \mu\text{m}$  as indicated in Fig. 24. Evidently, the fit is acceptable, and from here on we shall continue to employ the same definition of  $z^*$ , namely via  $\gamma(z^*) = \gamma_s/150$ , whether or not the dependence of  $\gamma$  on  $z$  is exponential. This has the disadvantage that the shear strain  $\gamma_0 = \gamma(z^*)$  may not be insignificant, namely  $\gamma_0 = 30$ , for example, if  $m = 5$  and  $\gamma_s = 4500$ , but it simplifies the subsequent considerations. Making a different choice for the thickness of the deformed layer is equivalent to changing the value of  $m$ , - maximally perhaps by as much as a factor of two in Fig. 24. However, it seems more logical to define  $z^*$  in terms of  $\gamma(z^*)/\gamma_s$  than in terms of some arbitrary value of strain and thereby making it also dependent on the value of  $\gamma_s$ .

From eq. 33 follows

$$\bar{\gamma} = \gamma_s/m = 0.2\gamma_s \quad (34)$$

and

$$\gamma_{\text{crit}} = \gamma(z^*/n) = \gamma_s \exp(-m/n) = \bar{\gamma}/f \quad (35)$$

Combining eqs. 34 and 35 renders

$$f = \exp(m/n)/m \quad (36a)$$

i.e. for  $m = 5$  and  $n \geq 4$

$$0.2 \leq f \leq 0.7 \quad (36b)$$

While  $\gamma_{\text{crit}}$  is always smaller than  $\gamma_s$ , it is evidently not very much

smaller, and will typically be comparable with it, e.g. for the example of  $n = 40$  appropriate to the data by Hirst and Lancaster<sup>(19)</sup>,  $\gamma_{crit} = 0.88\gamma_s$ . At its lowest, i.e. if  $n = 4$ , it is  $\gamma_{crit} = 0.29\gamma_s$ . Therefore, and because  $\gamma_s$  is more accessible to measurements than  $\gamma_{crit}$ , we rewrite the wear coefficient  $Z$  in terms of the surface shear strain,  $\gamma_s$ , using eqs. 31 and 35 as

$$Z = [f \gamma_s n \exp(-m/n)]^{-1} \quad (37a)$$

With  $m = 5$  and  $n \geq 4$  one thus obtains theoretically

$$0.015 \leq \gamma_s Z \leq 4.4 \quad (37b)$$

Comparing this with the experimental limits for metals, extracted from tables 41.07 and 41.09 in ref. 12 as quoted above, namely

$$2 \times 10^{-6} \leq Z \leq 2.7 \times 10^{-2} \quad (37c)$$

therefore requires

$$0.89 \leq \gamma_s \leq 160 \quad (37d)$$

for  $Z = 2.7 \times 10^{-2}$  and

$$7500 \leq \gamma_s \leq 2.2 \times 10^6 \quad (37e)$$

for  $Z = 2 \times 10^{-6}$  in steady state if the theory is to be acceptable. Similarly, from eq. 30, employing the same limiting values, one obtains

$$1 \leq L_{inc} / (A_t \sqrt{H/NP}) \leq 10^6 \quad (38)$$

for delamination wear in metals.

The above relationships will permit testing the theory presented here.

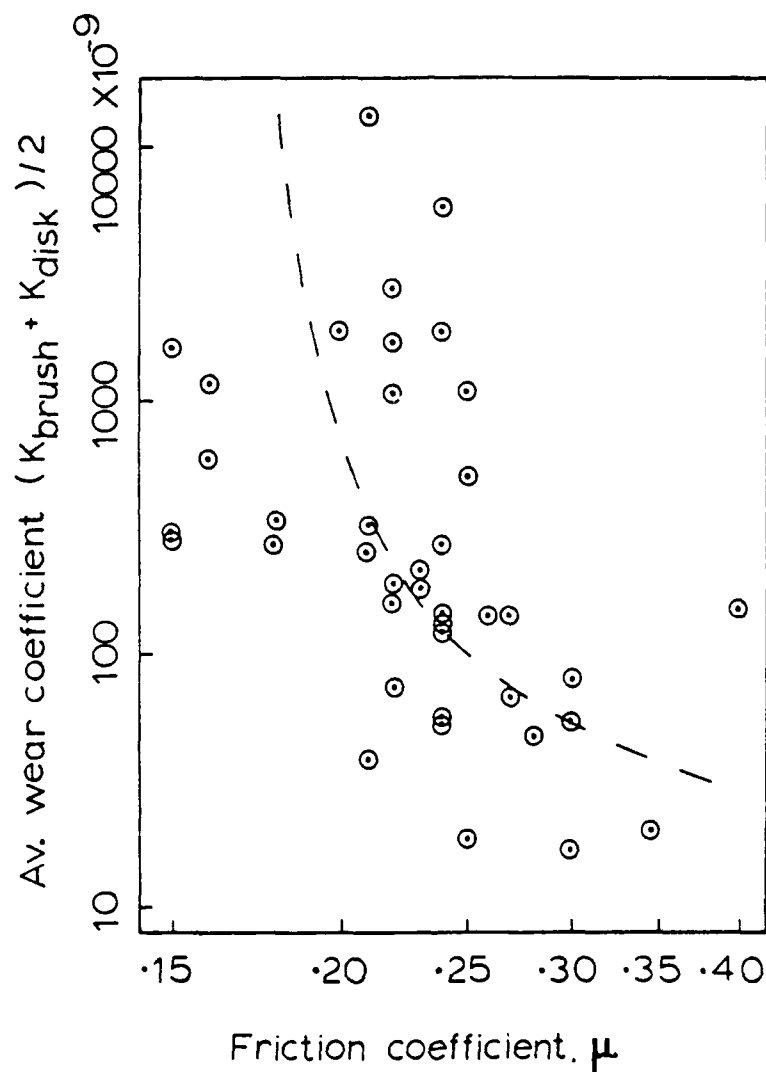


Fig. 25 Wear coefficients, averaged between the two sliding materials, namely a silver graphite (50 w/o Ag) brush and a disk made variously of Ag, Au, Cu, Pd, Pt, Ni, Rh, Re, Ru and Ir, plotted against the respective coefficients of friction as determined in different runs. (After E. Rabinowicz and P. Chan, ref. 78).

At this point little more can be done than to check general trends and order of magnitude values. In that spirit it may be pointed out that the theory does not provide for any connection between the coefficient of friction and delamination wear, - for it is only delamination wear which is considered in eqs. 26 to 38. Intuitively, one does expect a correlation between  $Z$  and the friction coefficient such that if one rises then so should the other, but experimentally, too, there is no real evidence that such a correlation exists. In fact, recently Rabinowicz and Chan<sup>(78)</sup> found the reverse relationship between  $\mu$  and  $Z$ , albeit with very much scatter, as shown in Fig. 25. Note that in this case the  $Z$  values are partly lying well below the lower limit indicated in eq. 37c. The reason is that Fig. 25 primarily concerns the wear of composite silver-graphite brushes, i.e. it involves graphite, a non-metal. It remains to be seen whether the wear also in that case can be treated by the above theory. In any event, one expects higher upper limits for  $\gamma_{crit}$  and  $n$  values in layer-type materials than in metals, and thus, optimally, lower  $Z$  values. This, then, is tentatively offered as an hypothesis to account for the excellent wear characteristics of layer-type materials, foremost among them graphite and molybdenite, to the point that they are often used as lubricants, as is well known.

One other relevant set of data concerns the variation of wear rates with sliding velocity. Hirst and Lancaster<sup>(19)</sup> have shown that, at least in the case investigated by them, the sliding speed does not act directly on wear rate but via the concomitant rise in surface temperature. Fig. 26 due to Hirst and Lancaster shows the typical resultant dependence of wear rate (of homogeneous metals, not subject to phase transformations) on sliding speed, including an initial significant decrease in wear rate followed by a

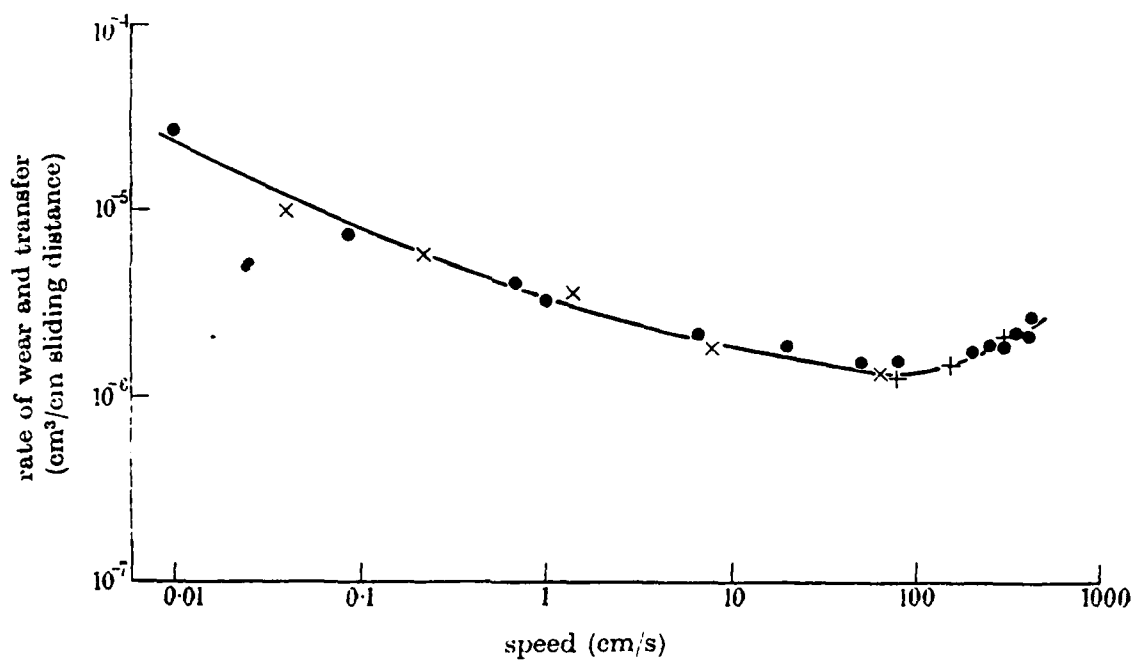


Fig. 26 Dependence of the wear rate on sliding speed for a 60/40 free cutting brass at 22.5 kg\* load. In this figure, due to W. Hirst and J. K. Lancaster<sup>19</sup>, a distinction is made between "rate of wear" (●) and "transfer" (× and +) which may be neglected for the present purposes. This dependence of wear rate on speed, namely an initial drop followed by a rise, is common for non-transforming metals.

rise. In terms of the present theory, that behavior is entirely to be expected because the strain to failure rises with increasing temperature, so that one should expect also  $\gamma_{crit}$  to increase with increasing temperature.

More complicated behavior, presumably responsible for the later increase in wear rates, will be expected when the surface temperature rises strongly: Already well below the point of surface melting one must expect chemical attack, principally oxidation for tests in the atmosphere, to raise the wear rate. Also, where freshly exposed surfaces touch, local welding will increasingly occur and increase wear. A further deviation from the simple theory outlined here occurs when phase transformations take place, a subject treated by O. Vingsbo in this volume. At melting, finally, the wear rates could become quite high, but also low, depending on the opportunities for healing of wear damage by re-solidifying material.

#### The Near-Surface Shear Strain Distribution as Determined from Workhardening

The fact that Hirst and Lancaster<sup>(19)</sup> found sliding velocity to have no direct influence on strain distribution and hardening (see Fig. 5), and the velocity dependence of wear rate to be due to surface temperature changes, suggests that within wide limits and presumably for a wide range of metals strain rate effects per se can be neglected. If so, plastic shear deformation will continue until the local flow stress as raised by workhardening equals the applied stress, i.e.  $\tau = \tau_y z_0 / (z + z_0)$  according to eq. 21. That this is so is strongly indicated by Fig. 5 in that much the same hardness distribution is caused by the different velocities. It follows that for the most simple case, i.e. linear hardening as in eq. 22 with a negligible  $a\dot{\gamma}$  term,

$$\tau_0 + \Theta_{II} \gamma(z) = \tau_y z_0 / (z + z_0) \quad (39)$$

i.e. that

$$\gamma(z) = \{z_0 / (z + z_0)\} s_{\tau_y} / \theta_{II} - \tau_0 / \theta_{II} \quad (40)$$

and

$$\gamma_s = (s_{\tau_y} - \tau_0) / \theta_{II} \quad (41)$$

while  $\gamma = 0$  for

$$z(\gamma = 0) \geq \frac{s_{\tau_y} - \tau_0}{\tau_0} z_0 \approx \frac{s_{\tau_y} - \tau_0}{\tau_0} K \sqrt{A_b} \approx z^* \quad (42)$$

with, say,  $0.1 \leq K \leq 10$ .

In this case of linear hardening with finite  $\tau_0$ , the assumption that  $z^*$ , the width of the deformed layer as introduced above in connection with eq. 33, is a measure of the size of the contact spot, i.e.  $\sqrt{A_b}$ , is evidently not true, except by occasional coincidence. Thus the distinction between  $z_0$ , a measure of the width of the layer subject to significant shear stress (roughly of size  $\sqrt{A_b}$ ) defined by eq. 21, and  $z^*$ , the width of the strongly shear strained layer defined by eq. 33, is very real for linear hardening, in which case  $z^*/z_0$  strongly depends on the prevailing conditions.

Depending on the choice of  $\theta_{II}$ ,  $s_{\tau_y}$  and  $\tau_0$ , the shear strain distribution represented by eq. 40 can vary widely. Thus, for very low workhardening, i.e.  $s_{\tau_y} = \tau_0 + \delta\tau$  with  $\delta\tau \ll \tau_0$ , eq. 40 reduces to

$$\gamma \approx [1 - z/z^*] \delta\tau / \theta_{II} = \gamma_s [1 - z/z^*] \quad (42a)$$

with

$$z^* = (\delta\tau / \tau_0) z_0 \quad (42b)$$

i.e. with eq. 26,

$$n \approx z_0 / z^* = \tau_0 / \delta\tau \quad (42c)$$

This, then, would be the strain distribution for the ideally plastic material so widely considered in continuums theory.

For  $s\tau_y = 2\tau_o$  it is  $z_o = z^*$ , i.e. the deformed zone would have a width comparable to  $\sqrt{A_o}$ , which has been the assumption in the earlier qualitative parts of this paper. In that case, i.e. for  $s\tau_y = 2\tau_o$  eq. 40 becomes

$$\gamma = (\tau_o / \theta_{II}) / (1 + z/z^*). \quad (43)$$

Finally, for  $s\tau_y \gg \tau_o$  one obtains

$$\gamma = \frac{s\tau_y / \theta_{II}}{1 + z/z_o} = \frac{\gamma_s}{1 + z/z_o} \quad (44a)$$

and, from  $\gamma(z^*) = \gamma_s/150$ ,

$$z^* = 149 z_o \quad (44b)$$

It is perfectly well possible (although as we shall see presently it is not common) that linear workhardening occurs during wear. At any rate, linear workhardening does not explain the data in Fig. 24. For one, when plotted logarithmically as in Fig. 24, eq. 40 is characterized by a very steep decline of shear strain near  $z^*$ , the edge of the deformed zone. Secondly, the shear strains in the deformed zone are typically much too large as if ordinary linear workhardening could be theoretically expected.

To put the values found in eq. 37d and e into perspective, it may be pointed out that in wire drawing, for slip planes oriented at  $45^\circ$  to the wire axis, the shear strain,  $\gamma$ , is related to the tensile strain,  $\Delta l/l$ , as  $\gamma = \sqrt{2} \Delta l/l$ , and to the "true" strain  $\epsilon$  as

$$\epsilon = \ln(\gamma/\sqrt{2}) \quad (45a)$$

Hence the limit  $\gamma = 7500$ , as in eq. 37e, corresponds to  $\epsilon = 8.5$  or less

in wire drawing, - less because in wire drawing textures the slip planes and directions do not have the ideal  $45^\circ$  orientations.

Such strains, while entirely unheard of in tensile tests, are commonplace in wire drawing, and are similarly expected to be realized in sliding wear. Namely, in wear even more so than in wire drawing, compressive stresses are superimposed on the shear stresses and retard cracking. This would not be so if  $n$ , defined by eq. 26, were near to, or less than, say, 2, because the delamination-type cracking would then take place at low compressive stress or even under dilatation. However, as we saw,  $n \geq 4$ , and the strain is strongly concentrated near the surface.

Taking, then, the standpoint that worn surface layers closely resemble highly drawn material, we turn to the work by Langford and Cohen<sup>(79)</sup> who investigated the flow stress and microstructure of iron wires as a function of true strains up to  $\epsilon = 7.4$  without intermediate annealing, which for the  $\langle 110 \rangle$  texture in their case corresponds to  $\gamma \approx 4000$ . Note that even this large strain can be easily exceeded in iron, while pure copper and platinum can be drawn without annealing practically indefinitely.

Langford and Cohen<sup>(79)</sup> observed a workhardening law of the type

$$\tau = \tau_0 + \theta_{II}' \ln \gamma \quad (45b)$$

This law is interpolated by eq. 22 for small changes in strain, provided strain rate effects can be neglected. It should indeed be quite prevalent, being expected whenever the workhardened state at any strain is essentially the same as the original state, i.e. is the potential beginning state for further workhardening, as is the case in so-called "stage II" behavior. Namely, stage II behavior goes hand in hand with a microstructure which shrinks

in scale but remains substantially unchanged geometrically<sup>(79-81)</sup>, as is demonstrated in Fig. 27.

Combining eq. 45b with eq. 21 renders

$$\gamma = \exp(-\tau_o/\theta'_{II}) \exp[(s\tau_y/\theta'_{II})/(1 + z/z_o)] \quad (46a)$$

and

$$\gamma_s = \exp[(s\tau_y - \tau_o)/\theta'_{II}] \quad (46b)$$

By the use of the previous convention that

$$\gamma(z^*)/\gamma_s = e^{-m} \quad (47)$$

where, specifically,  $m = 5$  was chosen above, one may rewrite eq. 46a into

$$\gamma = \gamma_s \exp[-2m/(1 + z^*/z)] \quad (48a)$$

with

$$z_o = z^* \quad (48b)$$

provided that

$$m = s\tau_y/2\theta'_{II} \quad (48c)$$

Eq. 48 has been entered into Fig. 24 as curve B, choosing  $m = 5$  as before and  $\bar{\delta}_s = 100$  (i.e.  $\gamma_s = \sqrt{3} 100 = 173$ ). Evidently, the agreement with the data is excellent, and it could still be bettered by a minor adjustment in the value of  $m$ . Therefore the only remaining question is whether  $s\tau_y/\theta'_{II} \approx 2m = 10$  is a reasonable value and is compatible with the requirement

of eq. 46b with eq. 48c, namely

$$\ln \gamma_s = (s\tau_y - \tau_o)/\theta'_{II} = 2m(1 - \tau_o/s\tau_y). \quad (49a)$$

With  $\gamma_s = 173$ , i.e.  $\ln \gamma_s = 5.15$ , and with  $m = 5$ , eq. 49a yields

$$\tau_o/s\tau_y = 1 - (\ln \gamma_s)/2m = 0.485 \quad (49b)$$

i.e.  $s\tau_y/\tau_o = 2.1$ . This result compares with the measurements by Langford and Cohen<sup>(79)</sup> in which at the true strain of  $\epsilon \approx 4.3$ , to which  $\gamma_s$  would correspond in the  $\langle 110 \rangle$  wire drawing texture,  $s\tau_y/\tau_o \approx 3$  was found. It thus seems that the strain distribution of Fig. 24, and by inference of a wide range of pure metals under sliding wear, is in all respects consistent with a logarithmic workhardening law of the type of eq. 45b without noticeable strain rate dependence.

For completeness sake it may be added that eq. 33 used for the interpolation curve A in Fig. 24 in conjunction with eq. 21 corresponds to the workhardening law

$$\tau = \tau_o/[1 - \text{const} \times \ln(\gamma/\tau_o)] \quad (50)$$

or more specifically for our case,

$$\tau = s\tau_y/[1 - (z^*/mz_o)\ln(\gamma/\gamma_s)] \quad (51)$$

Such a workhardening law has never been proposed but, given skillful choice of the disposable parameters, will also permit reasonable approximations to actual workhardening curves, - as may indeed be judged from curve A in Fig. 24 in comparison to curve B.

In summary of this section: For metals not subject to phase transforma-

tions, under a wide range of sliding conditions, flow stress gradients due to temperature and strain rate gradients can be neglected. Therefore the surface layer responds to the imposed shear stress (assumed to decrease as  $z_0/(z + z_0)$  in accordance with eq. 21) with plastic shear until the local flow stress has reached the local value of the applied stress. Stress and strain are related via workhardening laws. The workhardening law which from the theoretical viewpoint is most likely to be widely applicable has been observed in wire drawing of iron<sup>(79)</sup> as well as aluminum alloys<sup>(82)</sup>. According to it, the flow stress rises linearly with the logarithm of the strain. Available data on the shear strain distribution near a worn copper surface (Fig. 24) are completely explained with it.

It may be added that the logarithmic workhardening law is not the only one found in wire drawing, and in fact work softening is occasionally observed<sup>(82)</sup>. It would be most interesting to test the wear rates of materials that work-soften in wire drawing. For these, one would expect an extreme concentration of shear strain at the surface (i.e. large  $n$  values in eq. 37a) in conjunction with very large surface shear strains,  $\gamma_s$ , and thus low wear coefficients,  $Z$ .

For the ideal plastic material, without effective workhardening, one expects a simple linear decrease of  $\gamma$  with  $z$  and extremely concentrated at the surface, meaning a very large value of  $n$  and correspondingly very low wear rate according to eq. 37a. Also all other workhardening laws will concentrate the shear strain near the surface, but not as extremely, with the correspondingly expected moderate to large values of  $n$ .

The often debated, suspected soft surface layer, would appear to be impossible in the framework of the preceding analysis unless dynamic effects were very large, for which there is no evidence. However, all previous considerations concerned positive  $z$ -values, and the origin of our coordinate system, i.e.

$z = 0$ , was placed at the level of the valleys between cooperating hills, or of the micro-roughness, respectively. For negative  $z$ -values conditions are by far more complex: When a contact spot is released, while the two sides part, the roughened zone at negative  $z$ -values, which has not undergone systematic shear deformation and thus will be softer, will be subject to grooving which causes strong local deformation and hardening. Yet, even after grooving the top layer, of one micron or less, could still be softer than the layers below, and in that case would have the correspondingly lower dislocation density. However, if so, this softer layer is softer on account of a quite complex deformation history and not as the result of any particular dislocation mechanism.

The question of the suspected soft surface layer has been reviewed by Hirth and Rigney<sup>(51, 56)</sup> from the standpoint of dislocation theory, and even more extensively by Nabarro<sup>(83)</sup>. Rather earlier, and somewhat less searchingly, the same question has been addressed by the writer<sup>(84)</sup>, and it was further illuminated by some remarkable experiments<sup>(85, 86)</sup>. On balance, it seems clear that, on account of dislocation mechanisms, the top surface layer could be harder or softer, depending on detailed conditions, but that esoteric dislocation effects do not seem to play any appreciable role in modifying the hardness of surface layers in friction and wear.

#### Dislocation Behavior and Microstructures

The picture of regularity and simplicity of mechanical behavior during sliding wear that has been developed above for what we have termed the "basic" case, leaves little room for surprises in regard to microstructures: For homogeneous metals, at the least, one will expect the same kind of dislocation cell formation as in wire drawing, but with a texture much as in rolling.

The microstructure of drawn wire has previously been examined for the case

of iron<sup>(79)</sup> (of which Fig. 27 gives examples), and for the case of aluminum<sup>(82)</sup>, and it has been interpreted theoretically with considerable success<sup>(80)</sup>, albeit still leaving some unanswered problems<sup>(82, 87)</sup>.

The basic reasons for the formation of sub-boundaries have been given already above, namely energy reduction of the trapped dislocations which in the presence of more than one Burgers vector direction leads to the formation of dislocation cells. The cell interiors are almost free of dislocations and are rigidly rotated relative to the interiors of the neighboring cells.

"Similitude", as previously defined and illustrated in Fig. 27, causes stage II behavior. Included in "stage II behavior" is linear workhardening at small strains, and workhardening linear in log strain (i.e. linear from moment to moment with respect to the existing state) for large strains, as in eq. 45b. While similitude obtains, the dislocation cell size and mesh length in the cell walls are both nearly inversely proportional to the acting stress. This has indeed been found to be true in iron, in the work by Langford and Cohen<sup>(79, 80)</sup>, but a more complicated, though generally similar, behavior was reported for aluminum alloys<sup>(82, 87)</sup>.

The similarity between surface shear in wear, and the deformation in wire drawing, is sufficiently close that below wear tracks one expects to see dislocation cells resembling those in wire drawing, which follows stage II behavior, as explained, excepting perhaps the layer at  $z < 0$  in our coordinate system. Correspondingly, the dislocation cell diameter,  $D$ , should rise roughly linearly with  $z$ , i.e. distance from the surface, since the shear stress near the surface is  $\tau \approx \tau_y z_0 / (z + z_0)$  while  $D \propto 1/\tau$  in similitude, so that  $D = D_s + \text{const} \times z$ . Fig. 28 due to L. K. Ives<sup>(8)</sup> shows an increase about this type but, regrettably, micrographs are as yet too few.

AD-A093 451

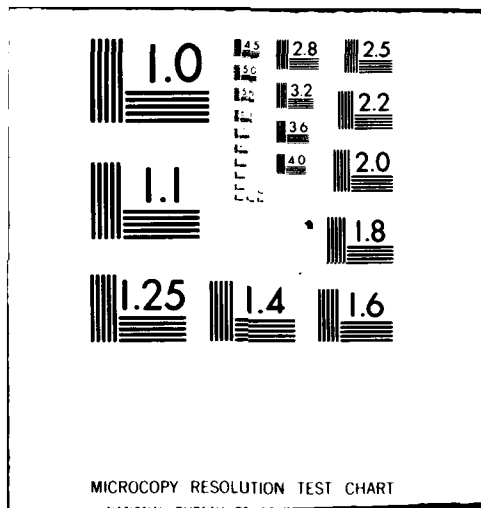
VIRGINIA UNIV CHARLOTTESVILLE DEPT OF MATERIALS SCIENCE F/6 20/2  
DISLOCATION CONCEPTS IN FRICTION AND WEAR.(U)  
DEC 80 D KUHLMANN-WILSDORF

N00014-76-C-1009  
NL

UNCLASSIFIED

2 of 2  
DATE  
FILMED

END  
DATE  
FILMED  
2-81  
DTIC



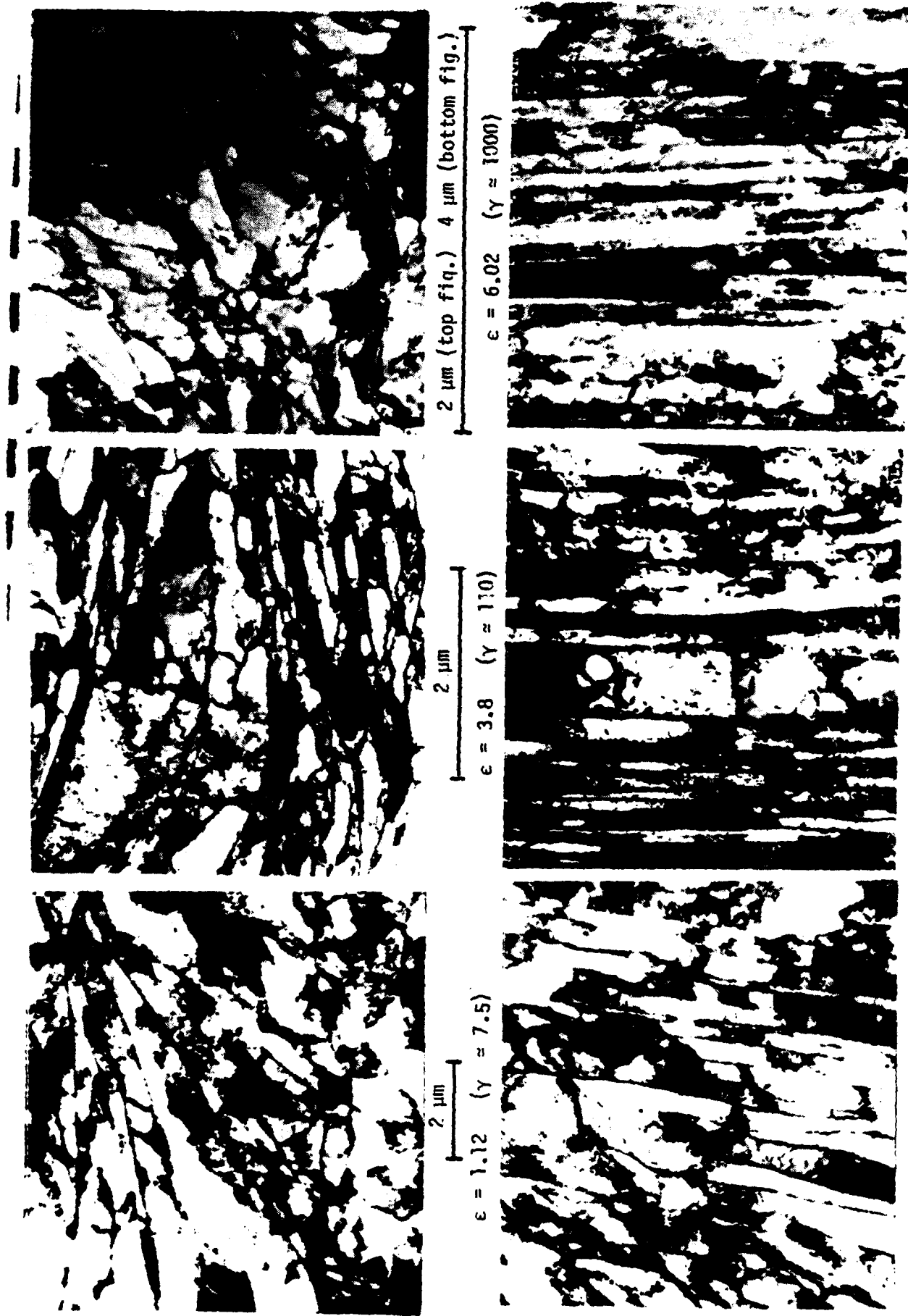


Fig. 27. Cross-sectional (top row) and longitudinal (bottom row) micrographs of the dislocation cell structure in drawn iron wire. The true strains ( $\epsilon$ ) and the shear strains ( $\gamma$ ) to which these would correspond in the surface deformation under wear tracks are as indicated, using the specific wear texture in the case concerned. Note that, due to "similitude", the cells shrink in size without changing shape; yet no recrystallization took place. (Courtesy of G. Langford and M. Cohen, - compare ref. 79).



Fig. 28 Cell structure beneath wear track in copper tested under lubricated sliding conditions. Note the qualitative similarity with Fig. 27, taking into consideration the relatively higher magnification in this figure. According to the theory in the present paper, the cell diameter should rise linearly with distance from the surface down to the thickness of the sheared layer, of roughly 0.1 mm in extent. (Courtesy of L. K. Ives, ref. 8).

this dependence definitely. Further, since  $\psi$ , the angle of relative misorientation across cell walls, is inversely proportional to the meshlength of the dislocations in the cell walls, one expects  $\psi \propto \tau$  i.e.  $\psi \propto z_0/(z + z_0)$ , more or less. This, too, should be tested. The qualifier "more or less" comes about due to a minor deviation from simple proportionalities by the intrusion of a logarithmic term in the dislocation line energy<sup>(80, 81)</sup>.

Dislocation cell walls are principally composed of mobile dislocations and are themselves mobile, always adjusting towards minimum energy configurations. Therefore it would be a mistake to expect dislocation cells to deform homologously with the shear of the surface material, and for the case of wire drawing Fig. 27 shows clearly that they don't; namely, the wire lengths in Figs. 27 are in the ratios of 1 : 14.6 : 134 i.e. a much wider spread than that of the cell lengths or crosssections. Because of the awesome variety of possible configurations and our present inability to compute the energy of even some of the most simple ones to an accuracy sufficient for relative comparisons, no quantitative predictions can be made as to the size of the cells in the deformed surface zone, however.

In drawn iron wire<sup>(79)</sup>, the cell diameters shrink in line with the rising stress (eq. 46) but, as evident from Fig. 27, less fast than the wire diameter, so that cell walls vanish continuously. It seems highly improbable that the eliminated cell walls simply dissolve, and equally improbable that, by and large, they leave through the free surfaces. Rather, they presumably annihilate pairwise, i.e. by the elimination of whole cells<sup>(81)</sup>. That effect is unlikely to be found in sliding wear, because the surface layer, though shearing, does not change its macroscopic area or thickness. Thus no cell walls need to be eliminated during cell refinement but cell walls must be

formed instead. Again, that process is believed to consist of the pairwise formation of opposite cell walls<sup>(81)</sup>. Furthermore, during sliding wear the average cell diameter as a function of  $z$  will not change beyond "run-in". Thereafter, the average cell length and shape is presumably maintained by the statistical pairwise formation of new cell walls, in whichever new areas become exposed as wear via delamination removes surface layers.

Going in the direction of smaller  $z$ -values, i.e. towards the surface, the cell walls will look more and more like grain boundaries, because as  $\psi$  and the dislocation density in the walls increases, so the wall thickness shrinks. For this reason the cells may often look like, and be mistaken for, recrystallized grains.

Measurements of shear strain below the surface by analyzing crystallite shapes<sup>(18, 77)</sup> are bedeviled by the discussed mobility of cell walls, the resulting impossibility of deducing the macroscopic shape change from them, and the difficulty of distinguishing cell walls from grain boundaries. The belief that "grain boundary" rearrangements are necessarily caused by recrystallization or dynamic recrystallization<sup>(18)</sup> is only too understandable and occasionally correct but, in connection with cell walls, it is generally erroneous as indicated. Fig. 27 demonstrates this clearly: The dislocation cells make the impression as if annealed, but the experimentally observed dependence of cell diameter on stress and strain<sup>(79)</sup>, as well as the theoretical interpretation<sup>(80)</sup> show without doubt that there was no recrystallization, dynamic or otherwise. This does not mean that recrystallization cannot take place at all during sliding wear. Fig. 29 by Ives<sup>(8)</sup> proves that it can; in this case unmistakable on account of the presence of annealing twins.

Rigney, Hirth and Glaeser<sup>(51, 55, 56)</sup> have recently suggested that the dislocation cells below the wear track are rectangular, with the largest face

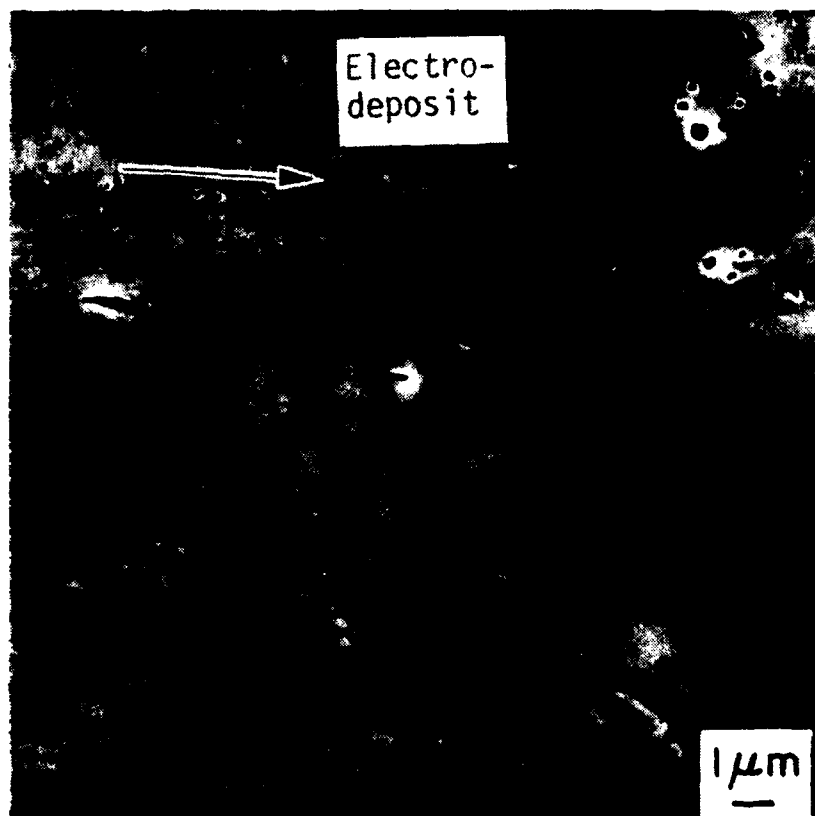


Fig. 29 Cross section through a wear track of copper tested under dry sliding condition, 1 kg\* load, 3.8 cm/sec sliding speed, after 200 m of sliding. Recrystallized grains can be clearly recognized by the presence of annealing twins in them. Note also fissures, partly in the recrystallized grains and partly in the fine-grained material, - which incidentally could also be recrystallized, a question which cannot be definitely decided without further information. (Courtesy of L. K. Ives, ref. 9).

parallel to the surface, and the cells being elongated in the direction of sliding. In addition to the arguments by Rigney et al., this is a most reasonable possibility also when viewed from the basis of a computational theory of dislocation cells<sup>(47, 88)</sup> which came to the following conclusions: The minimum energy configuration attainable with three equivalent, coplanar Burgers vectors forming an equilateral triangle, such as on close packed planes, is a set of rectangular cells whose relative misorientations are about a common axis and alternate left, right, left, right as if in a three-dimensional checker-board pattern.

In sliding wear, the sliding direction, as well as the normals to the sliding surface and to the sliding direction, are preferred directions. For symmetry reasons, either of the three could serve as the mentioned common axis of relative misorientation among the cells that should exist according to theory<sup>(88)</sup>. If it is the surface normal which so serves, there would be twist boundaries parallel to the surface, while the two sets of boundaries at right angles to the surface would be tilt walls. If, on the other hand, the axis of misorientation is the sliding direction, all cell walls containing the sliding direction (i.e. two thirds of the walls, and the larger ones at that) would have tilt character, while only the walls normal to the sliding direction would be twist boundaries. Finally, if the common axis of misorientation is parallel to the surface and normal to the sliding direction, the cell walls parallel to the surface and those normal to the sliding direction would have tilt character, whereas the cell walls parallel to the sliding direction would be twist boundaries.

Hirth and Rigney<sup>(51, 56)</sup> expect tilt walls at right angles to the sliding direction, composed of primary dislocations, which would imply a rotational

axis normal to the sliding direction, parallel to the surface. However, tentatively, Ives<sup>(89)</sup> has identified the majority of cell walls as of tilt type for the case of copper. If so, the sliding direction is the common axis. At any rate, now that the different simple possibilities have been stated, it becomes readily possible to search for the answer in a systematic manner.

We may conclude this discussion with two tantalizing micrographs due to Lawless<sup>(90)</sup> (Figs. 30 and 31). These give an example of that ideal cell geometry which was predicted by Rigney, Hirth and Glaesser<sup>(51, 55, 56)</sup>, and which is theoretically expected for the case of highly symmetrical conditions, including at least three coplanar Burgers vectors in a symmetrical orientation to surface and sliding direction<sup>(88)</sup>. These micrographs of the cell structure underneath a wear track were obtained from a 1000 Å thick (100)-oriented copper film that had been epitaxially grown on cleaved rock salt, and over which a very lightly loaded hemispherical sapphire was slid in [011] direction<sup>(90)</sup>.

Evidently, in this geometry, with  $\frac{1}{2}\langle 110 \rangle$  serving as Burgers vectors, the stipulated conditions for high symmetry are met, and evidently, too, the cell shapes are precisely those that were predicted. Yet, it is not possible to decide from Figs. 30 and 31 which direction served as the common axis of misorientation for the cells, that should be present according to theory. Namely, not all of the short boundaries normal to the sliding direction in Fig. 30 are necessarily cell walls, but some, namely specifically those showing no diffraction contrast change from one side to the other and composed of just one set of lines parallel to the surface, are probably stacking faults. If the dark lines in these features were dislocations, they could only be dipolar walls composed of equal numbers of positive and negative primary (i.e.

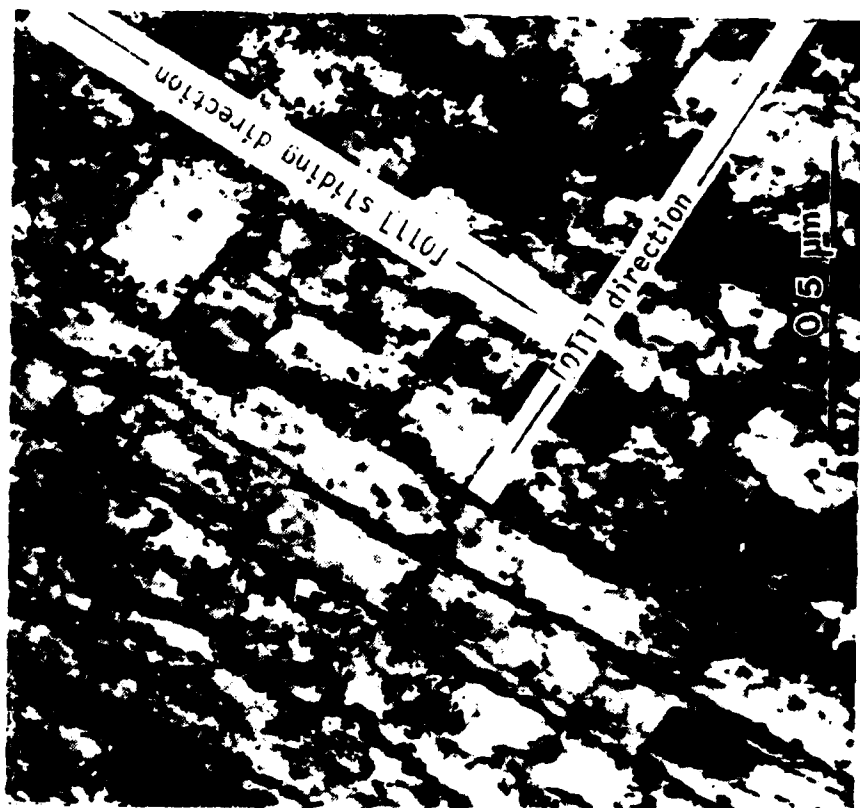


Fig. 30



Fig. 31

Dislocation cell structure under the wear track of a very lightly loaded sapphire ball slid over a 1000 Å thick, (100)-oriented copper film on cleaved rock salt. By geometry and orientation, the cells are exactly as had been predicted previously (refs. 51, 55, 56 and 88). However, it cannot be determined whether the cells have a common axis of misorientation, as predicted by theory (ref. 88) and, if so, which one. Part of the difficulty here arises because it is not entirely clear whether some of the features parallel to [011] in Fig. 31 are sets of dipolar edge dislocation pairs, or twin boundaries, or stacking faults. More experiments to clarify this point are needed. Fig. 30 as deformed, Fig. 31 after heating. (Courtesy of K. R. Lawless, ref. 90).

[011]) edge dislocations, and would thus not be associated with any relative rotation. Alternatively, also, these features could be twin boundaries.

The fact that another set of dislocations, steeply inclined to the surface, is appearing to move into those structures or to move towards extending them, is an argument in favor of interpreting them as dipolar walls which are in the process of converting into tilt walls with axis parallel to [100]. Also the cell walls parallel to [011] appear to be threaded with dislocations which are steeply inclined to the surface. It is thus possible that all of the walls either are, or are in the process of developing into, tilt walls with the rotation axis normal to the surface. This interpretation would be consistent with the lack of diffraction contrast in Fig. 31 but inconsistent with the rather pronounced diffraction contrast across the middle cell in Fig. 30. Perhaps, at the price of a further complication, that contrast could then be interpreted as due to an initial rotation about an axis parallel to the [011] sliding direction.

Alternatively, the common axis of misorientation could be parallel to the sliding direction. The lack of diffraction contrast in Fig. 31 in that case would be explained as due to a too great deviation from the Bragg condition. Altogether this hypothesis of [011] as the rotation axis is in better agreement with the micrographs. The features across which there is no evidence of misorientation, if they are not stacking faults or twin boundaries, could in that case be interpreted as close pairs of walls which are in the process of moving apart and thereby generating new dislocation cells as explained before in connection with cell size refinement in wear layers.

Altogether, therefore, Figs. 30 and 31 provide tantalizing support for the theoretical considerations presented in this paper but fall short of providing proof. Thus more experimental work is highly desirable also in this area.

### Summary and Outlook

Evidently, the various ideas, predictions and quantitative relationships in this paper provide much opportunity for experimental testing, which no doubt will lead to considerable refinements if not major modifications. As was shown, all of the above are in adequate agreement with existing data or better, so that the theory is certainly promising. If it is then assumed that it is basically correct, one may be impressed with the underlying simplicity of the mechanisms involved in friction and wear: A small number of relatively restricted contact spots, usually representing only a very small fraction of the geometrical area, interlock from one side of the sliding couple to the other, to enforce momentary relative rest. This enforces gliding, which is concentrated in the top layer of the softer of the two materials concerned, or is shared equally among two like materials. At the edges of these spots, as well as while spots part, the interlocking micro-roughnesses, - generated by inhomogeneities of local elastic and plastic deformation, - plough a shallow grooving pattern into the wear track. The shear stresses, due to the tangential tractions applied at the contact spots, extend into the materials to a depth comparable to the contact spot diameters, which typically is in the 0.1 mm range, whereas the micro-roughness has only about 1% of that depth, or less.

The two materials respond to the applied tractions with shear deformations. In the majority of technologically interesting dry sliding situations, those shear deformations cease when the local flow stress, as raised by work hardening, equals the applied resolved shear stress on the active glide systems, wherein each layer parallel to the surface may be assumed to act independently of its adjoining layers, and in which, typically, strain rate effects are negligible.

During the initial period of "running-in", statistically the contact spot migrations generate a rather uniformly sheared and work hardened surface layer. Local shearing off of asperities which are caught in the "valleys" of the opposing surface contour, continues throughout sliding. It acts to preferentially transfer

particles of the softer material to the harder, but not exclusively so. That transfer is initially stronger in the case of initially rough surfaces and is initially slower for the case of initially smooth surfaces, and should come to an equilibrium when the micro-roughness appropriate to the prevailing sliding conditions is established throughout. That shearing-off of asperities then should continue at some constant rate which, however, is slower than "delamination wear" which sets in gradually and reaches a constant rate after the running-in period.

"Delamination wear", consisting of the flaking off of a surface layer of more or less constant thickness, in flakes whose area is of little particular significance for the process, must occur whenever the flow stress of the softer (or both) material(s) is a monotonically rising function of cumulative strain. If so, there must typically a limit be reached, beyond which the material cannot be deformed, and cracking will result. This cracking takes the form of "delamination" because of the essential uniformity of stress/strain history and mechanical properties of layers parallel to the surface which, however, act rather independently of the neighboring layers. The simple formulae which describe this process give a wear rate parameter, and length of induction path for wearing-in, which are in general harmony with observations.

Complications of the above basic processes arise because the flow stress of the surface material subject to shearing, and the flow stress of the bulk material which determines the total extent of the contact spots, are not the same and are subject to different effects in regard to crystallographic texture and temperature gradients such as arise in the course of sliding. However, the semi-quantitative predictions of coefficient of friction and its dependence on crystal structure, sliding direction, development during running-in, and sliding velocity, are all in good accord with experimental observations.

Dislocation concepts are important in the understanding of the above derivations and conclusions, especially in regard to geometrical considerations. That the

dislocations behave according to the local conditions of stress and strain, without the obvious intervention of any peculiar effects, such as are otherwise known to occur at surfaces, is established to a high degree of confidence through comparing dislocation structures underneath wear tracks with those in drawn wires. The working conditions in the two cases are comparable, and similarly high shear strains are attained, - and the dislocation structures formed are also similar. Since those in wire drawing have previously been successfully interpreted in terms of basic dislocation properties, it is considered probable that also the structures under wear tracks are in accord with theoretical expectations, at the least in cases of sufficiently simple symmetry that predictions can be made. None such are at this point available with sufficiently much detail provided to permit a proof of this contention. However, in one specific case intriguing partial confirmation was obtained.

It is much to be hoped that the present theory will stimulate experimentation to test and expand it. If successful, the theory may become very useful in the prediction of coefficients of friction and wear rates. One particular application of the theory may be found in the opportunity it offers to improve wear behavior via purposefully selected textures.

### References

- 1) F. P. Bowden and D. Tabor, "Friction - An Introduction to Tribology" (Anchor Press/Doubleday, New York, 1973), pp. 16-24.
- 2) R. Holm, "Electric Contacts" (Springer, New York, first published 1958).
- 3) F. P. Bowden and D. Tabor, "Friction and Lubrication" (Methuen, London, 1967, first published 1956).
- 4) F. P. Bowden and D. Tabor, "Friction - An Introduction to Tribology" (Anchor Press/Doubleday, New York, 1973).
- 5) J. J. Bickerman, Wear, Vol. 39 (1976) 1.
- 6) N. P. Suh and coworkers, "The Delamination Theory of Wear" (Elsevier Sequoia, Lausanne, 1977).
- 7) E. Rabinowicz, "Friction and Wear of Materials" (John Wiley and Sons, New York, 1965).
- 8) L. K. Ives, "Microstructural Changes in Copper Due to Abrasive, Dry and Lubricated Wear" in "Wear of Materials - 1979" (Eds. K. C. Ludema, W. A. Glaeser and S. K. Rhee, Am. Soc. Mech. Eng., New York, 1979) p. 246.
- 9) J. A. Greenwood and J. B. P. Williamson, Proc. Roy. Soc. (London) Vol. 295A (1966) 300.
- 10) J. B. P. Williamson and R. T. Hunt, Proc. Roy. Soc. (London) Vol. A327 (1972) 147.
- 11) J. Pullen and J. B. P. Williamson, Proc. Roy. Soc. (London) Vol. A327 (1972) 159.
- 12) R. Holm "Electric Contacts" (Springer, New York, 1967) p. 34.
- 13) I. McNab, "Recent Advances in Electric Current Collection", Wear, Vol. 59 (1980) 259.
- 14) H. Kongsjorden, J. Kulsetås<sup>o</sup> and J. Sletbak, "Electrical Contacts - 1978" (Proc. Twenty-fourth Holm Conference on Electrical Contacts, Chicago, IL) p. 477.
- 15) "Thermal Deformation in Frictionally Heated Systems" (Ed. R. A. Burton, Elsevier Sequoia, Lausanne/New York, 1980).
- 16) R. A. Burton, Wear, Vol. 59 (1980) 1.
- 17) J. P. Netzel, Wear, Vol. 59 (1980) 135.
- 18) J. H. Dautzenberg, Wear, Vol. 60 (1980) 401.
- 19) W. Hirst and J. K. Lancaster, Proc. Roy. Soc., Vol. A259 (1961) 228.
- 20) R. M. Davies, Proc. Roy. Soc., A197 (1949) 416.

- 21) S. Jahanmir and N. P. Suh, Wear, Vol. 44 (1977) 17.
- 22) L. D. Dyer, Trans. ASM Quarterly, Vol 58 (1965) 620.
- 23) L. D. Dyer, Acta Met., Vol. 9 (1961) 928.
- 24) J. B. P. Williamson, private communication.
- 25) J. R. Whitehead, Proc. Roy. Soc., Vol. A201 (1950) 109.
- 26) J. F. Archard, Proc. Roy. Soc., Vol. A243 (1957) 190.
- 27) H. Hertz compare ref. 2, Fourth edition, 1967, pp. 367/8.
- 28) A. J. W. Moore, Proc. Roy. Soc. (London) Vol. A195 (1948) 231.
- 29) E. Holm, R. Holm and E. I. Shobert II, J. Appl. Phys., Vol. 20 (1949) 319.
- 30) D. Tabor, Proc. Roy. Soc. (London), Vol. A192 (1948) 247.
- 31) D. Tabor, "The Hardness of Metals" (Clarendon Press, Oxford, 1951).
- 32) R. Holm, "Electric Contacts" (Springer, New York, 1967) p. 373-375.
- 33) E. I. Shobert, "Carbon Brushes - The Physics and Chemistry of Sliding Contacts", Chemical Publ. Co., New York, 1965), p. 24.
- 34) R. Holm, loc. cit. p. 132.
- 35) C. M. Adkins and D. Kuhlmann-Wilsdorf, "Electrical Contacts - 1979" (Proc. Twenty-fifth Holm Conference on Electrical Contacts, Chicago, IL) p. 171.
- 36) C. M. Adkins and D. Kuhlmann-Wilsdorf, "Electrical Contacts - 1980" (Proc. Twenty-sixth Holm Conference on Electrical Contacts, Chicago, IL) p. 67.
- 37) E. Rabinowicz, ASLE Trans., Vol. 14 (1971) 198 and 206.
- 38) S. A. Barber and E. Rabinowicz, "Electrical Contacts - 1980" (Proc. Twenty-sixth Holm Conference on Electrical Contacts, Chicago, IL) p. 33.
- 39) J. H. van der Merwe, Proc. Phys. Soc., Vol. A62 (1949) 315.
- 40) J. H. van der Merwe, in "Single Crystal Films" (Eds. M. H. Francombe and H. Sato, MacMillan Co., N.Y., 1964) p. 139.
- 41) W. A. Jesser and D. Kuhlmann-Wilsdorf, phys. stat. sol., Vol. 19 (1967) 95.
- 42) E. Schmid and W. Boas, "Plasticity of Crystals" (F. A. Hughes and Co., London, 1950) p. 58; first published in German, 1934.
- 43) N. Brown, Trans. AIME, Vol. 221 (1961) 236.
- 44) G. Y. Chin, in "Constitutive Equations in Plasticity" (Ed. A. S. Argon, MIT Press, Cambridge, MA, 1975) p. 431.

- 45) R. E. Smallman, J. Inst. Met., Vol. 84 (1955) 10.
- 46) J. T. Moore and D. Kuhlmann-Wilsdorf, Surface Science, Vol. 31 (1972) 456.
- 47) M. N. Bassim and D. Kuhlmann-Wilsdorf, Crystal Lattice Defects, Vol. 4 (1973) 9.
- 48) D. Kuhlmann-Wilsdorf, J. Applied Physics, Vol. 33 (1962) 648.
- 49) G. I. Taylor, J. Inst. Met., Vol. 62 (1938) 307.
- 50) U. F. Kocks, Acta Met. 6 (1958) 85.
- 51) J. P. Hirth and D. Rigney in "Dislocations in Solids" (Ed. F. R. N. Nabarro, North Holland Publ. Co., Amsterdam), in press.
- 52) M. Antler, "Electrical Contacts - 1980", (Proc. Twenty-sixth Holm Conference on Electrical Contacts, Chicago, IL) p. 1.
- 53) P. Heilmann and D. A. Rigney, Leeds Conference, Sept. 1981.
- 54) E. Rabinowicz, "Friction and Wear of Materials" (John Wiley and Sons, N.Y., 1965), p. 67.
- 55) D. A. Rigney and W. A. Glaeser, Wear, Vol. 46 (1978) 241.
- 56) J. P. Hirth and D. A. Rigney, Wear, Vol. 39 (1976) 133.
- 57) J. R. Whitehead, Proc. Roy. Soc., Vol. A201 (1950) 109.
- 58) K. L. Johnson and D. V. Keller, J. Appl. Phys., Vol. 38 (1967) 1896.
- 59) D. H. Buckley, J. Appl. Phys., Vol. 39 (1968) 4224.
- 60) S. Dillich and D. Kuhlmann-Wilsdorf, "Electrical Contacts - 1979" (Proc. Twenty-fifth Holm Conference on Electrical Contacts, Chicago, IL) p. 185.
- 61) P. K. Lee, "Electrical Contacts - 1979" (Proc. Twenty-fifth Holm Conference on Electrical Contacts, Chicago, IL) p. 133.
- 62) D. Tabor, "The Hardness of Metals" (Clarendon Press, Oxford, 1951).
- 63) D. A. Rigney and J. P. Hirth, Wear, Vol. 53 (1979) 345.
- 64) N. Saka, A. M. Eleiche and N. P. Suh, Wear, Vol. 44 (1977) 109.
- 65) K. L. Hsu, T. M. Ahn and D. A. Rigney, Wear, Vol. 60 (1980) 13.
- 66) T. Tamai and K. Tsuchiya, "Electrical Contacts - 1978" (Proc. Twenty-fourth Holm Conference on Electrical Contacts, Chicago, IL) p. 469.
- 67) J. W. Beams, Physics Today, Vol. 12 (1959) 20.
- 68) ref. 7 p. 91.

- 69) P. Feinle and H. G. Feller, Z. Metallkunde, Vol. 68 (1977) 9.
- 70) J. R. Fleming and N. P. Suh, Wear, Vol. 44 (1977) 39.
- 71) A. R. Rosenfield, Wear, Vol. 61 (1980) 125.
- 72) P. Schwellinger, Z. Metallkunde, Vol. 71 (1980) 520.
- 73) R. N. Gardner, T. C. Pollock and H. G. F. Wilsdorf, Mat. Sci. Eng., Vol. 29 (1977) 169.
- 74) H. G. F. Wilsdorf in "Strength of Metals and Alloys" (Proc. ICSMA5, Aachen, Germany, Aug. 1979, Eds. P. Haasen, V. Gerold and G. Kostorz, Pergamon, N.Y. 1979) p. 169.
- 75) H. G. F. Wilsdorf, Kristall und Technik, Vol. 14 (1979) 1265.
- 76) N. Soda, Y. Kimura and A. Tanaka, Wear, Vol. 40 (1976) 23.
- 77) J. H. Dautzenberg and J. H. Zaat, Wear, Vol. 23 (1973) 9.
- 78) E. Rabinowicz and P. Chan, "Electrical Contacts - 1979" (Proc. Twenty-fifth Holm Conference on Electrical Contacts, Chicago, IL) p. 123.
- 79) G. Langford and M. Cohen, Trans. ASM, Vol. 62 (1969) 623.
- 80) D. Kuhlmann-Wilsdorf, Met. Trans., Vol. 1 (1970) 3173.
- 81) D. Kuhlmann-Wilsdorf in "Work Hardening in Tension and Fatigue" (Ed. A. W. Thompson, AIME, Warrendale, PA, 1977) p. 1.
- 82) D. J. Lloyd and D. Kenny, Acta Met., Vol. 28 (1980) 639.
- 83) F. R. N. Nabarro, in "Surface Effects in Crystal Plasticity" (Eds. R. M. Latanision and J. T. Fourie, Noordhoff, Leyden, 1977) p. 49.
- 84) D. Kuhlmann-Wilsdorf in "Environment-Sensitive Mechanical Behavior" (Eds. A. R. C. Westwood and N. S. Stoloff, Gordon and Breach, N.Y. 1966) p. 681.
- 85) G. E. Ruddle and H. G. F. Wilsdorf, Appl. Phys. Lett., Vol. 12 (1968) 271.
- 86) H. G. F. Wilsdorf and G. E. Ruddle, in "Surface Effects in Crystal Plasticity" (Eds. R. N. Latanision and J. T. Fourie, Noordhoff, Leyden, 1977) p. 565.
- 87) D. J. Lloyd, Metal Science, May 1980, p. 193.
- 88) M. N. Bassim and D. Kuhlmann-Wilsdorf, phys. stat. sol. (a) Vol. 17 (1973) 281; Vol. 17 (1973) 379; Vol. 19 (1973) 335.
- 89) L. K. Ives, 1980, private communication.
- 90) K. R. Lawless in "Interdisciplinary Approach to Friction and Wear" (Ed. P. M. Ku, NASA SP-181, 1968) p. 433.

DISTRIBUTION LIST FOLLOWS

Distribution ListNumber of Copies

Aero Material Department  
 Naval Air Development Center  
 Warminster, PA 18974  
 Attn: Mr. M.J. Devine, Code 30-7

1

Air Force Aero Propulsion Laboratory  
 Wright Patterson Air Force Base  
 Dayton, OH 45433  
 Attn: Mr. C. Hudson

1

Air Force Materials Laboratory  
 Wright Patterson Air Force Base  
 Dayton, OH 45433  
 Attn: Mr. F. Brooks

1

Defense Documentation Center  
 Building 5  
 Cameron Station  
 Alexandria, VA 22314

6

National Bureau of Standards  
 Department of Commerce  
 Washington, D.C. 20234  
 Attn: Dr. E. Passaglia  
 Attn: Dr. A.W. Ruff

1

1

National Science Foundation  
 Engineering Mechanics Division  
 1800 G Street  
 Washington, D.C.  
 Attn: Mr. M.S. Ojalvo

1

Naval Air Engineering Center  
 Group Support, Equipment Division  
 Lakehurst, NJ 08733  
 Attn: P. Senholzi, Code 92724

1

Naval Air Systems Command  
 Washington, D.C. 20361  
 Attn: B. Poppert, Code 340E

1

Director Naval Research Laboratory  
 Washington, D.C., 20375  
 Attn: Technical Information Division  
 Dr. L. Jarvis, Code 6170

6

Naval Research Laboratory  
 Washington, D.C. 20375  
 Attn: R. C. Bowers, Code 6170

1

Naval Sea Systems Command Washington, D.C. 20362 Attn: Mr. M. Hoobchack	1
Naval Ship Research and Development Laboratory Annapolis, MD 21402 Attn: Mr. N. Glassman Attn: Mr. W. Smith	1 1
Assistant Chief for Technology Office of Naval Research, Code 200 800 N. Quincy Street Arlington, VA 22217	1
Office of Naval Research 800 N. Quincy Street Arlington, VA 22217 Attn: Commander H.P. Martin, Code 211	6
Office of Naval Research 800 N. Quincy Street Arlington, VA 22217 Attn: D. Lauver, Code 411	1
Mr. D. Anderson Foxboro Analytical P.O. Box 435 Burlington, MA 01803	1
Mr. N.L. Basdekas Office of Naval Research 800 N. Quincy Street Arlington, VA 22217	1
Mr. J.R. Belt, Code 28 David W. Taylor Naval Ship R&D Center Annapolis, MD 21402	1
Dr. M.K. Bernett, Code 6176 Naval Research Laboratory Washington, D.C. 20375	1
Mr. W.J. Bohli Daedalean Assoc., Inc. Springfield Research Center 15110 Frederick Rd. Woodbine, MD 21797	1
Dr. R.N. Bolster, Code 6170 Naval Research Laboratory Washington, D.C. 20375	1

Dr. G. Bosmajian, Code 283 David W. Taylor Naval Ship R&D Center Annapolis, MD 21402	1
Dr. R.C. Bowers, Code 6170 Naval Research Laboratory Washington DC 20375	1
Mr. C.L. Brown, Code 2832 David W. Taylor Naval Ship R&D Center Annapolis, MD 21402	1
Dr. R.A. Burton, Code 473 Office of Naval Research 800 N. Quincy St. Arlington, VA 22217	1
Mr. J.W. Butler, Code 6070 Naval Research Laboratory Washington DC 20375	1
Mr. C. Carosella Naval Research Laboratory Washington DC 20375	1
Mr. M.A. Chaszeyka Office of Naval Research - BRO Chicago, IL 60605	1
Professor H.S. Cheng Northwestern University Dept. of Mechanical Engineering & Astronautical Sciences Evanston, IL 60201	1
Mr. A. Conte, Code 60612 Naval Air Development Center Warminster, PA 18974	1
Mr. R.J. Craig, Code 2832 David W. Taylor Naval Ship R&D Center Annapolis, MD 21402	1
Dr. J.F. Dill, Code SFL Air Force Aero Propulsion Lab Wright Patterson Air Force Base. Dayton, OH 45433	1
Mr. A.J. D'Orazio Naval Air Propulsion Center Trenton, NJ 08628	1

Dr. T. Dow Battelle Columbus Lab 505 King Avenue Columbus, OH 43201	1
Mr. E.C. Fitch FPRC - Oklahoma State University Stillwater, OK 74074	1
Dr. P. Genalis, Code 1720.1 David W. Taylor Naval Ship R&D Center Bethesda, MD 20084	1
Mr. N. Glassman, Code 2832 David W. Taylor Naval Ship R&D Center Annapolis, MD 21402	1
Dr. P.K. Gupta Mechanical Technology Inc. Latham, NY 12110	1
Mr. A.B. Harbage, Code 2723 David W. Taylor Naval Ship R&D Center Annapolis, MD 21402	1
Mr. P.T. Heyl Pratt & Whitney Aircraft E. Hartford, Ct 06108	1
Mr. L.F. Ives National Bureau of Standards Washington DC 20234	1
Dr. D. Jewell, Code 1170 David W. Taylor Naval Ship R&D Center Bethesda, MD 20084	1
Professor J.H. Johnson Michigan Technical University Houghton, MI 49931	1
Mr. J.W. Kannel Battelle Columbus Lab 505 King Avenue Columbus, OH 43201	1
Mr. S.A. Karpe, Code 2832 David W. Taylor Naval Ship R&D Center Annapolis, MD 21402	1

Mr. T. Kiernan, Code 1720.1  
David W. Taylor Naval Ship R&D Center  
Bethesda, MD 20084

1

Dr. J.P. King  
Pennwalt Corp.  
King of Prussia, PA 19406

1

Dr. M. Klinkhammer, Code 2832  
David W. Taylor Naval Ship R&D Center  
Annapolis, MD 21402

1

Mr. M. Kolobielski  
U.S. Army MERADCOM  
Ft. Belvoir, VA 22061

1

Dr. I.R. Kramer  
David W. Taylor Naval Ship R&D Center  
Annapolis, MD 21402

1

Mr. A.I. Krauter  
Shaker Research Corp.  
Ballston Lake, NY 12120

1

Capt. L. Krebes  
AFOSR/NC  
Bolling Air Force Base  
Washington DC 20332

1

Mr. S.P. Lavelle  
ROYCO Institute  
62 Prospect St.  
Waltham, MA 02154

1

Professor A.O. Lebeck  
University of New Mexico  
Mechanical Engineering Dept.  
Albuquerque, NM 87131

1

Dr. M. Lee  
General Electric Corp. Res. & Dev.  
P.O. Box 8  
Schenectady, NY 12301

1

Dr. L. Leonard  
Franklin Research Center  
20th & Race St.  
Philadelphia, PA 19103

1

Mr. S.J. Leonardi Mobil R & D Corp. Billingsport Rd. Paulsboro, NJ 08066	1
Mr. D.E. Lesar, Code 1720.1 David W. Taylor Naval Ship R&D Center Carderock Laboratory Bethesda, MD 20084	1
Mr. A. Maciejewski, Code 92724 Naval Air Engineering Center Lakehurst, NJ 08733	1
Mr. W.E. Mayo Rutgers College of Engineering P.O. Box 909 Piscataway, NJ 08854	1
Dr. R.S. Miller, Code 473 Office of Naval Research 800 N. Quincy St. Arlington, VA 22217	1
Dr. C.J. Montrose Catholic University of America Washington DC 20060	1
Dr. R.W. McQuaid, Code 2832 David W. Taylor Naval Ship R&D Center Annapolis, MD 21402	1
Dr. P. Nannelli Pennwalt Corp. King of Prussia, PA 19406	1
Mr. A.B. Neild, Code 2723 David W. Taylor Naval Ship R&D Center Annapolis, MD 21402	1
Mr. R.N. Pangborn Rutgers College of Engineering P.O. Box 909 Piscataway NJ 08854	1
Mr. M.B. Peterson Wear Sciences Inc. 925 Mallard Arnold, MD 21012	1
Mr. G.J. Philips, Code 2832 David W. Taylor Naval Ship R&D Center Annapolis, MD 21402	1

Mr. B.L. Poppert, Code 304E Naval Air Systems Command Washington DC 20361	1
Dr. A.L. Pranatis, Code 6320 Naval Research Laboratory Washington DC 20375	1
Professor E. Rabinowicz Room 35-014 Massachusetts Institute of Technology 77 Massachusetts Avenue Cambridge, MA 02139	1
Mr. B.B. Rath, Code 6320 Naval Research Laboratory Washington DC 20375	1
Mr. H.P. Ravner, Code 6176 Naval Research Laboratory Washington DC 20375	1
Professor D. Rigney Metalurgical Engineering Department Ohio State University Columbus, OH 43210	1
Mr. F.G. Rounds General Motors Research Labs F & L Dept. 12 Mile & Mound Road: Warren, MI 48090	1
Mr. R.C. Rosenberg General Motors Research Labs General Motors Technical Center Warren, MI 48090	1
Mr. W. Rosenlied SKF Industries Inc. King of Prussia, PA 19406	1
Dr. A.W. Ruff National Bureau of Standards Washington DC 20234	1
Dr. N. Saka Room 35-014 Massachusetts Institute of Technology 77 Massachusetts Avenue Cambridge, MA 02139	1

Dr. E.I. Salkovitz, Code 470 Office of Naval Research 800 N. Quincy St. Arlington, VA 22217	1
Mr. K. Sasdelli, Code 2723 David W. Taylor Naval Ship R&D Center Annapolis, MD 21402	1
Mr. J. Schwartz, Code 2842 David W. Taylor Naval Ship R&D Center Annapolis, MD 21402	1
Mr. P.B. Senholzi, Code 92724 Naval Air Engineering Center Lakehurst, NJ 08088	1
Mr. H-C. Sin Room 35-136 Massachusetts Institute of Technology 77 Massachusetts Avenue Cambridge, MA 02139	1
Dr. I.L. Singer, Code 6170 Naval Research Laboratory Washington DC 20375	1
Dr. P. Sniegowski Naval Research Laboratory Washington DC 20375	1
Mr. L. Stallings, Code 60612 Naval Air Development Center Warminster, PA 18974	1
Professor N.P. Suh Room 35-136 Massachusetts Institute of Technology 77 Massachusetts Avenue Cambridge, MA 02134	1
Professor R.K. Tessman Fluid Power Research Center Oklahoma State University Stillwater, OK 74074	1
Dr. A. Thiruvengadam Daedalean Assoc., Inc. Woodbine, MD 21797	1

Dr. J. Tichy Rensselaer Polytechnical Institute Troy, NY 12181	1
Dr. R. Valori Naval Air Propulsion Center Trenton, NJ 08628	1
Mr. V.D. Wedeven NASA/ Lewis Research Center Cleveland, OH 44135	1
Mr. P. Weinberg Naval Air Systems Command Washington DC 20361	1
Professor D. Wilsdorf School of Engineering & Applied Science University of Virginia Charlottesville, VA 22903	1
Mr. A.D. Woods, Code 5243 Naval Sea Systems Command Washington DC 20360	1
Dr. C.C. Wu, Code 6368 Naval Research Laboratory Washington DC 20375	1
Lt.Col. E.F. Young Joint Oil Analysis Program Technical Support Center Bldg. 780 Naval Air Station Pensacola, FL 32508	1

## **UNIVERSITY OF VIRGINIA**

### **School of Engineering and Applied Science**

The University of Virginia's School of Engineering and Applied Science has an undergraduate enrollment of approximately 1,400 students with a graduate enrollment of approximately 600. There are 125 faculty members, a majority of whom conduct research in addition to teaching.

Research is an integral part of the educational program and interests parallel academic specialties. These range from the classical engineering departments of Chemical, Civil, Electrical, and Mechanical and Aerospace to departments of Biomedical Engineering, Engineering Science and Systems, Materials Science, Nuclear Engineering and Engineering Physics, and Applied Mathematics and Computer Science. In addition to these departments, there are interdepartmental groups in the areas of Automatic Controls and Applied Mechanics. All departments offer the doctorate; the Biomedical and Materials Science Departments grant only graduate degrees.

The School of Engineering and Applied Science is an integral part of the University (approximately 1,530 full-time faculty with a total enrollment of about 16,000 full-time students), which also has professional schools of Architecture, Law, Medicine, Commerce, Business Administration, and Education. In addition, the College of Arts and Sciences houses departments of Mathematics, Physics, Chemistry and others relevant to the engineering research program. This University community provides opportunities for interdisciplinary work in pursuit of the basic goals of education, research, and public service.